MOLECULAR DYNAMICS STUDY OF THE INTERACTIONS BETWEEN THYMOQUINONE AND LIPID BILAYERS

by

Esra Ülgey

B.S., Chemical Engineering, Boğaziçi University, 2019

Submitted to the Institute for Graduate Studies in
Science and Engineering in partial fulfillment of
the requirements for the degree of
Master of Science

Graduate Program in Chemical Engineering

Boğaziçi University

2022

ACKNOWLEDGEMENTS

First of all, I would like to express my sincere gratitude to my supervisor, Assoc. Prof. Nazar İleri Ercan. Her guidance, encouragement, and continuous support made it possible to finish my thesis. I consider myself very lucky to have had the opportunity to work under her supervision; she guided me with politeness and showed me patience throughout my study.

I would like to thank my thesis committee members, Prof. Türkan Haliloğlu and Assoc. Prof. Özge Kürkçüoğlu Levitas, for devoting their valuable time and providing guidance and recommendations.

I want to express my love and thanks to the members of KB441 Laboratory; Özlem Özbek and Destina Ekingen Genç, for their emotional support and friendships. We became companions and made ourselves laugh when feeling overwhelmed and discouraged, for which I am endlessly grateful. I also want to sincerely thank another member of our laboratory, Gülşah Gül, who helped me overcome the problems I encountered during the research.

Moreover, I want to thank Rüveyda Karakoyun for being there through every step of the undergraduate and graduate years. I also want to thank my friends and colleagues, Ayşe Saliha Korkut, Duygu Kaya, Akarun Ayça Ersoy, and Abdullah Aladağ, for their friendship, support, and encouragement.

I want to express my special thanks and gratitude to Akın Cihan Akgün for believing in me and supporting me in every aspect of my life. I am also thankful to Gizem Kalyoncu for our eternal and sincere friendship for many years. I also thank my close friends, Maral Dicle Maral, İlayda İlerten, Kardelen Kanığ, and Aslınur Doğan, who made the time we spent in room 301 and beyond joyful and meaningful. Finally, I thank Ata Oruç and Serra Kirsch for their cheerful friendship. I wish all the best for

all these people.

I want to send my heartfelt thanks to my parents, Fatma Nilgün Ülgey and Cuma Ülgey, for their endless support, love, and belief in me. I also want to thank my twin brother Bahadır Ülgey, my other half, who helped and supported me not only on this journey but throughout my entire life. My last thanks go to Maya, the sweetest and fluffiest cat in the world, for biting and scratching me every day. I appreciate the love and support from my small family deeply.

This work was partially funded by grants from The Scientific and Technological Research Council of Turkey (TUBITAK) under BIDEB 2247-A (Grant No: 120C133).

ABSTRACT

MOLECULAR DYNAMICS STUDY OF THE INTERACTIONS BETWEEN THYMOQUINONE AND LIPID BILAYERS

Thymoquinone, a phytochemical with antitumor activity, and its derivative aminothymoquinone were investigated using Molecular Dynamics (MD) Simulations to understand their interactions with simple and complex bilayer models. MD simulations of the models were performed using all atom (AA) and coarse-grained (CG) force fields, i.e., the OPLS-AA and MARTINI 3. Although the resolution of the molecules decreased during coarse-graining, the chemical and thermodynamic properties of the molecules were mostly retained. The bond and dihedral distributions validated the matching of AA and CG models, and the free energy calculations showed the reproducibility of new models apart from the agreement with the experimental logP values with less than 10% of error. AA and CG thymoquinone models were used with DOPC and POPC bilayers and the systems were compared with the sole bilayers. The structural properties of bilayers including area per lipid, bilayer thickness, order parameters, and lateral diffusion coefficients were computed. The interaction of CG molecules with two different normal and cancer membrane models was also investigated through the orientation of the molecules in the bilayers, the density distribution, and radial distribution function (RDF) in addition to the methods used for simple bilayer. Both molecules resulted in bilayer thinning with decreased bilayer thicknesses but increased the area per lipid values. Similarly, both molecules decreased the ordering of the bilayers, but the effect was slightly more significant with thymoquinone in normal membrane models. While thymoquinone diffused inside the model membranes, aminothymoquinone preferred to reside near the head groups of lipids. Overall, both molecules interacted similarly, in general, with the lipids of the model membranes, apart from small differences.

ÖZET

TİMOKİNON VE ÇİFT TABAKALI LİPİT ETKİLEŞİMİNİN MOLEKÜLER DİNAMİK ÇALIŞMASI

Antitümör aktiviteye sahip bir fitokimyasal olan timokinon ve onun türevi aminotimokinonun, basit ve kompleks çift tabakalı lipit modellerle etkileşimlerini anlamak için Moleküler Dinamik (MD) Simülasyonları kullanılarak çalışmalar yapıldı. Modellerin MD simülasyonları, tüm atom (AA) ve kaba taneli (CG) kuvvet alanları, yani OPLS-AA ve MARTINI 3 kullanılarak gerçekleştirilmiştir. Kaba taneleme sırasında moleküllerin çözünürlüğünün azalıyor olmasına rağmen, moleküllerin kimyasal ve termodinamik özellikleri büyük bir çoğunlukla korunmuştur. Bağlar ve iki düzlemli açıların dağılımları, AA ve CG modellerinin eşleşmesini doğruladı ve serbest enerji hesaplamaları, %10'dan daha az hata ile deneysel logP değerleriyle uyumuyla yeni modellerin tekrarlanabilirliğini gösterdi. AA ve CG timokinon modelleri DOPC ve POPC çift tabakalı lipitleri üzerinde kullanılmış ve sistemler sade çift tabakalar ile karşılaştırılmıştır. Lipit başına alan, çift tabaka kalınlığı, lipit zincirlerinin düzen parametreleri ve yanal difüzyon katsayıları ile çift tabakalı lipitlerin yapısal özellikleri hesaplandı. CG moleküllerin iki farklı model olan normal ve kanser membran modeli ile etkileşimi, basit çift tabakalar için kullanılan yöntemlere ek olarak, çift tabakalardaki moleküllerin oryantasyonu, yoğunluk dağılımı ve radyal dağılım fonksiyonu (RDF) yoluyla da araştırıldı. Her iki molekül de azalmış çift tabaka kalınlıkları ile birlikte çift tabakada incelmeye yol açmış, ancak lipit başına düşen alan değerleri de artmıştır. Benzer şekilde, her iki molekül de çift tabakaların düzenini azalttı, ancak timokinonun normal membran modellerindeki etkisi biraz daha net görüldü. Timokinon model membranların içinde diffüz ederken, aminotimokinon lipitlerin baş gruplarının yakınında bulunmayı tercih etti. Genel olarak, her iki molekül de, küçük farklılıklar dışında, model membranların lipitleri ile benzer şekilde etkileşime girdi.

TABLE OF CONTENTS

LIST OF FIGURES

LIST OF TABLES

LIST OF SYMBOLS

a_i	Acceleration of the particle i
A_L	Area per lipid
A_{XY}	Cross-sectional area of the box
D	Diffusion coefficient
f	Force between the corresponding atom and the other atoms
F_i	Force applied on the particle i
G	Gibbs free energy
k	Force constant
m_i	Mass of the particle i
n	Multiplicity
N_L	Total number of lipids in the bilayer
P	Partition coefficient
q_i	Charges of atom i
q_j	Charges of atom j
r	Bond length
R	Gas constant
r_{eq}	Equilibrium position
r_i	Position of the particle i
r_{ij}	Distance between atom i and j
r_m	Distance of the minimum potential
S	Order parameter
t	Time
T	Temperature of the system
U	Potential energy function
v_i	Velocity of the particle i
γ	Phase shift
Δ	Change

ϵ_0	Dielectric constant
ϵ_{ij}	Lennard-Jones well depth
θ	Angle
θ_{eq}	Equilibrium angle
λ	Coupling parameter
φ	Dihedral angle
ω	Improper dihedral angle
ω_{eq}	Equilibrium dihedral angle

LIST OF ACRONYMS/ABBREVIATIONS

AA	All-atom
ATQ	Aminothymoquinone
CG	Coarse-grained
COG	Center of geometry
COM	Center of mass
DOPC	1,2-dioleoyl-sn-glycero-3-phosphocholine
DOPS	1,2-dioleoyl-sn-glycero-3-phospho-L-serine
HDAC	Histone deacetylase
HSA	Human serum albumin
IC50	Half-maximal inhibitory concentration
MD	Molecular dynamics
MSD	Mean square displacement
NVE	Microcanonical ensemble
NPT	Isothermal-isobaric ensemble
NVT	Canonical ensemble
PC	Phosphatidylcholine
PME	Particle mesh Ewald
POPC	1-palmitoyl-2-oleoyl-sn-glycero-3-phosphocholine
POPS	1-palmitoyl-2-oleoyl-sn-glycero-3-phospho-L-serine
PS	Phosphatidylserine
RDF	Radial distribution function
Rg	Radius of gyration
RMSD	Root mean square displacement
RMSF	Root means square fluctuation
ROS	Reactive oxygen species
TQ	Thymoquinone
VMD	Visual Molecular Dynamics

1. INTRODUCTION

Phytochemicals obtained from nuts, whole grains, fruits, and vegetables are the chemical components of plants with high bioactivity potential in animal cells [1]. Phytochemicals have various health benefits on many diseases in animals and humans, including cancers, diabetes, inflammatory diseases, coronary heart disease, microbial, viral, and parasitic infections, ulcers, psychotic diseases, etc [2]. Many phytochemicals are specifically investigated for their anti-carcinogenic effects at both cellular and molecular levels, and chemoprevention is proven for many of them by in vitro studies [3].

Thymoquinone is a phytochemical obtained from the Nigella sativa, which is also known as black seed [4]. As the main component of the volatile oil of Nigella sativa, thymoquinone exerts antimicrobial, antioxidant, and anti-inflammatory properties [5]. Besides, it is found non-toxic to normal tissues. Thymoquinone protects the organs from the damage of chemotherapy but increases the effect of chemotherapeutic agents in cancer-resistant cells [6]. Moreover, aminothymoquinone, which is a derivative of thymoquinone, has significant antifungal, antibacterial and anticancer activity against diseased cells [7]. However, both are hydrophobic molecules with poor solubility in aqueous media, resulting in poor transport to the cells and causing major challenges in drug formulations [5]. Despite the experimental limitations caused by its chemical properties, the necessity of anticancer drug discovery has reflected the significance of both thymoquinone and aminothymoquinone as promising anticancer agents and resulted in several recent research both in vitro and in vivo [6].

The mechanism of the diffusion of drug molecules through targeted cells is an important stage of drug discovery. Drug molecules that contain bioactive components encounter the plasma membranes in the first place [8]. Generally, these molecules penetrate cells through plasma membranes by direct diffusion, which is the transportation of molecules due to a concentration difference between two environments [9]. Cell mem-

branes consist of lipids as their primary structure. Phospholipids, a prominent type of lipids consisting of hydrophilic-head and hydrophobic-tail groups [10], form a bilayer to separate cell components from the external environment and provide a special milieu for many biophysical/biochemical processes, specifically the diffusion of small molecules to phospholipid bilayers. Therefore, the interaction between the bilayer and drug molecule is crucial for understanding the diffusion mechanism and enhancing the efficiency of the drug formulations in the development stage [11].

The interaction and transport of small pharmaceutical compounds are investigated both experimentally and computationally. Although the experimental studies have yielded significant information about this interaction, the fluidity of the bilayer systems has caused only one-dimensional findings in the direction of the plane normal to the membrane far from its dynamic structure. In other words, experimental techniques fail to prove the required molecular resolution. However, molecular dynamics (MD) simulations provide three-dimensional structures together with the dynamic behavior of phospholipid bilayers in solutions at atomic resolution. Additionally, the difference in time and spatial scales indicates the importance of MD simulations in large systems. The structural properties extracted from experimental studies are obtained for longer periods, such as hours. On the other hand, the findings from MD simulations are obtained after short periods, such as in nanoseconds [12]. To retain the resolution at the level of small molecules, MD simulations are more promising for investigating the drug molecule – lipid bilayer interactions compared to the experimental approaches in particular [13].

MD simulations can be performed at an atomic or coarse-grained (CG) scale. Atomistic simulations successfully provide insight into the underlying atomic-scale processes. Yet, they are limited by small system sizes and time scales. Coarse-grained models differ from atomistic simulations in representing groups of atoms, monomers, or ions as beads, providing a bridge between atomistic and mesoscopic scales [14]. Although both models offer thermodynamical, structural, and dynamical properties of various systems, coarse-grained models are more suitable alternatives for the simula-

tion of large-scale samples in terms of size-scale, time-scale, and computational cost. In other words, the CG force field allows the simulations of larger systems to run for longer time scales with less computational cost and hence enables the study of more realistic complex systems such as cell membranes. However, the CG model should reproduce the properties of atomic-level models during the coarse-graining procedure since a lower resolution scale of the atomistic model is used. The quality of the CG model depends on the model's resolution, mapping procedure, and potential energy function, together with the experimental and atomic level simulation properties used to optimize the parameters of the CG model [15]. The widely used atomistic force fields are AMBER [16], CHARMM [17], GROMOS [18], OPLS [19], the ones that follow the same functional form of potential energy proposed by Levitt and Lifson [20]. The most popular CG model is the MARTINI force field for the modeling of membrane proteins and membrane environment [21].

In this study, the interactions of thymoquinone and its derivative aminothymoquinone with lipid bilayers are simulated by MD simulation using both atomistic and CG force fields. In the second chapter, the literature data on the benefits and properties of thymoquinone and aminothymoquinone, the importance of the interaction of small drug molecules with lipid bilayers, the effectiveness of MD simulations, the comparison between atomistic and CG models, and similar previous studies using different phytochemicals are explained in detail. In the third chapter, the properties of the studied systems, the parameters used in the simulation runs, and the assumptions made are explained. In the fourth chapter, the results and analyses of the simulations are presented and discussed. In the fifth chapter, the final remarks of the study are made, and the recommendations for future studies are stated.

2. LITERATURE SURVEY

Humans have benefited from the easy availability, safe and non-toxic effects of active components in herbal medicines for a long time. Phytochemicals, non-nutrient bioactive components coming from nature, maintain not only health but also offer treatment for many chronic diseases, including diabetes, cardiovascular diseases, cognitional diseases, and cancer [22]. The health-promoting properties of phytochemicals studied in recent years have proven their antioxidant, anti-inflammatory, and anticarcinogenic effects both in vivo and in vitro [23]. Thymoquinone, the main bioactive component of black seed (*Nigella sativa*) [24], is one of the phytochemicals that has been demonstrated to have therapeutic potential on various diseases, including the anticarcinogenic effects on a wide range of cancer types. Thymoquinone was studied for over 50 years, yet most of the papers were published in the last 15 years. Thus, the interest in thymoquinone's therapeutic and anticancer properties has been increasing lately [6].

2.1. Antitumor Effects of Thymoquinone and Aminothymoquinone

The anticancer effects of thymoquinone and its derivatives have been widely studied, and promising results have been achieved for various cancer types, including leukemia, breast, colon, lung, skin, prostate, and ovarian cancers. For example, Dastjerdi *et al.* (2016) have shown that thymoquinone inhibits the migration and invasion of breast cancer cells. MCF-7 breast cancer cell line was treated with thymoquinone for 24 hours. The half-maximal inhibitory concentration (IC50) from the MTT (3-(4, 5-dimethylthiazolyl-2)-2, 5-diphenyltetrazolium bromide) assay has demonstrated that thymoquinone induces apoptosis in MCF-7 through up-regulation of P53 gene expression after the treatment time [25].

Chen *et al.* (2015) have found that 2.0 µM of thymoquinone induces apoptosis in an irinotecan-resistant LoVo colon cancer cell line and activates mitochondrial outer

membrane permeability. Thymoquinone triggers the autophagy proteins, which leads to the induction of autophagic cell death [26].

Pang *et al.* (2017) have reported that 3.0 and 10.0 µM of thymoquinone suppresses cancer growth in THP-1 and MV4-11 leukemia cell lines. Besides decreasing total DNA methylation, thymoquinone induces apoptosis and reduces colony formation by activating caspases [27].

Yang *et al.* (2015) injected different amounts of thymoquinone (10, 20, and 40 µM) into the A549 non-small lung cancer cell line. They have found that thymoquinone inhibits the growth of cancer cells by reducing the expression of the proliferation marker cyclin D1. ERK1/2 signaling pathway was controlled during thymoquinone treatment, inhibiting migration and invasion of A549 cells [28].

Furthermore, Jeong *et al.* (2019) observed the effect of 10, 15, and 20 µM of thymoquinone on the proliferation, differentiation, and cell motility of the B16F10 melanoma cell line. They have shown that thymoquinone reduces the expression of microphthalmia-associated transcription factor (MITF) as well as the activity and expression of tyrosinase, which leads to the inhibition of the Wnt signaling pathway [29].

Moreover, Kou *et al.* (2017) have studied the effect of thymoquinone on prostate cancer and shown that the migration metastasis is inhibited by the reduction in the expression of EMT markers in DU145 and PC3 prostate cancer cell lines. Thus, thymoquinone affects the essential intracellular signaling components of cell growth [30]. In general, the anticancer effect of thymoquinone is proven by those and many other studies.

Aminothymoquinone, the synthetic derivative of thymoquinone, also has a high anticarcinogenic potential proven in the literature. For instance, several analogs of thymoquinone were investigated on ovarian cancer cells by Johnson-Ajinwo *et al.* (2019). Aminothymoquinone, one of the analogs used in this study, has shown to increase the

activity of cancer drugs paclitaxel and carboplatin compared to thymoquinone due to its higher solubility in water [31].

Glamoclija *et al.* (2018) tested aminothymoquinone's and its derivatives' effectiveness on SW620, CFPAC, HepG2, and HeLa carcinoma cell lines, along with WI38 healthy control human fibroblast cell line. IC50 values from the MTT assay have demonstrated a significant antitumor activity on all cancer cell lines that were tested with aminothymoquinone. Additionally, all thymoquinone derivatives had no toxic effect on the WI38 healthy control cell line [7].

Bhosale *et al.* (2021) have reported that crystallized aminothymoquinone demonstrates high anticarcinogenic activity against pancreatic cancer cells [32]. Similarly, Eldin Salem *et al.* (2019) have invented new synthesis techniques for thymoquinone derivatives and have reported that aminothymoquinone shows the best anticancer potential against A549 human lung, HT29 colorectal, and MDA-MB-231 human breast cancer cell lines [33].

Moreover, Gobinath *et al.* (2022) have demonstrated that aminothymoquinone connected to 1,4-dihydropyridine molecules along with doxorubicin exhibit cytotoxic activity on the liver (HepG2), breast (MCF-7) and cervical (HeLa) cancer cell lines, based on the results of growth inhibition (GI50), tumor growth inhibition (TGI) and lethal concentration (LC50) [34]. Even though an increasing number of studies have been published in recent years, the anticancer potential of aminothymoquinone should be investigated further to develop more effective treatments against cancer.

2.2. Other Therapeutic Effects of Thymoquinone and Aminothymoquinone

Thymoquinone and aminothymoquinone have anti-inflammatory, antioxidant, antibacterial, and antifungal activities alongside their anticarcinogenic effects, and many studies have proven their therapeutic properties in this context. Studies tested thymo-

quinone and black seed oil on inflammation-based models, including arthritis, colitis, and edema, and immune responses were reported to be enhanced by the active pharmaceutical ingredients in black seed oil [35].

Tekeoğlu *et al.* (2007) have investigated the anti-inflammatory effect of thymoquinone on rheumatoid arthritis in vivo. Rats with arthritis and the healthy control group were observed, and TNF-alpha and IL-1beta values were measured in blood using ELISA kits. The measurements indicated that thymoquinone reduces adjuvant-induced arthritis in rat models [36]. Similarly, Mahgoub (2003) tested thymoquinone on acetic-acid-induced colitis in rats. Platelet-activating factor (PAF), glutathione level, and myeloperoxidase activity measurements have shown that pretreatment of rats with thymoquinone for three days completely protects against acetic-acid-induced colitis [37]. Al-Ghamdi (2001) has investigated the anti-inflammatory activity of black seed extract on Carrageenan-induced paw edema. The results of the analgesic study have indicated that the group treated with the extract experienced a lack of increase in paw volume compared to the group treated with aspirin. The black seed extract also induced an analgesic effect but not an antipyretic effect, compared to the effect of aspirin [38].

Moreover, Nagi *et al.* (2000) and Mansour *et al.* (2002) have studied the effect of oral administration of thymoquinone and demonstrated the antioxidant activity of thymoquinone against reactive oxygen species (ROS) including singlet molecular oxygen, superoxide anion, and hydroxyl radical by suppressing the level of ROS in hepatic, cardiac and kidney disorders. The findings from in vitro assays indicate that thymoquinone has the potential as an endogenous antioxidant [39, 40].

Glamoclija *et al.* (2018) have demonstrated that both thymoquinone and aminothymoquinone have significant antibacterial effects on the Gram-positive and Gram-negative bacterial strains. Additionally, aminothymoquinone has shown higher antifungal activity against three different types of fungi that are tested [7]. The studies discussed above, and many others established the therapeutical properties of thymo-

quinone and aminothymoquinone as being promising in drug development studies.

The properties and pharmacological features of thymoquinone should be known for its applicability in experiments. Thymoquinone has limitations in its bioavailability and drug formation due to its hydrophobicity. Solubility of thymoquinone depends on the duration in the aqueous solutions, which is found as 549 μg/mL - 669 μg/mL at 24 h, and 665-740 μg/mL at 72 h [41]. Regarding its toxicology, an oral dose of 100 mg/kg or less does not have any toxic effect [42]. Thymoquinone is sensitive to light and the pH of the solvent; exposure to light causes degradation regardless of the solvent type, and alkaline solutions decrease the stability of thymoquinone with increasing pH [41, 43]. Bioavailability and stability of thymoquinone cause problems when developing drug formulations and limit its use in clinical trials. Therefore, computational studies are necessary to understand the behavior of thymoquinone and aminothymoquinone in biological environments.

2.3. Computational Studies of Thymoquinone and Aminothymoquinone

The computational studies of thymoquinone and aminothymoquinone in the literature are mainly molecular docking studies on binding these molecules to several proteins, followed by MD simulations to investigate the stability of the complexes formed. These studies aim to understand the therapeutic potential of thymoquinone and aminothymoquinone completely. For example, Woo *et al.* (2011) have performed a molecular docking study to identify the anti-tumor effect of thymoquinone on breast cancer cells. The results have revealed that thymoquinone binds to the binding pocket of the PPAR-γ, inhibiting breast cancer cell proliferation successfully [44]. Similarly, El-Baba *et al.* (2014) have investigated the activity of thymoquinone on colorectal cancer by a molecular docking model. They have demonstrated that thymoquinone binds to and induces the PAK1 expression in colorectal cancer cell lines, pointing out the applicability of thymoquinone in targeted anticancer therapies [45].

Yin *et al.* (2012) have conducted a small molecule-protein binding in silico study on thymoquinone-complexed Plk1-PBD crystal structure. After MD production runs, root means square fluctuation (RMSF) and radial distribution function (RDF) of docked conformation were analyzed. Quantum mechanical calculations were performed to measure the cation-pi interaction of the conformation since the force fields did not include this interaction when the article was published [46].

The inhibition effect of thymoquinone on human histone deacetylase (HDAC) was investigated through molecular docking and MD simulations by Parbin et al. (2016), and in silico findings were supported by in vitro experiments. Molecular structures obtained from RCSB Protein Data Bank and ChEBI database were used in an automated docking program Autodock. The stability of the docked complex was analyzed via MD simulation program GROMACS 4.5.4 and GROMOS96 43a1 force field. It has been demonstrated that the binding affinity of thymoquinone to HDAC is higher, and the stability of the complex is better than the reference molecules, which have been validated by root mean square displacement (RMSD) and average hydrogen bonding analyses. The findings were complemented by in vitro experiments, revealing the help of in silico approach in explaining the elementary interactions between thymoquinone and HDACs [47].

Saffari-Chalestori *et al.* (2019) conducted an in vitro and MD study to analyze the energy changes and molecular interactions of thymoquinone with BCL-XL, BCL-2, and MCL-1 anti-apoptotic factors on prostate cancer cells. Protein-ligand docking simulations were completed by Autodock. MD simulations of both ligand-docked and no-ligand protein systems were performed by GROMACS 4.5.4. RMSD, RMSF, and radius of gyration (Rg) values were computed to validate the accuracy of MD simulation outputs, observe the flexibility of residues, and measure the structure and function of the protein. The results of MD analysis have demonstrated a more stable docking on BCL-XL than other studied factors, supported by the in vitro results [48].

The computational studies of natural compounds have gained momentum for the drug discovery against COVID-19 during the pandemic since a treatment is greatly needed. To meet this urgent need, thymoquinone, along with the other phytochemicals, has been investigated in MD simulation studies to treat the SARS-CoV-2 virus. A molecular docking conducted by Srivastava *et al.* (2021) tested thymoquinone, cinnamic acid, and andrographolide with ACE2 receptor, allowing SARS-CoV-2 to enter human cells. Molecular docking was performed using the Autodock tool to predict the binding scores, confirmation, and affinity. After protein-ligand docking, MD simulation was performed using Desmond v12 to investigate the stability and conformational changes on the ligand-binding site. The binding energy and RMSD analysis have proven that thymoquinone has a strong binding affinity, better stability, and structural conformation on the binding site of ACE2 receptor, indicating the prevention of viruses entering human cells by binding ACE2 [49]. Similarly, thymoquinone-ACE2 binding was investigated via other computational molecular docking studies along with in vitro experiments [50]. Moreover, the docking of thymoquinone with Mpro, the main protease of SARS-CoV-2, has been studied by Khan *et al.* (2022), the most recent computational study on thymoquinone. The docking complex was simulated by MD using the Amber force field. RMSD and RMSF analyses were conducted for stability and flexibility of the binding site, while Rg was measured for protein folding effect. Strong binding activity of thymoquinone on Mpro has been demonstrated [51].

Alam *et al.* (2021) performed a docking study on thymoquinone for its apoptotic potential on Bax and Bcl2, which are the targets for non-small lung cancer. After molecular docking and MD simulations, RMSD, RMSF, Rg, and free energy landscape analysis were performed. Thymoquinone with Bax and Bcl2 complexes have shown a strong conformational fitting, and they were stable throughout the MD runs [52]. Zhou *et al.* (2021) also followed molecular docking and MD simulations with a free energy landscape and an additional principal component analysis on thymoquinone and breast cancer cell mutations using GROMOS96 v43a1 force field on GROMACS v5.1.3. Thymoquinone inhibited PI3K/Akt1 pathway in tumor cells by binding to the PIK3CA kinase domain [53]. Taghvaei *et al.* (2022) predicted the SENP2 inhibitory effect of

natural products, including thymoquinone, with molecular docking via Autodock, MD simulation, binding free energy, and trajectory analysis via GROMACS 4.6.5 GROMOS53a6 force field consecutively. Thymoquinone has been found to have moderate stability of binding to SENP2 compared to the other natural compounds [54].

The interaction between aminothymoquinone and the crystal structures of human serum albumin (HSA) (1BM0, 2BXD, and 2BXF) has been investigated by Bhosale *et al.* (2021) through molecular docking using the Autodock software package. Aminothymoquinone has been shown to bind to HSA by forming hydrogen bonds in the docking cavity. The study also underlined the potential of aminothymoquinone for the future of aminothymoquinone-based drug design [32]. Additionally, Yusufi *et al.* (2013) have studied the compounds ATQTHB and ATQTFB, which are synthesized from aminothymoquinone, and revealed their anticancer activity against pancreatic cancer cells by molecular docking analysis [55].

It is important to note that all studies explained in this section include atomistic simulations of thymoquinone-protein interactions. There is no study on the MD simulation of thymoquinone with other types of biological compounds and environments, both in atomistic and CG scales. Likewise, there is no MD simulation of aminothymoquinone found. As described, the interactions of thymoquinone and aminothymoquinone with cell membranes is an open research topic in both atomistic and coarse-grained MD simulations.

2.4. Studies on the Interaction between Drug Molecules with Lipid Bilayers

The ability of a drug to diffuse through the cell membrane is one of the key factors in the bioavailability of the drug molecule. The diffusion mechanism of the drug molecule can be observed more thoroughly at the molecular level by analyzing the interaction between lipid bilayers and pharmaceutical compounds [56]. MD simulations provide a better understanding of the diffusion and orientation of small drug molecules

in cell membranes on the atomic-level resolution [57].

The interactions between model lipid bilayers and small bioactive molecules are widely studied in the literature. For example, Ingolfsson *et al.* (2014) investigated the biological activity of five phenolic phytochemicals on the cell membrane and membrane proteins. The tested phenols were capsaicin, curcumin, EGCG, genistein, and resveratrol from chili peppers, turmeric, green tea, soybeans, and grapes, respectively. POPC (1-palmitoyl-2-oleoyl-sn-glycero-3-phosphocholine) bilayer was used in these CG simulations using the MARTINI force field. The phytochemicals were localized in the solution near the bilayer with a molar ratio of 1 phytochemical to 10 POPC lipids. The placement of phytochemicals in the lipid bilayer was observed along with the bilayer properties such as area per lipid, bilayer thickness, lipid order, and bilayer compressibility. All tested phytochemicals have altered the bilayer properties due to cell membrane perturbations [58].

Saha *et al.* (2020) have performed atomistic MD simulations of flavonols, which are fisetin, apigenin, and morin, to observe their antioxidant and lipid-peroxidation inhibition effect at the molecular resolution. POPC bilayers with 0% mol and 40% mol cholesterol were computed with and without flavonols using the OPLS-AA force field in Desmond 2016 MD package. The location and orientation of flavonols in the lipid bilayers, area per lipid, bilayer thickness, hydrogen bond, and free energy profiles were analyzed to observe the interaction between flavonols and bilayer models. The results have shown that morin has the highest affinity, depending on the model membrane's cholesterol content. An increase in cholesterol concentration reduces membrane permeability of the flavanols by increasing the bilayer thickness and decreasing the area per lipid correspondingly [59].

Eid *et al.* (2021) have constructed an atomistic MD simulation to analyze the effect of another flavonoid, quercetin, on membrane rigidity at the molecular level. The topology of quercetin was built on the LigParGen server based on the OPLS-AA force field. The 138-lipid bilayer model included three types of lipids, which were 80

POPC, 10 POPE (1-palmitoyl-2-oleoyl-sn-glycero-3-phosphatidylethanolamine), and 48 cholesterol molecules. The trajectory analysis consisted of membrane thickness, area per lipid, deuterium order parameters, and diffusion coefficient, along with the density distribution and RDF showing the softening effect of quercetin on the model membrane [57].

There is no study in the literature on the thymoquinone/aminothymoquinone interactions with lipid bilayers both at atomistic and CG scales. Thus, in this study, atomistic (OPLS-AA) and coarse-grained (MARTINI) force fields are used to simulate the interactions between thymoquinone/aminothymoquinone and lipid bilayers. CG models of thymoquinone and aminothymoquinone are constructed using MARTINI force field. In addition to AA simulations, CG simulations are studied as an alternative, low-cost and fast simulations for large systems. The density distributions, lateral diffusion coefficients, area per lipid, bilayer thickness, and order parameters are investigated for bilayers alone and ligand-bilayer complexes.

3. MATERIALS AND METHODS

3.1. Theory of Molecular Dynamics Simulations

The computer simulation methods are developed to simulate the dynamic responses of a system and are used in many areas. Monte Carlo and Molecular Dynamics (MD) Simulations are the two widely used computational approaches that apply to macromolecular systems and molecular biology. The Monte Carlo method constructs an ensemble of configurations and conformations with lower total energy and highest probability by applying random perturbations to the corresponding macromolecular system. However, Monte Carlo simulations do not provide information on the changes in a system with time. On the other hand, MD simulations compute the position and momentum of the system in a given time interval. The time evolution of the system is called a trajectory and it is used for time-dependent analysis. The interactions between various molecules and biomolecular systems can be observed using MD simulations [60].

MD simulation algorithms need specific thermodynamic conditions to compute the time evolution of a system. These conditions are called thermodynamic ensembles that represent the large systems on the microscopic scale subjected to certain constant constraints, such as the number of particles (N), temperature (T), volume (V), pressure (P), and total energy (E) of the system. The general thermodynamic ensembles used in MD simulations are listed below [61].

- Canonical (NVT) ensemble: An ensemble of a system with a constant number of particles, volume, and temperature.
- Isothermal-isobaric (NPT) ensemble: An ensemble of a system with a constant number of particles, pressure, and temperature.
- Microcanonical (NVE) ensemble: The system is isolated. Thus, it has constant total energy, number of particles, and volume [61].

The two thermodynamic properties, temperature, and pressure are kept constant via temperature and pressure coupling. Temperature coupling with Berendsen [62], Nose-Hoover [63, 64], and V-rescale [65] thermostats, and pressure coupling with Berendsen [62] and Parrinello-Rahman [66] are used for MD simulations in this study and are implemented in the GROMACS software package [67]. In general, one should decide on the types of thermostats and barostats to use in MD simulations based on the studied system.

3.1.1. The Basics of Molecular Dynamics Simulations Algorithm

MD simulations predict the movement of every atom in a particular system over time by solving the classical equations of motion [68]. The dynamic evolution of a system can be observed from the trajectory of the system for a fixed time period. The input of the MD simulation is the initial positions of atoms in the system box. The algorithm calculates the forces exerted on each atom by the other atoms [69].

Newtonian mechanics is used to find the accelerations, and velocities are calculated together with the positions of the atoms at the next time point [69]. Newton's law of motion is described as

$$a_i = \frac{F_i}{m_i} = \frac{dv_i}{dt} = \frac{d^2 r_i}{dt^2}, \tag{3.1}$$

where F is applied force on particle i, t is time, a is the acceleration, v is the velocity, r is the position, and m is the mass of the ith particle [70].

The positions and velocities of each atom are predicted by integrating the corresponding equations of motion. The integration algorithm solves Newton's equation of motion numerically. The integration algorithms used in MD simulations are the leap-frog stochastic dynamics integrator [71], and Velocity-Verlet integrator [72], being the most used algorithm in MD simulations.

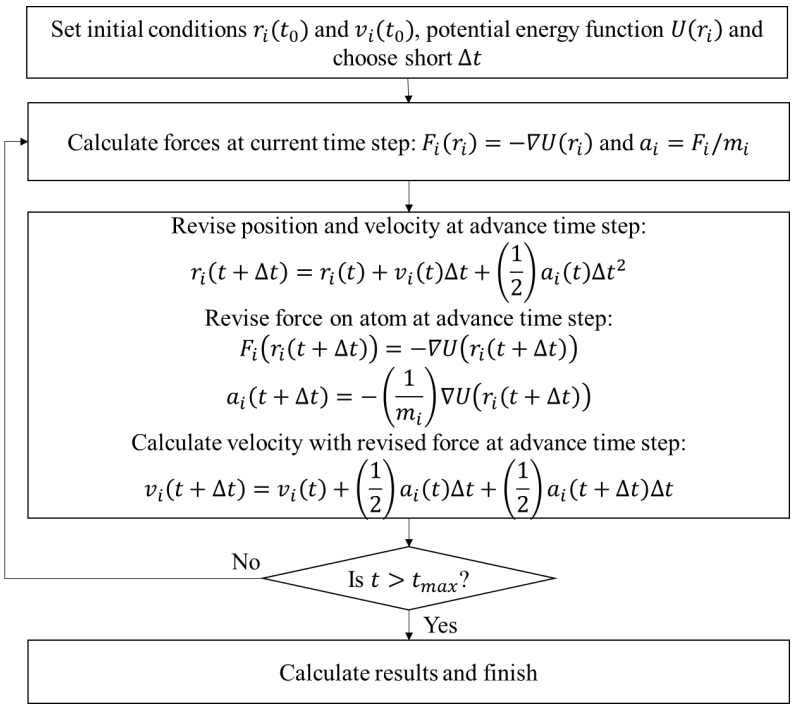

Figure 3.1. The basic algorithm of MD simulations [73].

The prediction of the position at the next time step of a particle is approximated by a Taylor series expansion. The position of the ith particle r_i is expanded at $t + \Delta t$ and the derivative of r_i is taken to form the velocity expression as

$$r_i(t + \Delta t) = r_i(t) + v_i(t)\Delta t + \left(\frac{1}{2}\right) a_i(t)\Delta t^2, \tag{3.2}$$

$$v_i(t + \Delta t) = v_i(t) + \left(\frac{1}{2}\right) a_i(t)\Delta t^2 + O(t^3) + \left(\frac{1}{2}\right) a_i(t + \Delta t)\Delta t^2, \tag{3.3}$$

in which Equation (3.3) represents the basic form of the Velocity-Verlet algorithm. The algorithm continues by calculating Equation (3.2) and deriving the acceleration term from potential energy using $r_i(t + \Delta t)$ as

$$a_i(t + \Delta t) = -\left(\frac{1}{m_i}\right) \nabla U(r_i(t)), \tag{3.4}$$

where U is the potential energy function. After calculating $a_i(t + \Delta t)$, Equation (3.3) is computed, and the integration continues [72].

3.1.2. Force Field

The force field is a mathematical function with parameters for the potential energy of the particles in molecular modeling. The parameters of force field functions are obtained from the experiments and the high-level quantum mechanical calculations [74].

The acceleration of a particle is the negative derivative of the potential energy function with respect to the position of the particle divided by its mass, as shown in Equation (3.4). Thus the total force exerted on the corresponding atom can be represented as the gradient of the potential energy as

$$F_i = \sum_{j \neq i} f_{ij}, \tag{3.5}$$

$$f_{ij} = -\nabla U_{ij}, \tag{3.6}$$

where f is the force between the corresponding atom and the other atoms, and U is the potential energy function [73]. The potential energy includes both bonded and non-bonded interactions between each atoms as

$$\begin{aligned} U(R) = &\sum_{bonds} k_r(r - r_{eq})^2 + \sum_{angles} k_\theta(\theta - \theta_{eq})^2 + \sum_{dihedrals} k_\varphi(1 + \cos[n\varphi - \gamma]) \\ &+ \sum_{impropers} k_\omega(\omega - \omega_{eq})^2 + \sum_{i<j}^{atoms} \epsilon_{ij} \left[\left(\frac{r_m}{r_{ij}} \right)^{12} - 2 \left(\frac{r_m}{r_{ij}} \right)^{6} \right] + \sum_{i<j}^{atoms} \frac{q_i q_j}{4\pi\epsilon_0 r_{ij}}, \end{aligned} \tag{3.7}$$

where k_r, k_θ, k_φ and k_ω are the force constants; r is the bond length; θ is the angle; φ is the dihedral angle; r_{ij} is the distance between atom i and j; r_{eq}, θ_{eq} and ω_{eq} are the equilibrium positions; γ is phase shift; n is multiplicity; ϵ_{ij} is Lennard-Jones well depth; r_m is the distance of minimum potential, ϵ_0 is the dielectric constant; q_i and q_j are the charges of atom i and j [75].

This equation is the definition of the classical force field used for MD simulations. The summed terms correspond to the energies of bonds, angles, dihedrals, and improper

dihedrals, which represent bonded interactions; and van der Waals and electrostatic energy, which represent non-bonded interactions [75].

Every force field, designed for different systems, assigns different force constants for their purposes. For instance, the AMBER force field is mainly used for protein and DNA systems [16]. The CHARMM force field is designed for small molecule and macromolecule simulations [17]. GROMOS force field is adapted for aqueous solutions of proteins, nucleotides, and sugars [18]. OPLS-AA is a general force field for organic molecules and peptides [19].

The applicability of atomistic MD simulations is limited to the size of the simulation systems. Large-scale applications require a faster but reliable approach. Coarse-grained MD simulation is a convenient way of simulating large-scale systems as long as it reproduces the properties of smaller-scale atomistic models. CG models can be used for larger systems with less computational costs and short time intervals [76].

The coarse-graining procedure lowers the resolution of the model [15]. Two, or more atoms are grouped and represented as a bead, which is defined as the smallest unit of CG models [21, 77]. Each molecule consists of one or more beads and the properties of the beads are obtained from the reference atomistic simulations or experiments [15]. CG force fields have different parameters from atomistic force field paremeters. For CG MD simulations, MARTINI is one of the most used force fields [21]. Although many fundamental molecules are defined in the MARTINI force field, the parametrization of many others is an ongoing process [77].

The MARTINI force field has been developed by the research groups of Marrink and Tieleman to provide computationally feasible simulation models. The application of the force field has been improved by including lipids, peptides, proteins, and small molecules in polar and nonpolar versions. MARTINI models are developed by two, three, or four-to-one mapping, which are determined in a way that increases the computational efficiency without the loss of molecular information [78].

3.2. Atomistic Simulations

3.2.1. Initial Configurations

The initial structures of thymoquinone, aminothymoquinone, DOPC (1,2-Dioleoyl-sn-Glycero-3-Phosphocholine), POPC, and 1-octanol were constructed via the LigParGen server for the OPLS-AA force field [79]. The visualization of the molecules and all systems were captured via the Visual Molecular Dynamics (VMD) v1.9.4a53 program [80]. Of the studied molecules, the molecular representations on the atomic scale are given in Figure 3.2.

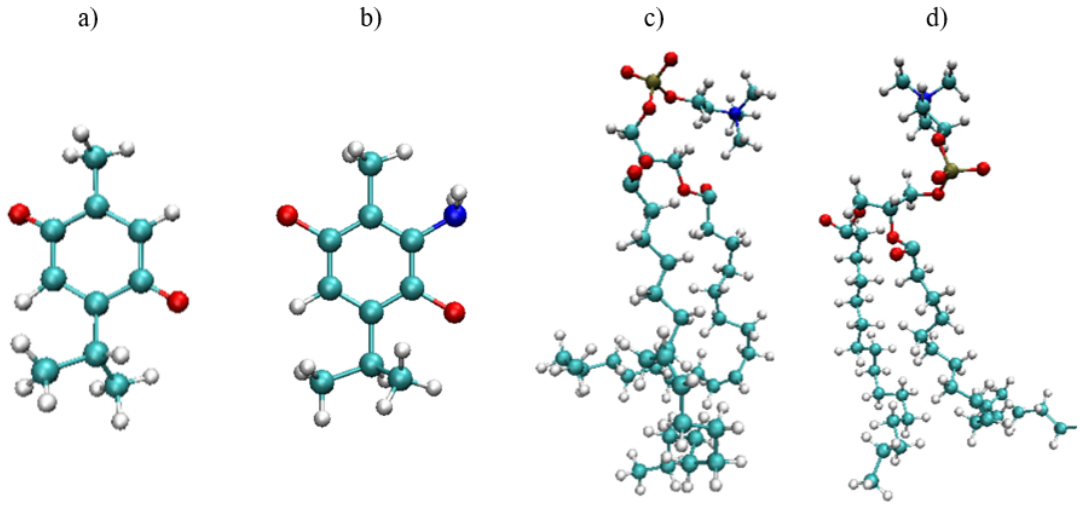

Figure 3.2. Molecular representations of a) thymoquinone, b) aminothymoquinone, c) DOPC, and d) POPC.

The simulation boxes for free energy calculations were constructed using GROMACS version 2021.3 [67]. Thymoquinone or aminothymoquinone was solvated in water or 1-octanol separately within a simulation box of dimensions of 5 nm x 5 nm x 5 nm. Solvated systems ran for 100 ns to reach the equilibrium before the simulations of free energy calculations were started, and their output trajectories were used in free energy simulations.

The systems with lipid bilayers consisted of 64 lipids in each leaflet and the total number of lipids was 128 for both DOPC and POPC bilayer-only systems. The number of TIP3P water molecules was determined by the hydration number of 60 water molecules per lipid, which was equal to 7680 water molecules in total. 0.15 M of NaCl salt was added to mimic the biological environments [81]. DOPC-only and POPC-only bilayer systems were constructed using VMD, and the systems were equilibrated for further simulations with thymoquinone. Thymoquinone molecules were added at two different concentrations (i.e., 1 and 10 thymoquinone molecules) to the equilibrated output trajectories of DOPC-only and POPC-only bilayer systems. The addition of thymoquinone was performed using VMD. 1 thymoquinone was placed in between the two leaflets of the bilayers, while 10 thymoquinone were added to the solvent phase at random distribution. The reason of the random distribution is to mimic the biological environment as the molecules diffuse in random ordering. The initial configurations can be seen in Figure 3.3.

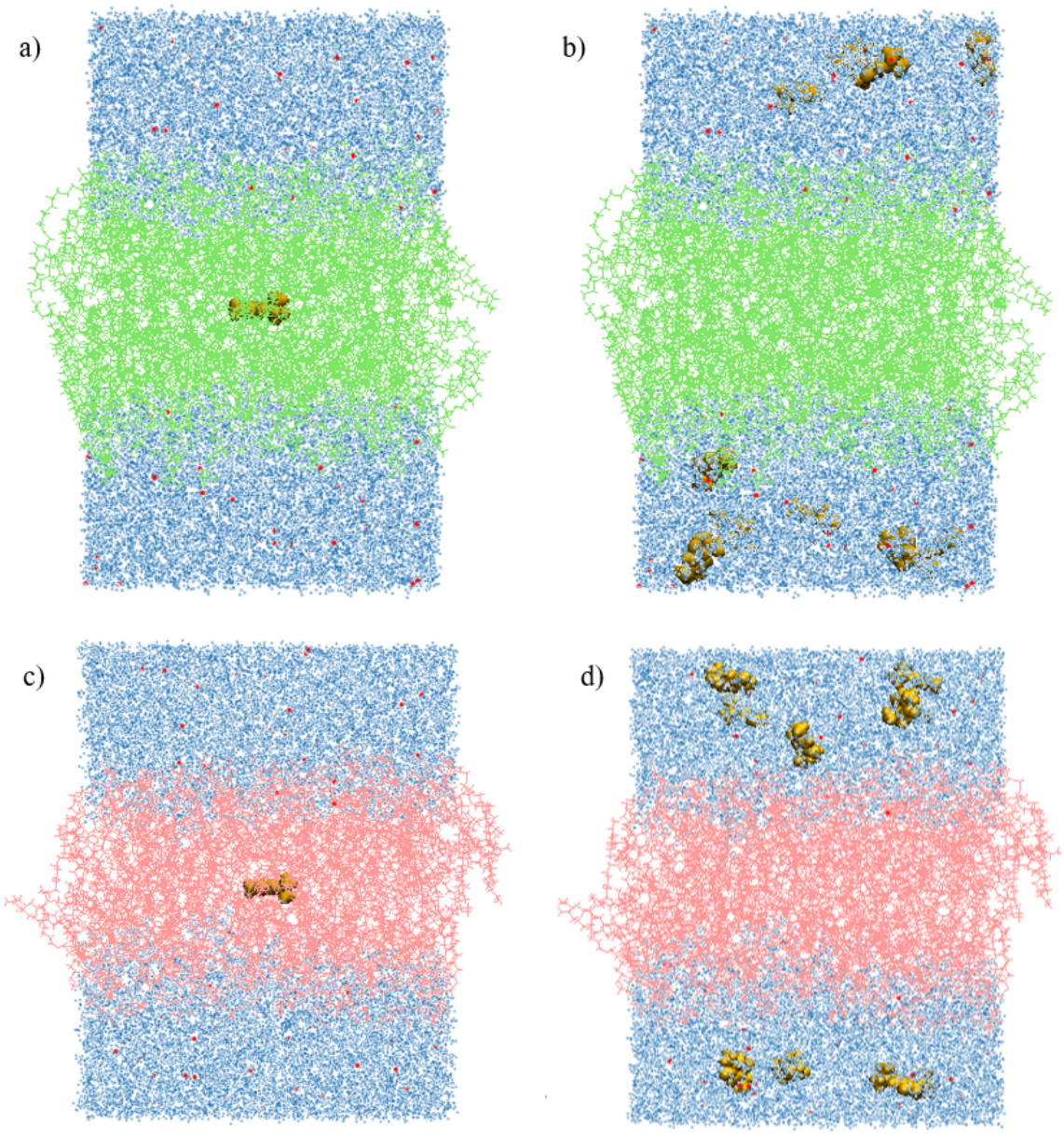

Figure 3.3. The initial configurations for DOPC bilayers with a) 1, b) 10 thymoquinone molecules, and POPC bilayers with c) 1, d) 10 thymoquinone molecules.

3.2.2. Simulation Parameters

The atomistic simulations were carried out by the OPLS-AA force field with GROMACS 2021.3 [19]. The parameters for lipids were from the study of the revised OPLS-AA version of lipids [81]. All atomistic simulations, including the free energy

calculations of thymoquinone, and bilayer systems with and without thymoquinone were energy minimized with the steepest descent algorithm. All systems were run only once, indicating that there is no replica used for the simulations.

The free energy simulations were performed for 21 different systems, from λ=0 to λ=1, where the non-bonded interactions were on and off respectively. Both Coulombic and van der Waals interactions were coupled sequentially. The λ values were equally spaced and identical in each simulation. For free energy calculations, 1 ns of NVT and 1 ns of NPT equilibrations were performed before the production run [82]. The temperature was set to 310 K for both NVT and NPT runs, and pressure was controlled by Parrinello-Rahman barostat [66] at 1 atm with a time constant of 4.0 for the NPT run. The long-range dispersion correction was applied for energy and pressure. The stochastic dynamics integrator was used with a time step of 0.002. The long-range electrostatic interactions were calculated by the particle mesh Ewald (PME) method [83,84] with a grid spacing of 0.12 and PME order of 6. Non-bonded interaction cutoff values were set to 1 nm. Linear interpolation of Coulomb interactions is included for free energy simulations with soft-core power of 1 and soft-core alpha parameter of 0.5. After equilibration, an MD production run was performed with an NPT ensemble for 40 ns using the same parameters of NPT equilibration. The trajectory outputs were used for free energy calculations as explained later under the analysis title.

For bilayer systems, the steepest descent minimizations were followed by 1 ns or 5 ns of NPT equilibration without or with thymoquinone, respectively. The pressure was kept constant with semi-isotropic Parrinello-Rahman barostat [66] at 1 atm with a time constant of 4.0 and a compressibility factor of 4.5×10^{-5} bar^{-1}, and the temperature was controlled by Nose-Hoover thermostat [63, 64] at 310 K with a time constant of 1. The long-range electrostatic and van der Waals interactions were handled with the force-switch cut-off using the same parameters of the free energy NPT simulations. The LINCS algorithm was used to constrain the hydrogen bonds [85,86]. These parameters were also used in the MD production runs which were performed in the NPT ensemble. The time step of MD production runs was 0.002 ns for all systems. The duration

of production runs was 250 ns, 400 ns, and 500 ns for bilayer-only, bilayer with 1 thymoquinone molecule, and bilayer with 10 thymoquinone molecules, respectively. The last 100 ns of the production trajectories were used for analysis, where all systems were in equilibrium. The equilibrium states were decided based on the energy profiles, given in Appendix B.

3.3. Coarse-Grained Simulations

3.3.1. Parametrization of CG Models

Atom-to-bead mapping was done by grouping 3 or 4 non-hydrogen atoms into 1 bead. By performing the mapping on the structure files of the atomistic simulations, the coarse-grained structure and index files were obtained. Center of geometry (COG) mapping is used to prevent the loss of resolution during mapping in the MARTINI v3.0.0 force field [77]. COG mapping requires the inclusion of hydrogen atoms in the mapping while transferring the atomistic properties to the CG resolution. After mapping, the initial parameter file was generated by defining the appropriate bead types of MARTINI 3.0.0 [77, 87]. The bead types and the representations used for thymoquinone and aminothymoquinone are explained in Section 4.2.

The beads, angles, and dihedrals were defined in the initial parameter file by making initial guesses for the force constants and angle values. The force constants are altered via trial and error, by comparing AA (all-atom) and CG distributions of bonds, angles, and dihedral distributions. The fitted distributions and the parameters of thymoquinone and aminothymoquinone are given in Section 4.2.

3.3.2. Initial Configurations

Except for thymoquinone and aminothymoquinone, the initial configurations and parameters of molecules were obtained for MARTINI 3.0.0 force field. The lipid, MARTINI water, and ion parameters were taken from the general MARTINI 3 force field [77]

while the parameters for 1-octanol were obtained from the small molecule implementation of MARTINI 3.0.0 [87].

For the free energy calculations, thymoquinone and aminothymoquinone were solvated in MARTINI water [21] or 1-octanol, and simulations were performed with GROMACS 2021.3. The box dimensions were identical to those used in the atomistic free energy calculations. The systems were equilibrated for 500 ns and the output structure files were used in free energy simulations.

The numbers of lipids and water molecules in coarse-grained DOPC and POPC bilayer systems were equal to the atomistic systems to compare both force fields. 1920 MARTINI waters were solvated to reach the hydration number used in the atomistic simulations since one MARTINI water represents four water molecules. 0.15 M NaCl salt was added to the bilayer-solvent complexes. The bilayer-only systems were constructed using CHARMM-GUI Input Generator [88]. After the equilibration of the bilayer-only systems, 1 or 10 molecules of thymoquinone were added to DOPC and POPC systems. Similarly, 10 molecules of aminothymoquinone were added to DOPC or POPC bilayers to compare the effects of thymoquinone and aminothymoquinone. The insertion of molecules into the bilayer systems was carried out via VMD [80]. The initial configurations of CG simulations are given in Figure 3.4.

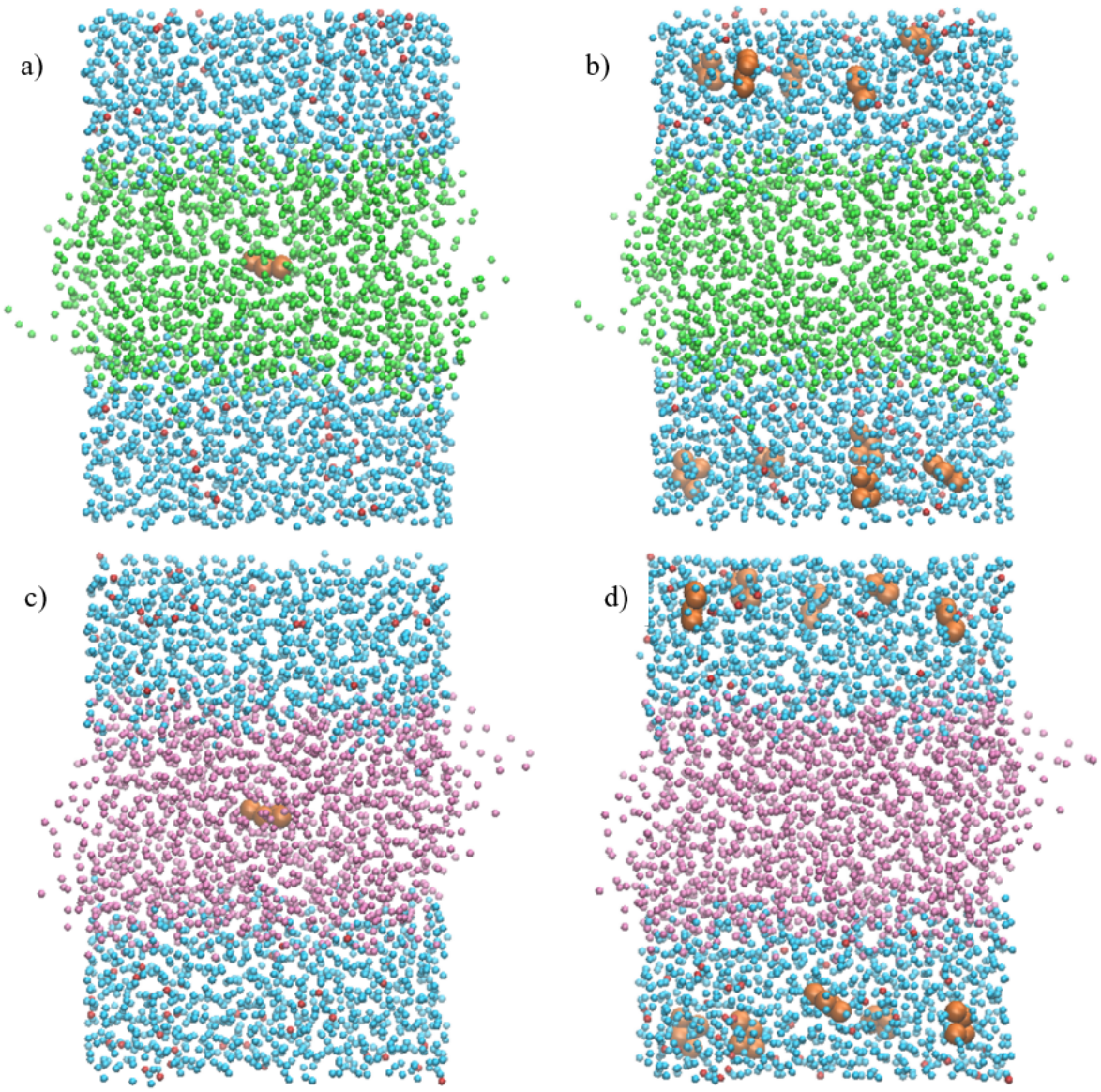

Figure 3.4. The initial configurations for DOPC bilayers with a) 1, b) 10 thymoquinone molecules, and POPC bilayers with c) 1, d) 10 thymoquinone molecules.

The model bilayers representing normal and cancer cell membranes were constructed to observe the effect of high concentrations of thymoquinone/aminothymoquinone on asymmetric and more complex bilayers using the CHARMM-GUI Input Generator [88]. The types and composition of the lipids were based on the studies of Radhakrishnan et al. (2022) and Shahane et al (2019) [89, 90]. Each leaflet of normal and cancer bilayer models had 500 lipids, which makes 1000 lipids in total. The com-

positions of the model bilayers, which are Model 1 and Model 2, are shown in Tables 3.1 and 3.2, respectively.

Table 3.1. The composition of complex bilayer Model 1.

	Normal Cell Bilayer			**Cancer Cell Bilayer**		
Lipids	**Outer**	**Inner**	**Total**	**Outer**	**Inner**	**Total**
Cholesterol	170	170	340	85	85	170
DOPC	330	110	440	277	277	554
DOPS	0	220	220	138	138	276

Table 3.2. The composition of complex bilayer Model 2.

	Normal Cell Bilayer			**Cancer Cell Bilayer**		
Lipids	**Outer**	**Inner**	**Total**	**Outer**	**Inner**	**Total**
Cholesterol	170	170	340	85	85	170
DOPC	330	110	440	277	277	554
DOPS	0	220	220	138	138	276

The number of MARTINI waters added to the system was 17500 corresponding to a hydration number of 70. 0.15 M of NaCl was added to the system with additional Na^+ ions to neutralize the systems. The normal and cancer model bilayers were run for 10 μs to equilibrate the system, then 100 thymoquinone or aminothymoquinone were added to both bilayer systems separately. The introduction of the molecules to bilayer systems was performed by VMD, and the molecules were placed at least 1 nm away from the bilayers in random distribution. The initial configurations of Model 1 are given in Figure 3.5 as an example.

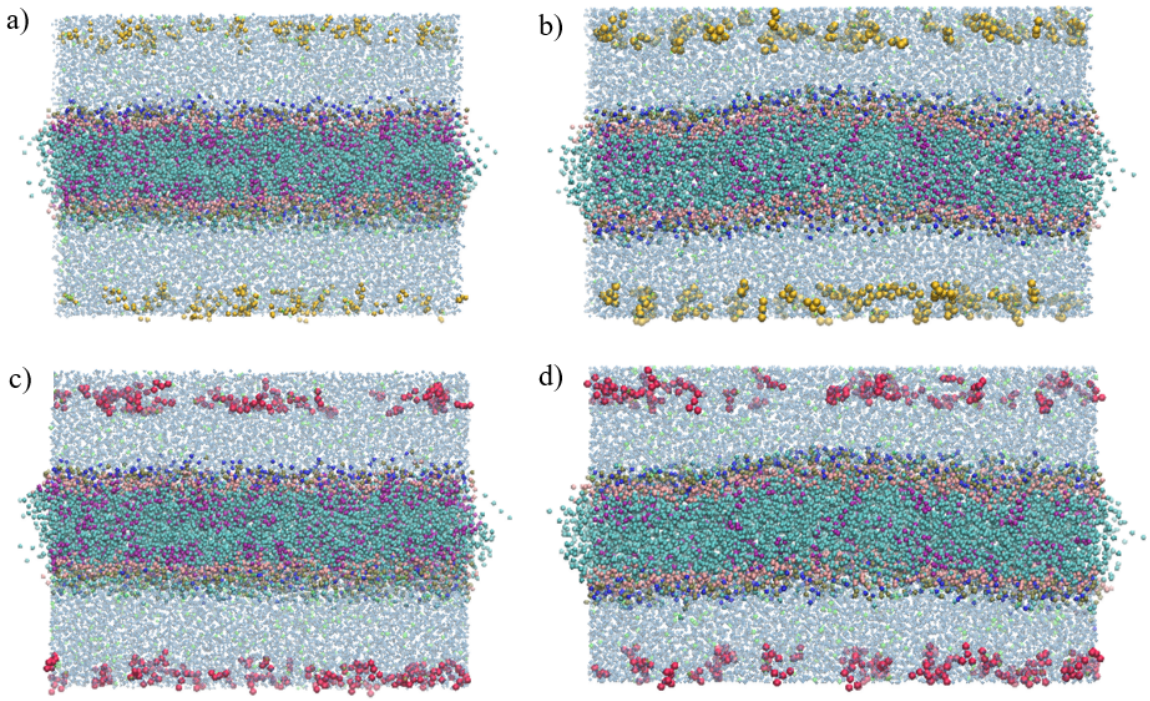

Figure 3.5. The initial configurations for thymoquinone in a) normal, b) cancer, and aminothymoquinone in c) normal, d) cancer membrane models of Model 1.

3.3.3. Coarse-Grained Simulation Parameters

The coarse-grained simulations were performed via GROMACS 2021.3 using the MARTINI 3.0.0 force field [77, 87]. The coarse-grained simulations include free energy simulations of thymoquinone and aminothymoquinone in water or 1-octanol; simple or complex bilayer models with no thymoquinone or aminothymoquinone; and simple or complex bilayer simulations with thymoquinone or aminothymoquinone at different concentrations.

The free energies of transfer of thymoquinone and aminothymoquinone were computed for 11 different lambda states, from full to zero interactions corresponding to λ=0 and λ=1, respectively. Only van der Waals interactions were coupled since both thymoquinone and aminothymoquinone have no charges in their CG bead definitions. After energy minimization by the steepest descent algorithm, NVT and NPT equilibration runs were performed for 1 ns. The production run was performed for 50 ns

using the NPT ensemble. The temperature was set to 310 K with a time constant of 1 by velocity-rescale thermostat [65] for both NVT and NPT runs, while pressure is kept at 1 atm using Parrinello-Rahman barostat [66] with a time constant of 12 and compressibility factor of 4.5×10^{-5} bar^{-1} for NPT runs. The long-range interactions for different lambda states included only van der Waals interactions, with a cut-off distance of 1.1 nm. The stochastic dynamics integrator was used with a time step of 0.02 ns. The output files were used in the free energy calculations.

For the bilayer systems, minimizations by the steepest descent algorithm were followed by 1 ns or 10 ns of NPT equilibrations for simple bilayers with no thymoquinone/aminothymoquinone or all the other systems, respectively. MD productions were performed for 1 μs, 5 μs, and 10 μs for simple bilayers with no thymoquinone or aminothymoquinone, one thymoquinone in simple bilayer systems, and all other systems, respectively. The equilibration and production runs were performed with a semi-isotropic Berendsen barostat at 1 atm with a time constant of 5 and compressibility factor of 4.5×10^{-5} bar^{-1}, and a V-rescale thermostat [65] at 310 K with a time constant of 1. The Lennard-Jones interactions were shifted between 0 and 1.1 nm with the Potential-Shift-Verlet modifier while the Coulomb potential was modeled using the Reaction Field [91] with a dielectric constant of 15. The last 500 ns of the MD production runs were used for the analysis of the systems.

3.4. Simulation Analysis

3.4.1. Free Energy Calculations

Free energy change of a molecule from one state to another is crucial to understand the non-bonded interactions of the molecule during the parametrization of MD simulations [92]. Thus, free energy calculations are performed for thymoquinone and aminothymoquinone both at atomistic and CG scales.

Free energy calculations correspond to Gibbs free energy changes ΔG_{AB} of a system, from one state (A) to another (B). This change was controlled by the coupling parameter, λ. The simulations for free energy calculations were conducted with equally-spaced λ values from λ=0 to λ=1, representing the systems with interactions being on and off, respectively [93]. The thermodynamic cycle of free energy calculations is given in Figure 3.6.

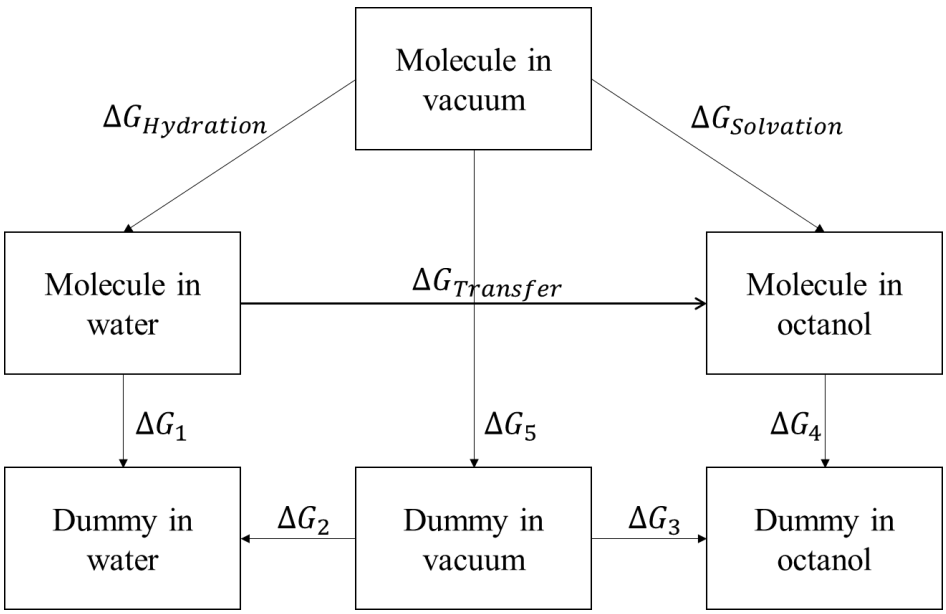

Figure 3.6. The thermodynamic cycle of free energy calculations.

Free energies of transfer of thymoquinone and aminothymoquinone were computed by subtracting the free energy of solvation of compounds in 1-octanol from the free energy of solvation of compounds in water as

$$\Delta G_{Hydration} = \Delta G_5 + \Delta G_2 - \Delta G_1. \tag{3.8}$$

$$\Delta G_{Solvation} = \Delta G_5 + \Delta G_3 - \Delta G_4, \tag{3.9}$$

$$\Delta G_{Transfer} = \Delta G_{Solvation} - \Delta G_{Hydration}, \tag{3.10}$$

where the terms ΔG_2 and ΔG_3 are equal to zero since the dummy molecule does not interact with the system. Additionally, the internal non-bonded interactions, ΔG_5,

were also set to zero due to the small sizes of thymoquinone and aminothymoquinone. The equations were simplified, and free energy of transfer was found as

$$\Delta G_{Transfer} = \Delta G_1 - \Delta G_2 + \Delta G_3 - \Delta G_4 = \Delta G_1 - \Delta G_4, \tag{3.11}$$

$$\Delta G_{Transfer} = \Delta G_{inwater} - \Delta G_{inoctanol}. \tag{3.12}$$

The partition coefficients, i.e., logP values, were calculated as

$$\log P = \frac{-\Delta G_{Transfer}}{RT \ln 10}, \tag{3.13}$$

where R is the gas constant and T is the temperature of the system [94].

Free energies of solvation were calculated by the thermodynamic integration (TI) method using Bennett's Acceptance Ratio (BAR) which estimates the free energy differences [95]. *gmx bar* command was used to obtain the free energy differences of the systems via GROMACS 2021.3.

3.4.2. Analysis of Simulation Trajectories

Simulation trajectories were analyzed along with the virtual observation of the systems to observe the effect of thymoquinone and aminothymoquinone on bilayer properties. Trajectory analysis included area per lipid, bilayer thickness, mean square displacement (MSD), order parameters, the orientation of molecules in bilayers, and density distributions, which are consecutively explained below.

Area per lipid was calculated by the cross-sectional area of the simulation box divided by half of the total number of lipids as

$$A_L = \frac{A_{XY}}{N_L/2}, \tag{3.14}$$

where A_L is area per lipid in nm^2, N_L is the number of lipids in the bilayer, and A_{XY} is the cross-sectional area of the box, which was calculated by the multiplication of box dimensions on the x and y axis [90].

Bilayer thickness, d_{HH} was found by calculating the distance between phosphate head groups of lipids using *gmx distance* command on GROMACS 2021.3. The indexes of phosphate groups of the lipids were used to compute the head-to-head distance for each frame of the time interval [90].

Mean square displacement (MSD), the change in the position of a particle or molecule with respect to a reference position [96], was computed to obtain the self-diffusion coefficients of the lipids in this study. The diffusion coefficients were found using the least square fitting on a linear line ($Dt + c$) on the MSD graphs, where D is the diffusion coefficient and t is time. This link between the diffusion coefficient and MSD with respect to time comes from the Einstein relation shown as

$$D = \lim_{t\to\infty} \frac{\partial}{\partial t} \frac{\langle |r(t) - r(0)|^2 \rangle}{6}, \tag{3.15}$$

where $r(t)$ and $r(0)$ is the positions of the particles at times $t = t$ and $t = 0$, respectively, and D is the self-diffusion coefficient of the corresponding particles [97].

The order parameters of the lipids are the time-averaged alignments of the lipids. Order parameters were found by

$$S = \frac{3}{2}\langle \cos^2 \theta \rangle - \frac{1}{2}, \tag{3.16}$$

where S is the order parameter of the lipid and θ is the angle between the corresponding tail and the bilayer normal on the z-axis [98]. $S = 1$, 0.5 and 0 indicate perfect alignment with the bilayer surface, an anti-alignment, and random orientation, respectively [99]. The order parameters of the lipids were computed for both atomistic and CG simulations using *gmx order* command on GROMACS and the order parameter calculator developed by Martini 3 developers [77], respectively.

Time-averaged density profiles of molecules are important to detect the relative locations along with their distributions in the simulation box [100]. The density distributions were obtained by *gmx density* command implemented in GROMACS, with an option for centering the bilayers.

The tilt angle distribution of thymoquinone and aminothymoquinone provides the orientation of molecules inside or at the surface of the bilayer. The tilt angles were calculated from the angle between the vector of two atoms or beads in the molecule and the bilayer normal on the z-axis using *gmx gangle* command in GROMACS.

The radial distribution function (RDF) gives the information about the density of particles as a function of distance from a reference particle [101]. In GROMACS, the distance between all center of mass of the reference and selected molecules were calculated and plotted using *gmx rdf* command.

4. RESULTS AND DISCUSSION

4.1. Production of Atomistic Models

The atomistic models of thymoquinone (TQ) and aminothymoquinone (ATQ) were tested to determine their accuracy compared with the experimental findings. Partitioning free energies of thymoquinone and aminothymoquinone were calculated both in water and 1-octanol on the atomistic scale. The free energy change of thymoquinone was calculated by summing the free energy changes of each *lambda* neighboring value, which are shown in Appendix A.1.

The solvation and hydration free energies of thymoquinone in 1-octanol and water are 40.63 kJ/mol and 24.49 kJ/mol, respectively. $\Delta G_{Transfer}$ was found using Equation (3.12) by subtracting the free energy in water from that in 1-octanol, calculated as

$$\Delta G_{Transfer} = 24.49\frac{kJ}{mol} - 40.63\frac{kJ}{mol} = -16.14\frac{kJ}{mol}.$$

The logarithm of the partition coefficient, $logP$, of thymoquinone was calculated using Equation (3.13). The gas constant is 8.314 J/molK [102] used in the calculation as

$$logP = \frac{-(-16.14\frac{kJ}{mol}) \times (\frac{10^3 J}{kJ})}{(8.314\frac{J}{molK}) \times (310K) \times (ln10)} = 2.72.$$

Different experimental and computational values for $logP$ of thymoquinone are reported in the literature. Johnson-Ajinwo *et al.* (2018), Anilkumar *et al.* (2020), Wayan Agung *et al.* (2016), Haq *et al.* (2018), Dwisari *et al.* (2019), and Alkharfy *et al.* (2015) have reported $logP$ values of 1.04 [103], 1.5 - 2.7 [104], 2.0 [105], 2.54 [106], 2.8 [107] and 2.2 [108], respectively. More results have been reported based on in vitro studies and computational calculations. Zuhroh *et al.* (2020) have reported values of 2.21, and 2.80 based on HPLC analysis, and Hyperchem predictions, respectively [109,110]. Similarly, Ulfa *et al.* (2021) performed HPLC analysis and used ALOGPS 2.1 prediction

program and reported $logP$ values of 2.17 and 2.80, respectively [111, 112]. Overall, reported $logP$ values of thymoquinone are in a range between 1.04 – 2.80, with the majority of values being between 2.2 and 2.8.

The free energy calculations for thymoquinone are tested using different force fields. $logP$ of thymoquinone is found as 0.77 using CHARMM force field and 3.07 using GROMOS force field. The partitioning free energy result using the OPLS-AA force field provided the closest $logP$ value of thymoquinone. The result from partitioning free energy calculations of atomistic simulations falls in the reported range.

The free energy differences of aminothymoquinone for different λ values can be found in Appendix A.1. The solvation and hydration free energies of aminothymoquinone in 1-octanol and water are found as 47.77 kJ/mol and 36.99 kJ/mol, respectively. $\Delta G_{Transfer}$ and $logP$ values are found by using Equations (3.12), and (3.13), respectively, and the calculations are given as

$$\Delta G_{Transfer} = 36.99\frac{kJ}{mol} - 47.77\frac{kJ}{mol} = -10.78\frac{kJ}{mol},$$
$$logP = \frac{-(-10.78\frac{kJ}{mol}) \times (\frac{10^3 J}{kJ})}{(8.314\frac{J}{molK}) \times (310K) \times (ln10)} = 1.82.$$

The information about partitioning coefficients of aminothymoquinone is limited compared to thymoquinone. Johnson-Ajinwo (2017) has reported computed $logP$ values of thymoquinone and aminothymoquinone as 1.04 and -0.71 respectively [113]. Additionally, $logP$ values are calculated using Chemicalize web-based source and they are found as 2.55 for thymoquinone and 1.39 for aminothymoquinone [114]. The summary of free energy differences and $logP$ values are given in Table 4.1.

In general, the difference in $logP$ values between thymoquinone and aminothymoquinone in the corresponding resources matches the difference in $logP$ values found from the atomistic free energy calculations in this study.

Table 4.1. The free energy differences and logP of thymoquinone and aminothymoquinone in atomistic simulations.

	$\Delta G_{inoctanol}$	$\Delta G_{inwater}$	$logP$
Thymoquinone	40.43	24.49	2.72
Aminothymoquinone	47.77	36.99	1.82

4.2. Construction and Validation of Coarse-Grained Models

The coarse-grained models of thymoquinone and aminothymoquinone are mapped using four different MARTINI 3 bead types based on the number and polarity of the mapped atoms. The grouping of the beads used in thymoquinone and aminothymoquinone models is shown in Figure 4.1.

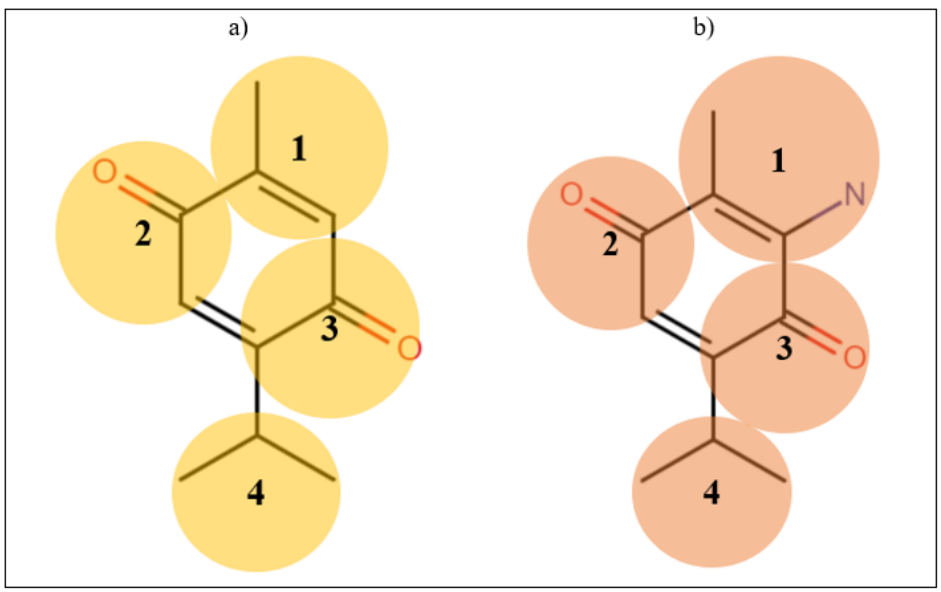

Figure 4.1. Coarse-grained representations of a) thymoquinone and b) aminothymoquinone.

The corresponding bead types to the bead numbers are given in Table 4.2. It is important to note that all beads of thymoquinone and aminothymoquinone are the same except for the first bead since the difference between these two molecules is the

addition of NH_2 to the third carbon. Moreover, the first bead of aminothymoquinone represents four non-hydrogen atoms instead of the other beads, including three non-hydrogen atoms.

Table 4.2. Coarse-grained beads of thymoquinone and aminothymoquinone.

Bead Number	**Thymoquinone**	**Aminothymoquinone**
1	SC5	N5d
2	SN4a	SN4a
3	SN4a	SN4a
4	SC3	SC3

Three constraints, one bond, and one improper dihedral are defined for both molecules' models. The lengths of bonds and constraints, the angle of improper dihedrals, and the corresponding force constants of thymoquinone and aminothymoquinone are shown in Tables 4.3 and 4.4.

Table 4.3. Bond definitions of thymoquinone and aminothymoquinone.

Thymoquinone				
Bond Pairs	1-2	2-3	1-3	3-4
Bond Type	Constraint	Constraint	Constraint	Bond
Length (nm)	0.329	0.325	0.368	0.295
Force Constant (kJ/mol/rad^2)	1000000	1000000	1000000	80000
Aminothymoquinone				
Bond Pairs	1-2	2-3	1-3	3-4
Bond Type	Constraint	Constraint	Constraint	Bond
Length (nm)	0.352	0.322	0.328	0.296
Force Constant (kJ/mol/rad^2)	1000000	1000000	1000000	90000

Table 4.4. Improper dihedral of coarse-grained thymoquinone and aminothymoquinone.

	Thymoquinone	**Aminothymoquinone**
Dihedral Group	4-2-1-3	4-2-1-3
Dihedral Type	Improper	Improper
Angle (Degree)	0	0
Force Constant (kJ/mol/rad^2)	150	50

Before the free energy calculations of coarse-grained models, bond and improper dihedral distributions are fitted to those in atomistic models by adjusting the force constants. The good agreement between atomistic and coarse-grained models on bond and improper dihedral distributions can be seen in Figure 4.2 for thymoquinone and in Figure 4.3 for aminothymoquinone.

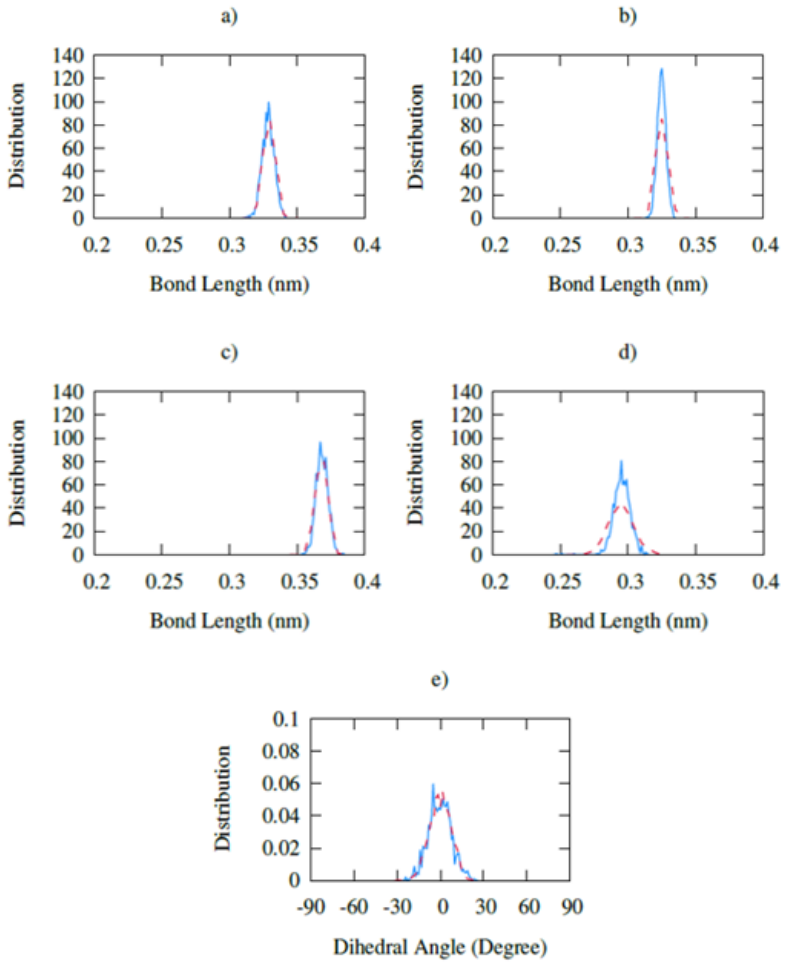

Figure 4.2. The distribution of the bonds between bead numbers a) 1-2, b) 2-3, c) 1-3, d) 3-4, as well as e) the improper dihedrals for the coarse-grained (red line) and atomistic (blue line) models of thymoquinone.

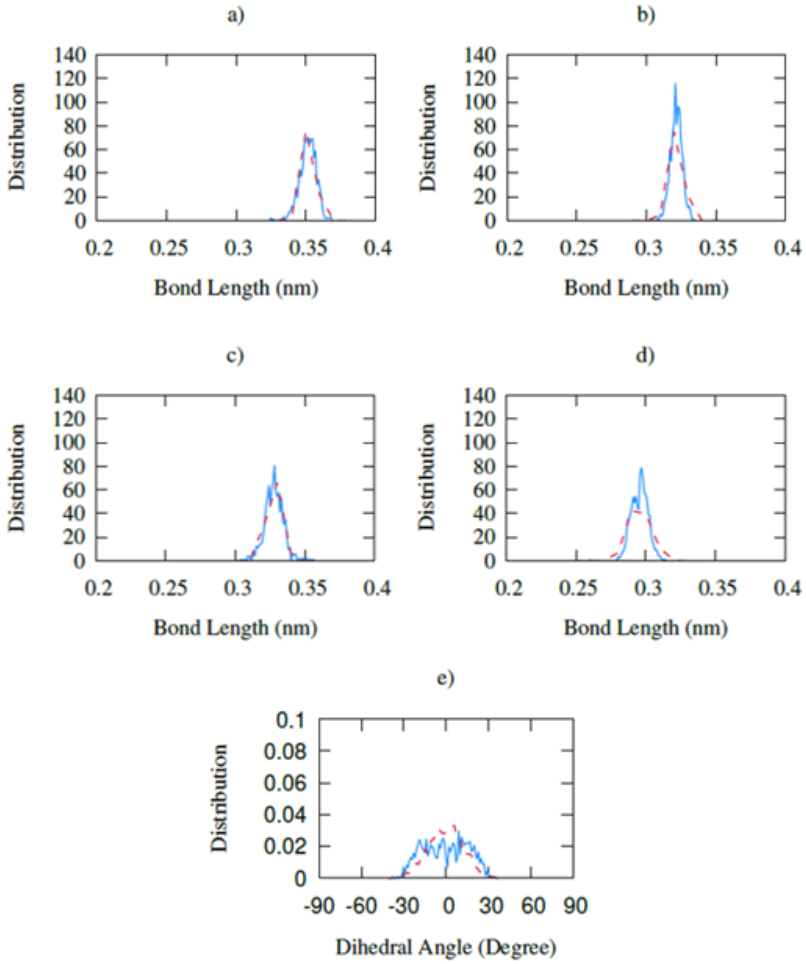

Figure 4.3. The distribution of the bonds between bead numbers a) 1-2, b) 2-3, c) 1-3, d) 3-4, as well as e) the improper dihedrals for the coarse-grained (red line) and atomistic (blue line) models of aminothymoquinone.

The free energy calculations have been performed for coarse-grained simulations to evaluate the models compared to the atomistic data and the data from the literature. The free energy changes of thymoquinone and aminothymoquinone for different *lambda* stages are shown in Appendix A.1. In the coarse-grained simulations, the solvation and hydration free energies of thymoquinone in 1-octanol and water are 25.23 kJ/mol and 10.27 kJ/mol, respectively. $\Delta G_{Transfer}$ and $logP$ values are calculated using Equations (3.12) and (3.13), respectively given as

$$\Delta G_{Transfer} = 10.27\frac{kJ}{mol} - 25.23\frac{kJ}{mol} = -14.96\frac{kJ}{mol},$$

$$logP = \frac{-(-14.96\frac{kJ}{mol}) \times (\frac{10^3 J}{kJ})}{(8.314\frac{J}{molK}) \times (310K) \times (ln10)} = 2.52.$$

The $logP$ value of the coarse-grained thymoquinone model also falls within the previously reported range mentioned in Section 4.1. Moreover, the percentage of the difference between $logP$ values obtained from the atomistic and coarse-grained simulations is calculated as

$$Error\% = \frac{|2.52 - 2.72|}{2.72} \times 100 = 7.31\%.$$

The solvation and hydration free energies of aminothymoquinone sum in 1-octanol and water are found as 32.15 kJ/mol and 22.37 kJ/mol, respectively. Then, $\Delta G_{Transfer}$ and $logP$ values are calculated using Equations (3.12) and (3.13) as

$$\Delta G_{Transfer} = 22.37\frac{kJ}{mol} - 32.15\frac{kJ}{mol} = -9.78\frac{kJ}{mol},$$
$$logP = \frac{-(-9.78\frac{kJ}{mol}) \times (\frac{10^3 J}{kJ})}{(8.314\frac{J}{molK}) \times (310K) \times (ln10)} = 1.65.$$

The deviation of the coarse-grained model from the atomistic one is calculated by the percentage of the difference between $logP$ values, and the result is given as

$$Error\% = \frac{|1.65 - 1.82|}{1.82} \times 100 = 9.34\%.$$

The solvation and hydration free energies and $logP$ of aminothymoquinone are given in Table 4.5.

Table 4.5. The free energy differences and logP of thymoquinone and aminothymoquinone in coarse-grained simulations.

	$\Delta G_{inoctanol}$	$\Delta G_{inwater}$	$logP$
Thymoquinone	25.23	10.27	2.52
Aminothymoquinone	32.15	22.37	1.65

The coarse-grained representation of aminothymoquinone is in the acceptable $logP$ range considering the difference in $logP$ values of thymoquinone and aminothymoquinone discussed in Section 4.1. The error percentages are also under 10%, and up to 10% deviation between coarse-grained and atomistic models is usually considered within the acceptable range [21]. Thus, atomistic and coarse-grained models are in good agreement with each other and with other experimental findings.

4.3. The Accuracy of the Models

In the following section, the accuracy and reproducibility of coarse-grained models are examined. The results from atomistic bilayer-only systems are analyzed and compared to the findings from the literature to validate the bilayer models. Bilayers with different concentrations of thymoquinone molecules are also analyzed to observe the behavior of bilayers and thymoquinone in simple bilayers having different lipid types. The area per lipid, bilayer thickness, diffusion coefficient, and lipid order parameters are analyzed to observe the change in structural properties of the bilayers. Additionally, thymoquinone orientation in the bilayers, RDF, density distribution, and residence time of thymoquinone in water are computed to further understand the behavior of thymoquinone in the presence of bilayers.

4.3.1. Structural Changes in Simple Bilayers

The structural properties of lipids are investigated through the area per lipid, bilayer thickness, and self-diffusion coefficient calculations for bilayer-only systems to-

gether with the systems in the presence of one or ten thymoquinone molecules. The area per lipid of DOPC and POPC bilayers with and without thymoquinone molecules are calculated. The variation of area per lipid value with respect to time can be found in Appendix A.2. The time averages of area per lipid with their standard deviations for all atomistic and coarse-grained systems are presented in Table 4.6.

Table 4.6. Area per lipid of DOPC and POPC bilayers (nm^2).

		Atomistic	**Coarse-Grained**
DOPC	**No TQ**	0.68 ± 0.01	0.68 ± 0.01
	1 TQ	0.68 ± 0.01	0.69 ± 0.01
	10 TQ	0.70 ± 0.01	0.70 ± 0.01
POPC	**No TQ**	0.71 ± 0.01	0.66 ± 0.01
	1 TQ	0.70 ± 0.01	0.66 ± 0.01
	10 TQ	0.70 ± 0.01	0.67 ± 0.01

Area per lipid values of DOPC only and POPC only bilayers are obtained from the literature to ensure the validation of the bilayer systems. Tristnam-Nagle *et al.* (1998) [115], Nagle *et al.* (2000) [116], Liu *et al.* (2004) [117], Kucerka *et al.* (2005) [118] , Pan *et al.* (2008) [119], and Kucerka *et al.* (2008) [120] have reported area per lipid values in the range between 0.67-0.73 nm2 for DOPC bilayer. For the POPC bilayer, Kucerka *et al.* (2011) [121] have reported area per lipid values between 0.63-0.68 nm^2 for temperatures between 20°C-60°C, while Leftin *et al.* (2014) [122] have found 60.4 ± 3.6 $\AA^2$ at 28°C and 70.5 ± 4.2 $\AA^2$ at 48°C. The results from both atomistic and coarse-grained simulations fall in the range of the reported area per lipid values in the literature. Adding one or ten thymoquinone molecules does not have a notable effect on either the area per lipid values or the bilayer thickness values (see Table 4.7) considering the error bounds.

Table 4.7. Bilayer Thickness of DOPC and POPC bilayers (nm).

		Atomistic	**Coarse-Grained**
DOPC	**No TQ**	3.89 ± 0.05	3.74 ± 0.05
	1 TQ	3.87 ± 0.05	3.74 ± 0.05
	10 TQ	3.86 ± 0.05	3.72 ± 0.05
POPC	**No TQ**	3.56 ± 0.05	3.86 ± 0.06
	1 TQ	3.59 ± 0.05	3.86 ± 0.05
	10 TQ	3.60 ± 0.06	3.84 ± 0.06

The bilayer thicknesses of DOPC and POPC bilayers have been investigated in several studies. Tristnam-Nagle *et al.* (1998) [115], Nagle *et al.* (2000) [116], Liu *et al.* (2004) [117], Kucerka *et al.* (2005) [118], Pan et al. (2008) [119], Kucerka *et al.* (2008) [120] and Attwood *et al.* (2013) [123] have reported DOPC bilayer thickness values as 3.67 nm, 3.61 nm, 3.53 nm, 3.69 nm, 3.67 nm, and 4.6 nm, respectively. Kucerka *et al.* (2005) [118] and Kucerka *et al.* (2011) [121] have reported POPC bilayer thickness values as 3.7 nm, and 3.77-3.98 nm between 60°C and 20°C, respectively. The bilayer thickness of DOPC bilayers is in the range of the reported values. However, the values for POPC bilayers found in atomistic simulations are out of the range of the experimental data, but closer to the previously computed values [124–126].

Upon the addition of thymoquinone, a slight decrease in the thickness of DOPC bilayers with both atomistic and coarse-grained simulations can be seen in Table 4.7. The difference in thickness values in the atomistic POPC bilayer simulations is larger than in the other reported data groups. However, the change is still in the error range considering the standard deviation of thickness values.

The lateral diffusion coefficients of DOPC and POPC bilayers were calculated by applying the least square fitting between 10-30 ns of the last 100 ns for atomistic simulations, between 100-300 ns of the last 500 ns of bilayer only systems, and between 200-600 ns of the last 1000 ns of bilayers in the presence of thymoquinone for coarse-

grained simulations. The results are given in Table 4.8.

Table 4.8. Lateral diffusion coefficients of phosphate groups in DOPC and POPC bilayers ($\mu m^2/s$).

		Atomistic	**Coarse-Grained**
DOPC	**No TQ**	8.10 ± 1.70	67.1 ± 19.1
	1 TQ	6.40 ± 0.40	66.7 ± 0.70
	10 TQ	12.6 ± 0.60	88.0 ± 1.50
POPC	**No TQ**	4.10 ± 0.10	55.3 ± 0.30
	1 TQ	3.70 ± 0.10	55.9 ± 8.30
	10 TQ	10.5 ± 2.80	53.4 ± 6.70

The diffusion coefficients of DOPC and POPC lipids in atomistic simulations were compared to the experimental data from the literature. Filippov *et al.* (2009) [127] and Akhunzada *et al.* (2019) [128] have reported the self-diffusion coefficient of DOPC lipids as 9.32 $\mu m^2/s$ and 11.5 $\mu m^2/s$ at 298 K and 303 K, and between 5.0-14.0 $\mu m^2/s$, respectively. Febo-Ayala *et al.* (2008) [129] and Saito *et al.* (2018) [130] have obtained the diffusion coefficient of POPC lipids as 1.8-2.5 $\mu m^2/s$ at 298 K and 7.49 $\mu m^2/s$ at 303 K. Additionally, Erimban, *et al.* (2019) [125] have used the same OPLS-AA lipid parameters developed by Kulig *et al.* (2015) [81] and have reported the diffusion coefficient of POPC lipids as 9.0 ± 3.0 $\mu m^2/s$ at 300 K. Considering the effect of temperature on diffusion coefficient data, it is sufficient to say that the results in atomistic simulations are in the range of literature data. The diffusion coefficient values of the coarse-grained DOPC and POPC models are larger than their atomistic counterparts. Coarse-grained simulations predict higher diffusion coefficients in general and the results reported here are in the acceptable range [131]. The addition of thymoquinone molecules to the bilayers increases the diffusion of the lipids in general.

Order parameters of acyl chains of DOPC and POPC lipids are calculated to observe if thymoquinone causes any disorder in the bilayers. Each carbon atom in the

acyl chains is used in the order parameter calculation in atomistic systems. All tail beads are included in the calculations in the coarse-grained systems. The changes in the order parameters of sn1 and sn2 acyl chains of the bilayers in the presence and absence of thymoquinone are shown in Figures 4.4 and 4.5.

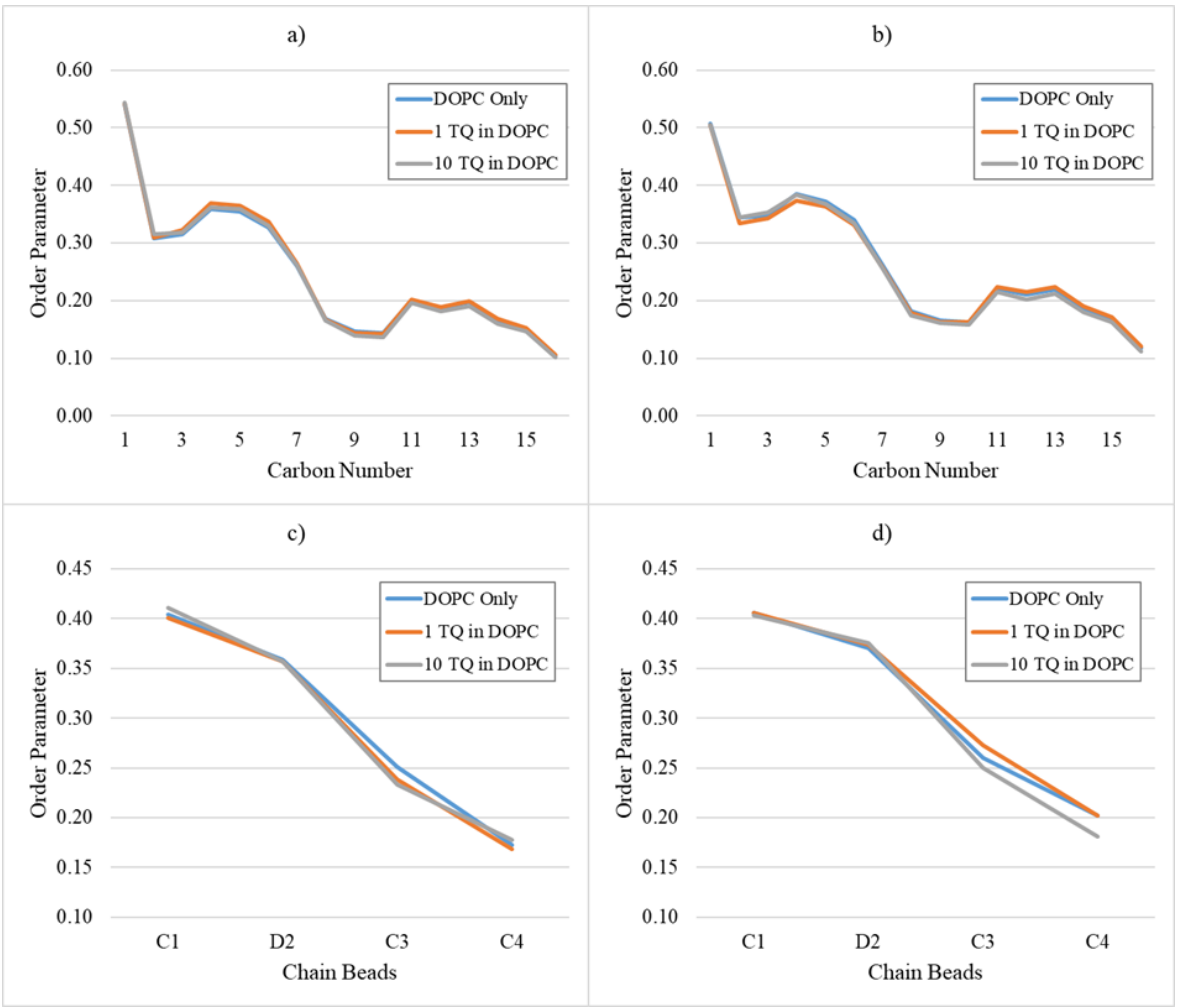

Figure 4.4. Order parameters of DOPC: a) sn1 and b) sn2 acyl chain in atomistic; and c) sn1 and d) sn2 acyl chains in coarse-grained simulations.

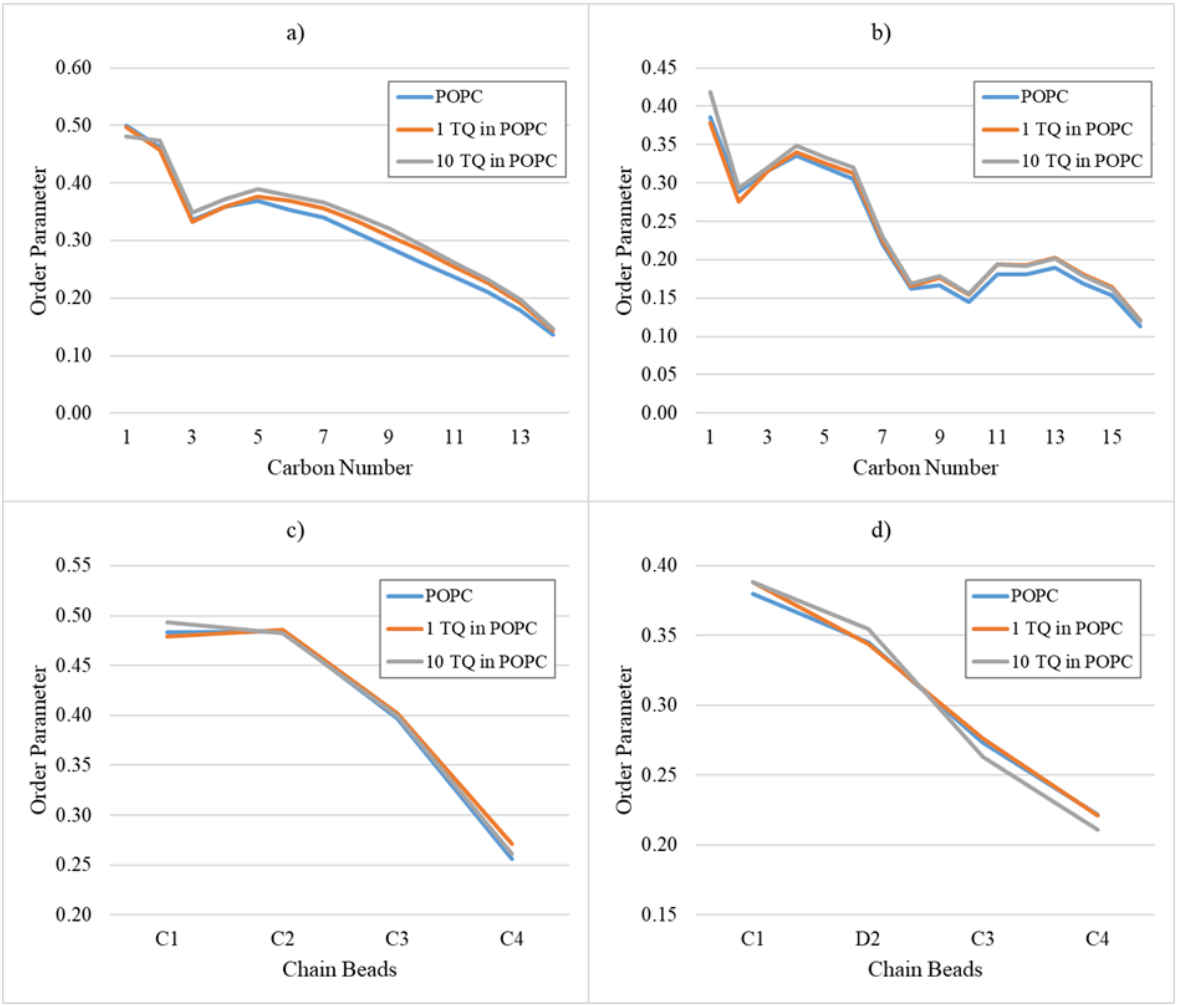

Figure 4.5. Order parameters of POPC: a) sn1 and b) sn2 acyl chain in atomistic; and c) sn1 and d) sn2 acyl chains in coarse-grained simulations.

The average of all acyl carbons of sn1 and sn2 chains is also calculated. The findings are given with the overall average order parameter for DOPC and POPC lipids in Table 4.9.

With both models, thymoquinone has slight disordering and ordering effects on POPC and DOPC bilayers, respectively. This change is generally negligible with the addition of one thymoquinone molecule to the POPC bilayers.

Table 4.9. Order parameters of DOPC acyl chains.

		Atomistic			Coarse-Grained		
		No TQ	**1 TQ**	**10 TQ**	**No TQ**	**1 TQ**	**10 TQ**
DOPC	**sn1 chain**	0.245	0.249	0.244	0.297	0.291	0.295
	sn2 chain	0.262	0.260	0.258	0.310	0.314	0.302
	Average	0.254	0.254	0.251	0.303	0.302	0.299
POPC	**sn1 chain**	0.310	0.321	0.329	0.405	0.410	0.409
	sn2 chain	0.227	0.233	0.238	0.305	0.307	0.304
	Average	0.266	0.274	0.280	0.355	0.358	0.357

4.3.2. The Interaction of Thymoquinone with Simple Bilayers

To understand the orientation and the behavior of thymoquinone in simple bilayers, the density distributions, the residence time of thymoquinone in the solvent, and RDF analysis are computed.

The density distributions of the bilayer components, solvent, ions, and thymoquinone molecules are plotted by centering the bilayer at 0 nm. The calculated bilayer components are the main groups of phospholipids, which are the phosphate head group (Head), glycerol group (Gly), and acyl chains (Acyl). Bilayers without and with ten thymoquinone molecules are chosen for this analysis to be able to make meaningful comparisons. The density profiles of bilayer only and thymoquinone bilayer complexes are given in Figures 4.6 and 4.7. The graphs are zoomed in to observe the placement of thymoquinone in the systems clearly. The original graphs are given in Appendix A.5.

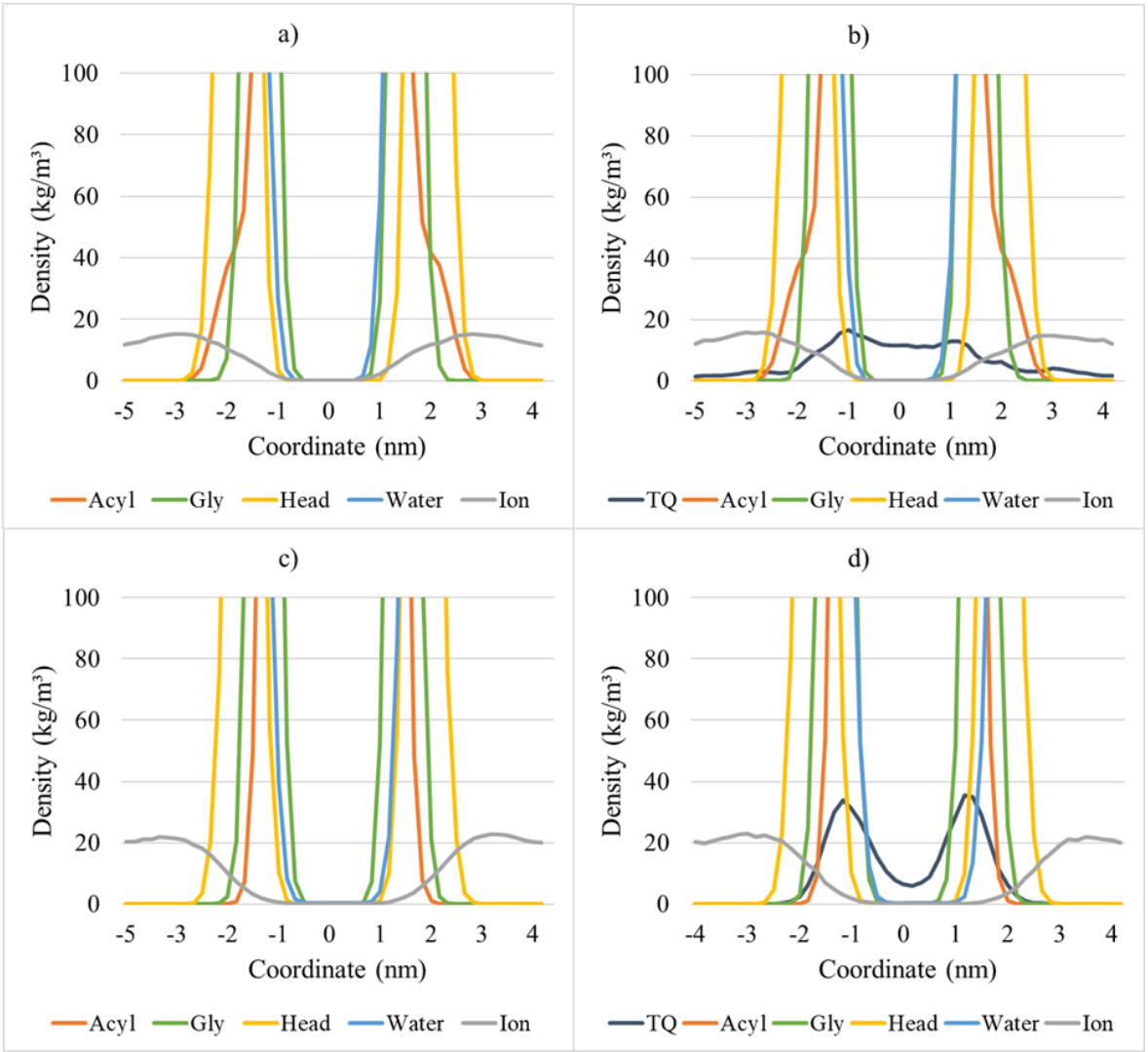

Figure 4.6. Density distributions of the systems with DOPC bilayer: a) without and b) with thymoquinone in atomistic; and c) without and d) with thymoquinone molecules in coarse-grained simulations.

The density profiles demonstrate the residence of thymoquinone inside the bilayers. When Figure 4.6.b and Figure 4.6.d are compared, the localization behavior of thymoquinone seems different from each other. Nearly all thymoquinone molecules seem to be inside the DOPC bilayer. On the other hand, the distribution of thymoquinone in coarse-grained bilayer systems is smoother than in the atomistic model. The sharp peaks of thymoquinone can be seen in the border of head groups, around -1.0 and 1.4 nm with respect to the bilayer center. The peaks of thymoquinone with wider

distributions in the atomistic model are also around the same coordinates. Moreover, when only-bilayer (Figure 4.6.a and 4.6.c) and thymoquinone-bilayer systems (Figure 4.6.b and 4.6.d) are compared, the bilayer components' distributions are observed to be similar.

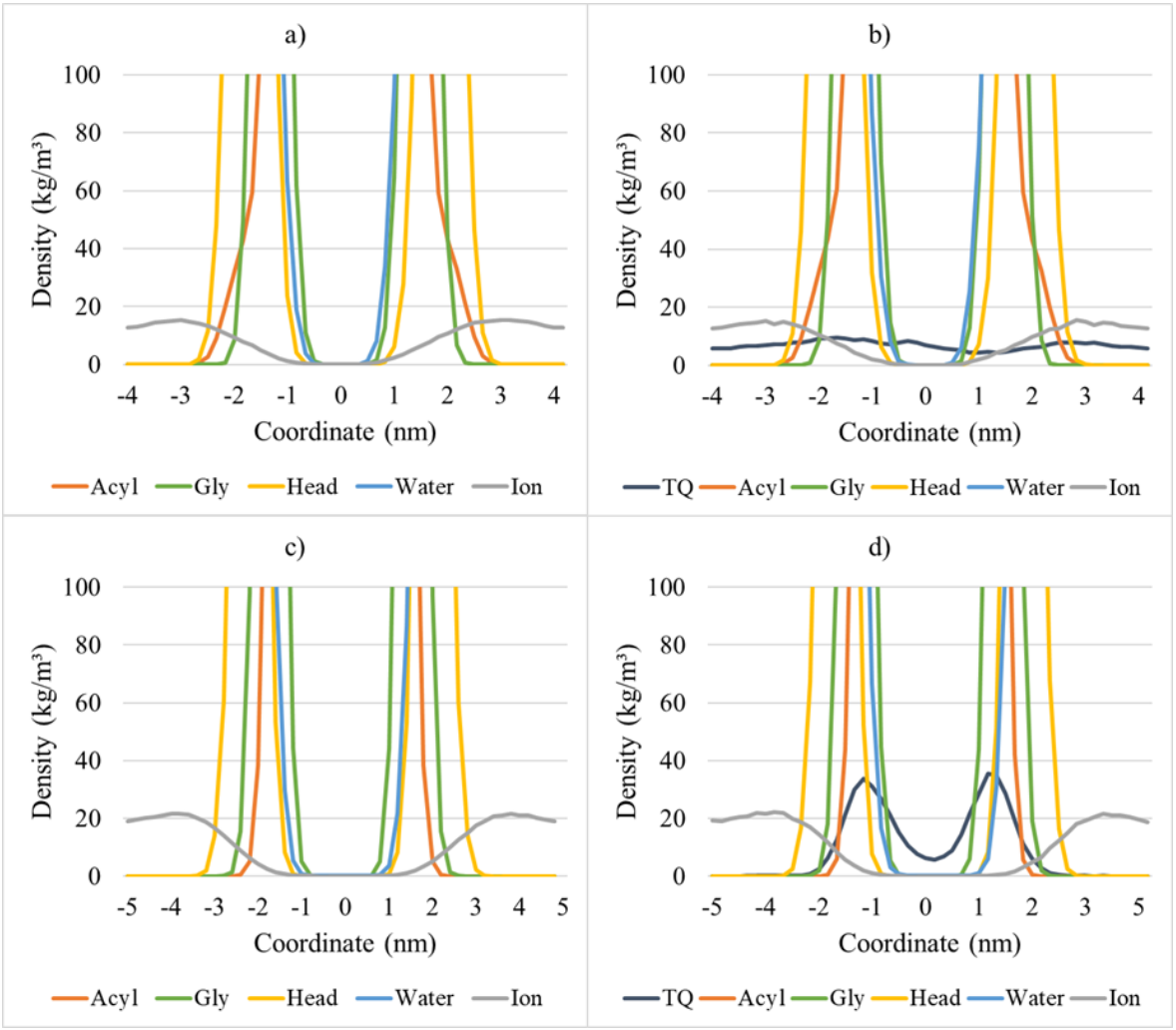

Figure 4.7. Density distributions of the systems with POPC bilayer: a) without and b) with thymoquinone in atomistic; and c) without and d) with thymoquinone molecules in coarse-grained simulations.

The distribution of thymoquinone in the POPC bilayer is different than in the DOPC bilayer. Thymoquinones exist both in the bilayer and solvent phase in the atomistic model. That is, only some of the thymoquinones are inside the bilayer.

On the other hand, all thymoquinones diffused into the bilayer in the coarse-grained models. The density peaks of thymoquinone in Figure 4.7.d indicate that most of them prefer to be close to the glycerol groups, which are around -1.5 and 1.5 nm with respect to the bilayer center.

The diffusion of thymoquinone into the lipid bilayers is clearly observed in coarse-grained simulations. However, some of the thymoquinone molecules do not seem to be diffusing into the bilayers in atomistic simulations. To support this observation, the average center of mass distance of each thymoquinone molecule from the bilayer center is calculated over all frames of the simulations. The beginning and the end of the distance measurements are taken as the beginning and the end of the MD production run, i.e., 0 and 500 ns respectively. Figures 4.8 and 4.9 exhibit the distance between thymoquinone and lipid bilayers with respect to simulation time.

According to Figure 4.8, all thymoquinone diffused into the DOPC bilayer except for two molecules. On the other hand, only four thymoquinone molecules diffused into and stayed in the POPC bilayer (see Figure 4.9). The reason for the non-smooth distribution of thymoquinone in the atomistic simulations can be understood due to the roaming of some thymoquinone molecules in the bilayer solvent throughout the simulations.

The difference in the behavior of thymoquinone between atomistic and coarse-grained simulations can be explained by the nature of atomistic simulations. It requires more time to evaluate the systems in atomistic simulations than the coarse-grained simulations, which has a faster dynamical behavior. If the atomistic systems would run for a longer simulation time, the diffusion of most of the thymoquinone molecules could have been observed. However, the atomistic simulations are not feasible to run larger systems for a long time even though they provide a higher resolution.

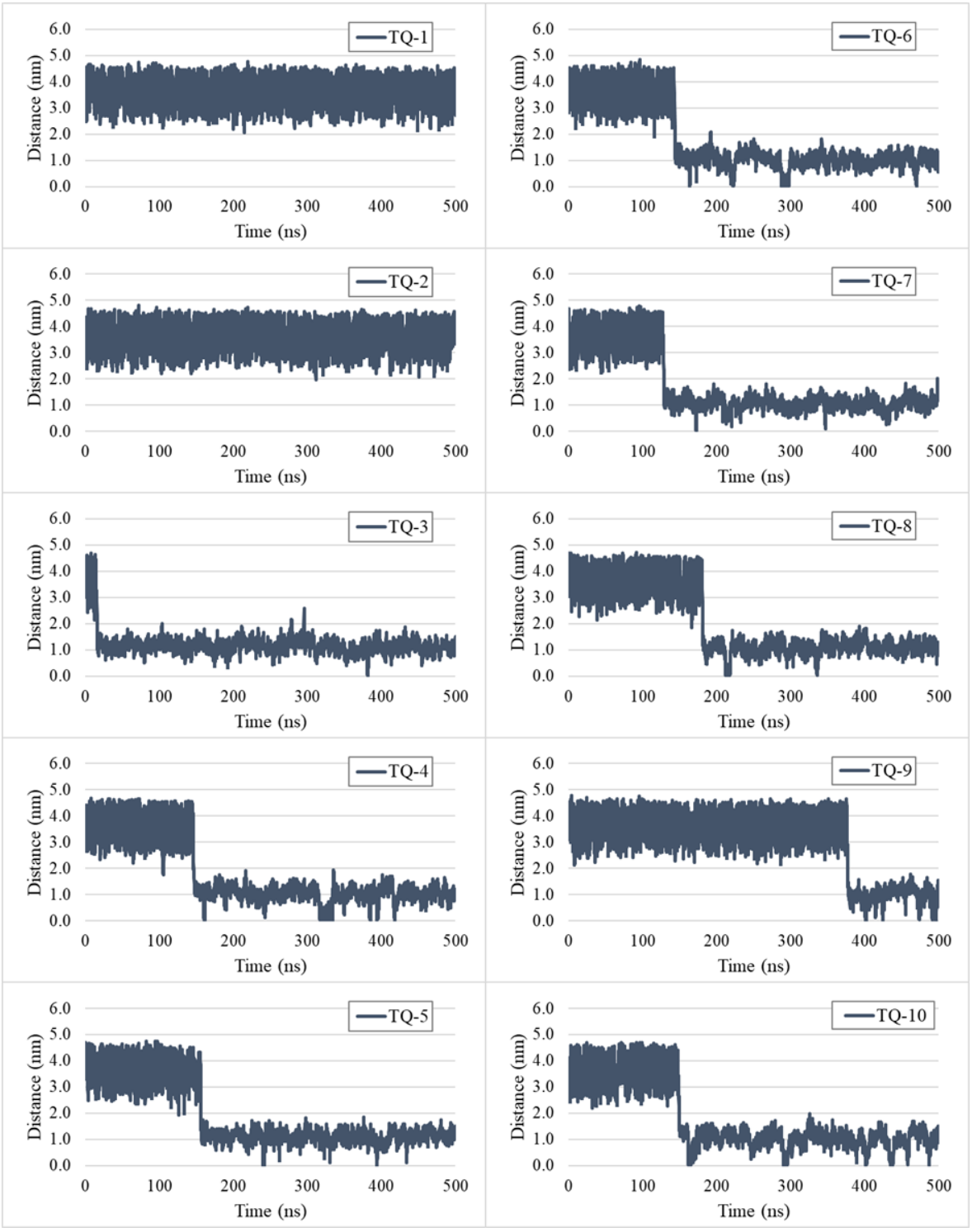

Figure 4.8. The absolute center of mass distance of thymoquinones from DOPC bilayer in atomistic simulations.

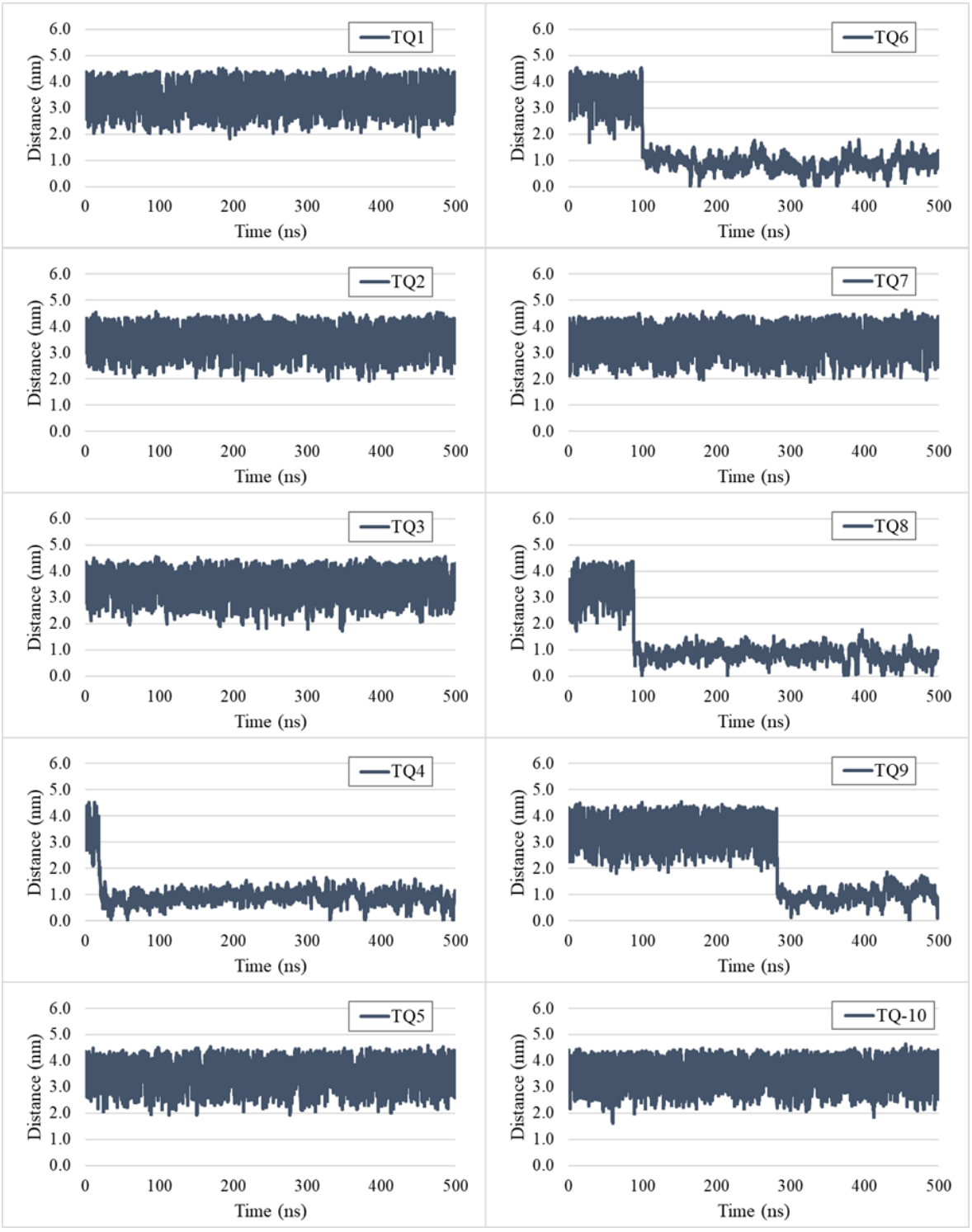

Figure 4.9. The absolute center of mass distance of thymoquinones from POPC bilayer in atomistic simulations.

The last analysis for thymoquinone in simple bilayer systems is the radial distribution function analysis, which is performed with respect to the center of mass of DOPC, POPC, and thymoquinone. The interaction of thymoquinone with the lipids can be seen in Figures 4.10 and 4.11.

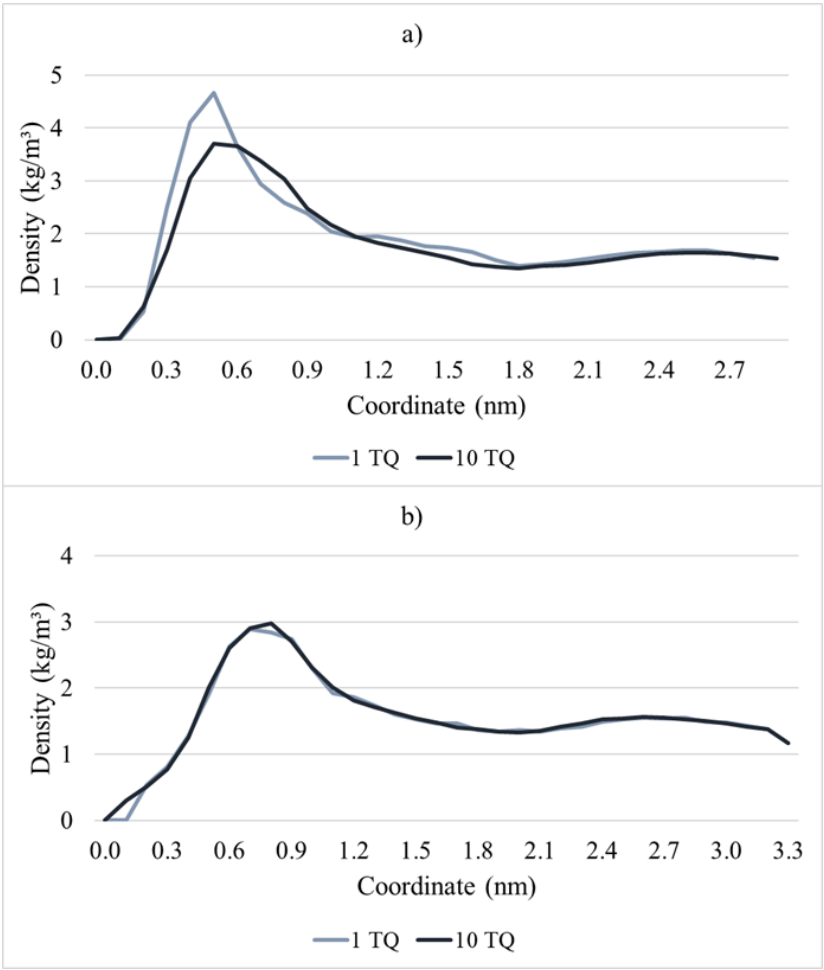

Figure 4.10. The radial distribution functions of thymoquinone with respect to the center of mass of DOPC molecules in a) atomistic and b) coarse-grained simulations.

The separation distance between thymoquinone and DOPC bilayers is closest when one thymoquinone is introduced into the systems in both atomistic and coarse-grained simulations. As concentration increases, this distance between thymoquinone and DOPC lipids decreases.

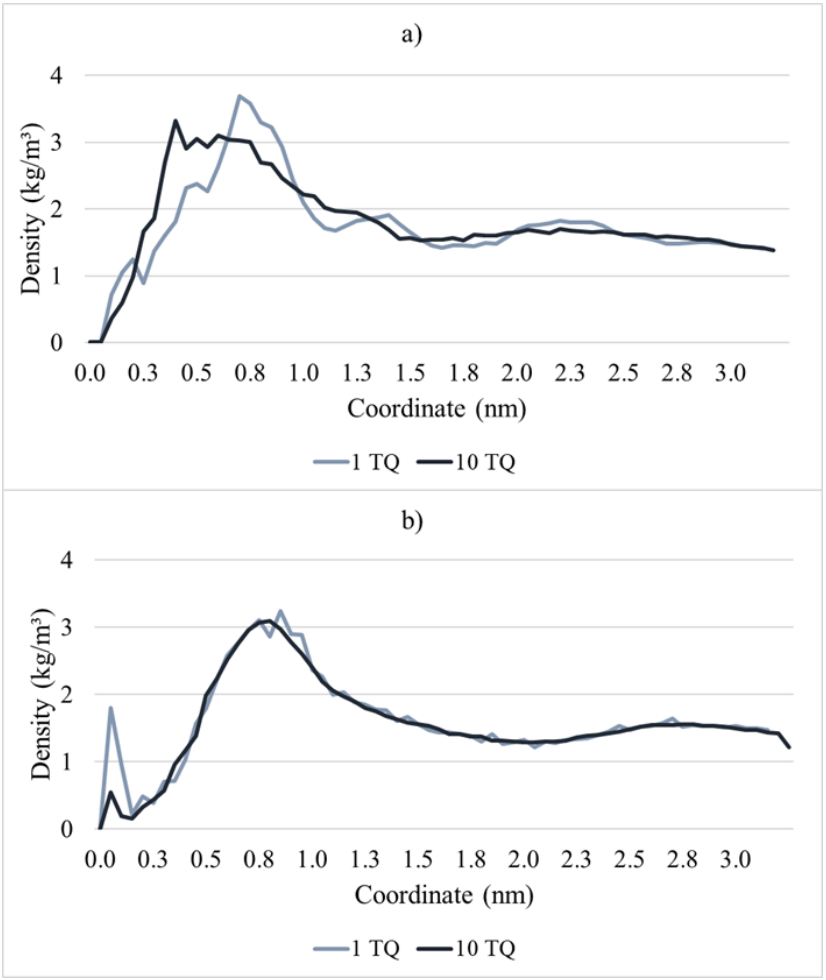

Figure 4.11. The radial distribution functions of thymoquinone with respect to the center of mass POPC molecules in a) atomistic and b) coarse-grained simulations.

In the atomistic model, the ordering of thymoquinone with the POPC bilayer decreases with the increasing concentration of thymoquinone. In coarse-grained simulations, the distributions have similar profiles. The peaks of the distributions are around 0.8-1.0 nm in coarse-grained systems and one thymoquinone system in the atomistic model, while 10 thymoquinone system in the atomistic POPC has a peak of around 0.5 nm. In both atomistic and coarse-grained simulations, a single thymoquinone molecule prefers a more widely spaced configuration with the lipids. The interaction distance decreases with increasing thymoquinone molecule. It is important to note that the interaction of thymoquinone with DOPC and POPC lipids is vice versa.

4.4. The Application of Coarse-Grained Models to Complex Bilayers

The normal and cancer cell bilayer models are constructed from two different lipid types, as explained in Section 3.3.2. Model 1 consists of cholesterol, DOPC, and DOPS (1,2-dioleoyl-sn-glycero-3-phospho-L-serine) lipids, and Model 2 contains cholesterol, POPC, and POPS (1-palmitoyl-2- oleoyl- sn -glycero-3-phospho- L-serine) lipids respectively. The last 1 μs of the trajectories of only-bilayer and the bilayers in the presence of thymoquinone or aminothymoquinone are used for the trajectory analyses. The changes in the bilayer properties are computed through the area per lipid, bilayer thickness, lateral diffusion coefficient, and order parameters. Moreover, thymoquinone and aminothymoquinone orientations in the model bilayers, density distributions, and radial distribution functions are analyzed to observe the effect and behavior of thymoquinone and aminothymoquinone.

4.4.1. Structural Changes in Complex Bilayers

Area per lipid of complex bilayers with and without thymoquinone or aminothymoquinone are given in Table 4.8.

Table 4.10. Area per lipid of normal and cancer cell model bilayers (nm^2).

		Model 1	**Model 2**
Normal	**No TQ/ATQ**	0.52 ± 4.0x10^{-3}	0.49 ± 4.0x10^{-3}
	100 TQ	0.53 ± 4.0x10^{-3}	0.51 ± 4.0x10^{-3}
	100 ATQ	0.53 ± 4.0x10^{-3}	0.51 ± 4.0x10^{-3}
Cancer	**No TQ/ATQ**	0.60 ± 4.0x10^{-3}	0.57 ± 4.0x10^{-3}
	100 TQ	0.61 ± 4.0x10^{-3}	0.59 ± 4.0x10^{-3}
	100 ATQ	0.61 ± 4.0x10^{-3}	0.58 ± 4.0x10^{-3}

The area per lipid of both model bilayers increases systematically in the presence of thymoquinone or aminothymoquinone. The effect of both molecules on normal and

cancer cell bilayer models is similar. In one of the reference studies of Model 1 and 2, Radhakrishnan *et al.* (2022) have reported the area per lipid value of around 0.60 and 0.65 nm^2 in both normal and cancer model bilayers, which consist of POPC and POPS lipids [89]. The reason for the lower area per lipid values obtained in this study is the addition of cholesterol to Model 1 and 2. As the cholesterol concentration increases in a phospholipid bilayer, the thickness of the bilayer increases, and the area per lipid decreases inversely [132].

The bilayer thicknesses of the complex bilayer models are presented in Table 4.11.

Table 4.11. Bilayer Thickness of normal and cancer cell model bilayers (nm).

		Model 1	**Model 2**
Normal	**No TQ/ATQ**	3.92 ± 0.02	4.08 ± 0.02
	100 TQ	3.90 ± 0.02	4.04 ± 0.02
	100 ATQ	3.90 ± 0.02	4.05 ± 0.02
Cancer	**No TQ/ATQ**	3.83 ± 0.02	3.97 ± 0.02
	100 TQ	3.81 ± 0.02	3.94 ± 0.02
	100 ATQ	3.81 ± 0.02	3.94 ± 0.02

The thicknesses of all model bilayers decrease as thymoquinone or aminothymoquinone molecules are introduced to the systems. This result agrees with the area per lipid values since the area per lipid and bilayer thickness is inversely proportional to each other. The decrease in bilayer thickness and the increase in area per lipid indicate the bilayer thinning effect of both aminothymoquinone and thymoquinone. It is important to note that the effect of thymoquinone on the simple bilayers can be seen in the complex bilayer models indicating the applicability of the coarse-grained models to different systems.

The lateral-diffusion coefficients for cholesterol, DOPC, and DOPS lipids in Model 1 and Model 2 complex bilayers are calculated separately. The least-square fitting on

mean square displacement data is performed between 200-800 ns of the last 1000 ns of the output trajectories. The results are shown in Tables 4.12 and 4.13.

Table 4.12. Lateral diffusion coefficients of cholesterol, DOPC and DOPS lipids in Model 1 normal and Model 1 cancer cell bilayers ($\mu m^2/s$).

		Cholesterol	**DOPC**	**DOPS**
Normal	**No TQ/ATQ**	96.3 ± 2.9	50.7 ± 1.1	55.5 ± 1.6
	100 TQ	95.9 ± 3.7	47.9 ± 3.1	52.4 ± 4.5
	100 ATQ	102.1 ± 3.5	50.8 ± 0.9	41.2 ± 2.4
Cancer	**No TQ/ATQ**	123.4 ± 4.2	65.4 ± 5.9	59.7 ± 3.4
	100 TQ	123.8 ± 4.0	65.3± 0.5	61.5 ± 0.4
	100 ATQ	141.2 ± 1.8	59.9 ± 0.8	65.2 ± 7.3

The diffusion coefficients of cholesterol, DOPC, and DOPS do not change too much when thymoquinone is added to both normal and cancer model bilayers considering the standard deviations. However, diffusion coefficients of cholesterol for normal and cancer model bilayers show a gradual increase in the presence of aminothymoquinone. The diffusion coefficient of DOPC decreases or remains nearly equal for all model systems. Likewise, the diffusion coefficients of DOPS do not follow a trend in the model systems.

Table 4.13. Lateral diffusion coefficients of cholesterol, POPC and POPS lipids in Model 2 normal and Model 2 cancer cell bilayers ($\mu m^2/s$).

		Cholesterol	**POPC**	**POPS**
Normal	**No TQ/ATQ**	79.3 ± 1.9	44.3 ± 2.3	36.7 ± 1.9
	100 TQ	82.5 ± 2.6	48.8 ± 0.2	51.2 ± 0.1
	100 ATQ	85.0 ± 0.9	49.9 ± 2.3	39.7 ± 5.9
Cancer	**No TQ/ATQ**	94.0 ± 1.8	51.3 ± 6.5	56.5 ± 4.5
	100 TQ	105.0 ± 5.2	55.3± 5.3	62.1 ± 6.4
	100 ATQ	108.1 ± 6.7	55.4 ± 8.8	55.2 ± 3.2

Similar to the results of Model 1, cholesterol's diffusion coefficient in Model 2 increases in the presence of thymoquinone, and this increase is more significant in the presence of aminothymoquinone. Indeed, cholesterol has the largest diffusion coefficient among the other bilayer components. The diffusion coefficients of POPC and POPS also increase as thymoquinone or aminothymoquinone are added to the systems. The diffusion rates of POPC increase in both normal and cancer bilayer models in the presence of thymoquinone. On the other hand, POPS diffuses more in the presence of aminothymoquinone compared to the change in diffusion coefficient on thymoquinone in both normal and cancer bilayer models. The order parameters of acyl chains of DOPC and DOPS lipids of Model 1 and POPC and POPS lipids of Model 2 are calculated to observe any ordering effect of thymoquinone and aminothymoquinone on the complex bilayers. The time-averaged order parameters of each bead are plotted for their corresponding acyl chain. The changes in the acyl chains are shown in Figures 4.12-15. The time average values of sn1, sn2 chains, and total lipid order parameters are given in Tables 4.14-17.

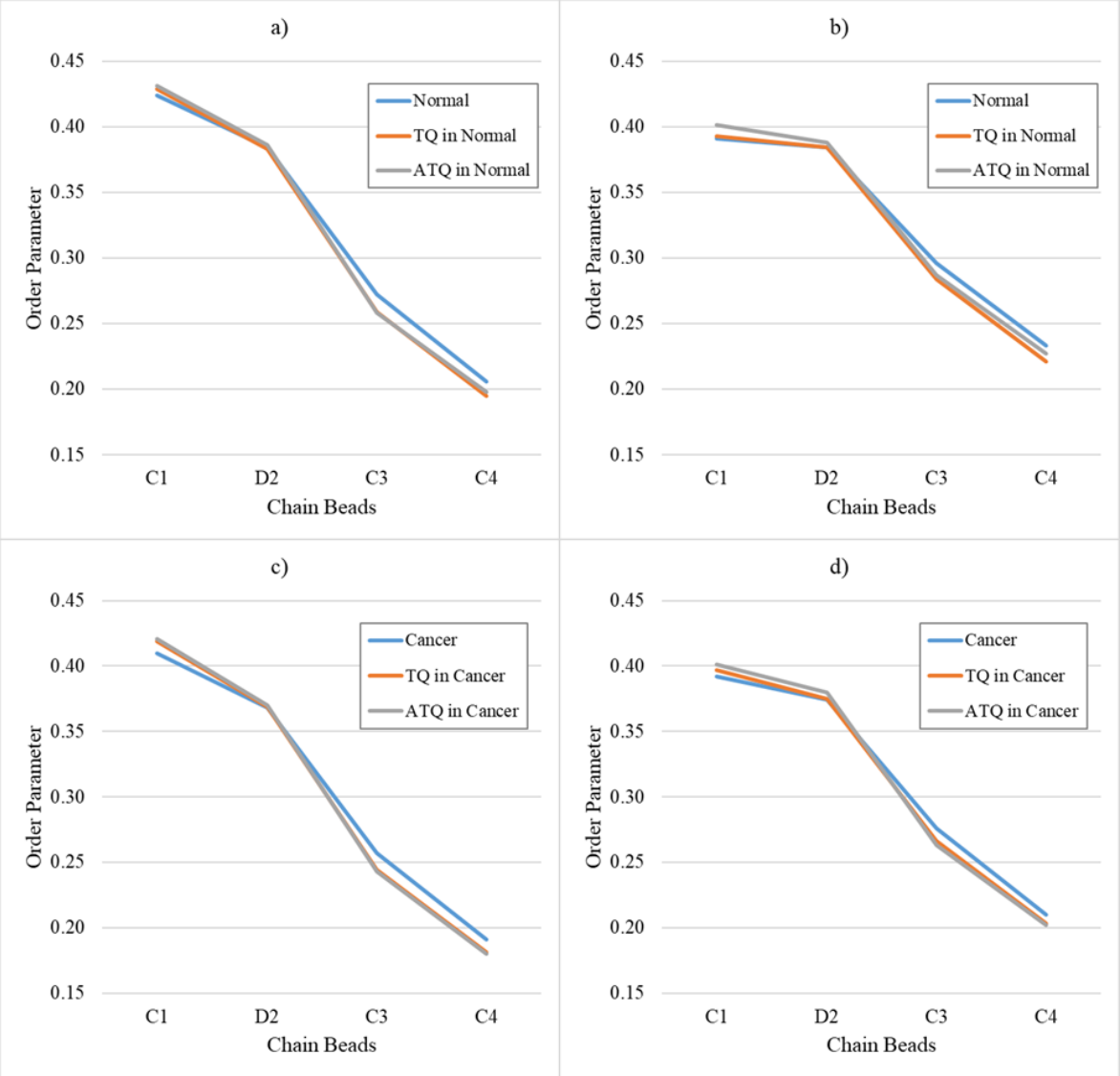

Figure 4.12. Order parameters of DOPC a) sn1 and b) sn2 acyl chains in Model 1 normal cell bilayer, and c) sn1 and d) sn2 acyl chains in Model 1 cancer cell bilayer.

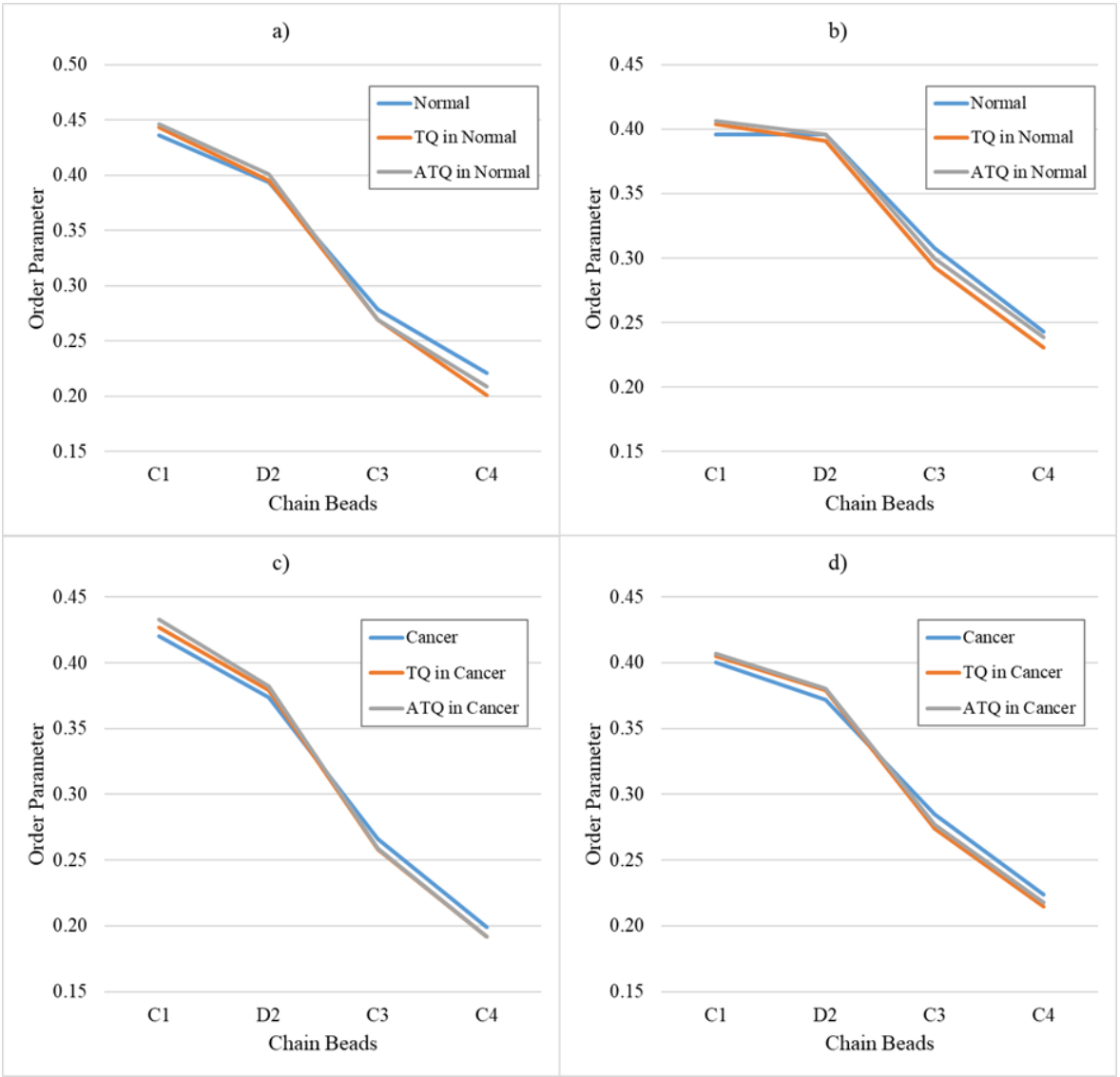

Figure 4.13. Order parameters of DOPS a) sn1 and b) sn2 acyl chains in Model 1 normal cell bilayer, and c) sn1 and d) sn2 acyl chains in Model 1 cancer cell bilayer.

Table 4.14. Order parameters of acyl chains of DOPC lipids in Model 1 normal and cancer cell bilayers.

		No TQ/ATQ	**100 TQ**	**100 ATQ**
Normal	**sn1 chain**	0.322	0.317	0.318
	sn2 chain	0.326	0.321	0.326
	Average	0.324	0.319	0.322
Cancer	**sn1 chain**	0.307	0.303	0.304
	sn2 chain	0.313	0.310	0.312
	Average	0.310	0.307	0.308

Table 4.15. Order parameters of acyl chains of DOPS lipids in Model 1 normal and cancer cell bilayers.

		No TQ/ATQ	**100 TQ**	**100 ATQ**
Normal	**sn1 chain**	0.333	0.327	0.331
	sn2 chain	0.336	0.330	0.335
	Average	0.334	0.328	0.333
Cancer	**sn1 chain**	0.315	0.314	0.317
	sn2 chain	0.320	0.318	0.321
	Average	0.318	0.316	0.319

The order parameters of DOPC acyl chains decrease more when thymoquinone molecules are present in both normal and cancer cell bilayers. Thymoquinone induces disorder in the DOPC lipids more than aminothymoquinone. The same disordering effect of thymoquinone on DOPS lipids is observed in both normal and cancer bilayers. Aminothymoquinone decreases the order in the normal bilayer model slightly. However, it increases the ordering of DOPS in the cancer Model 1.

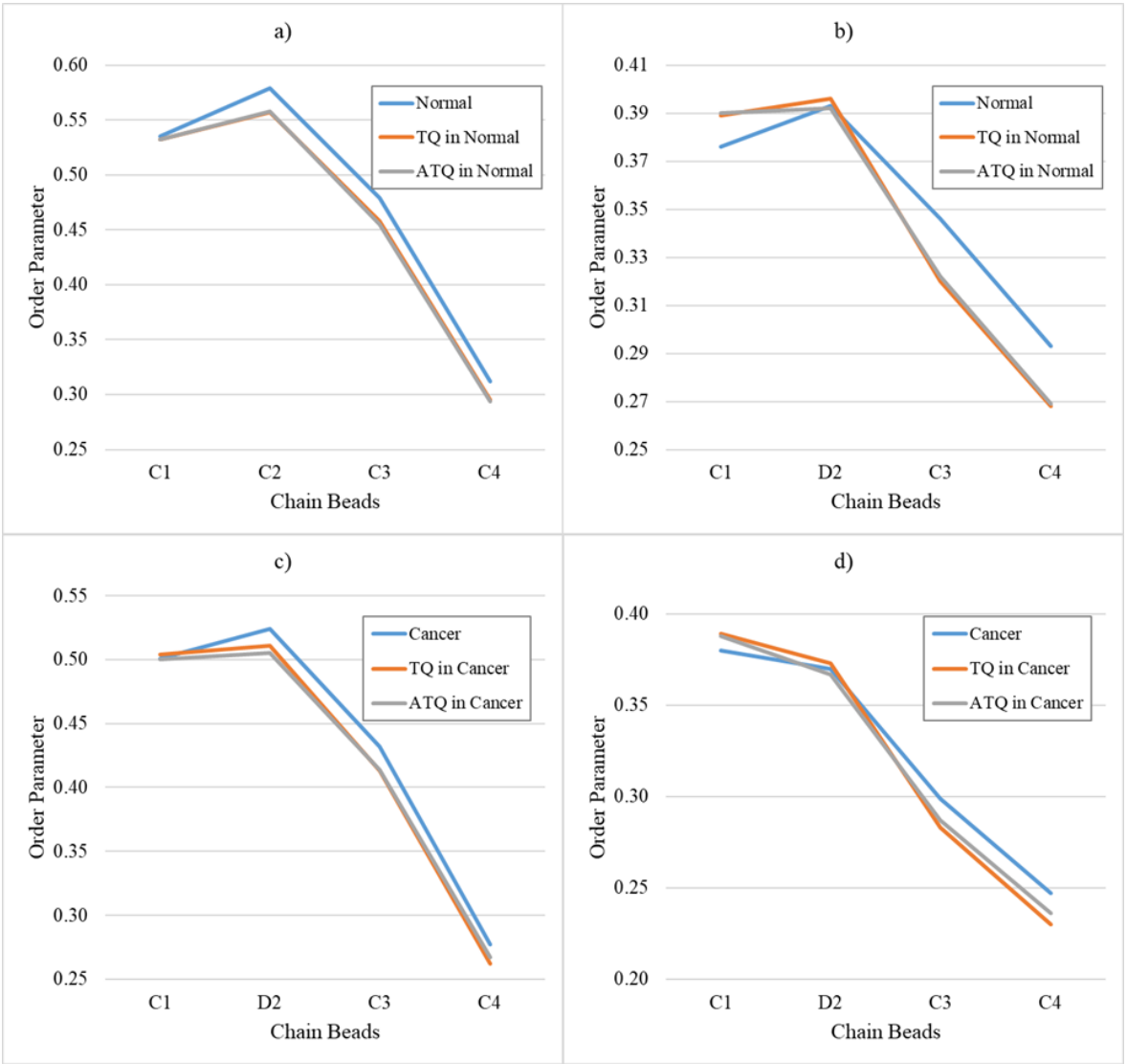

Figure 4.14. Order parameters of POPC a) sn1 and b) sn2 acyl chains in Model 2 normal cell bilayer, and c) sn1 and d) sn2 acyl chains in Model 2 cancer cell bilayer.

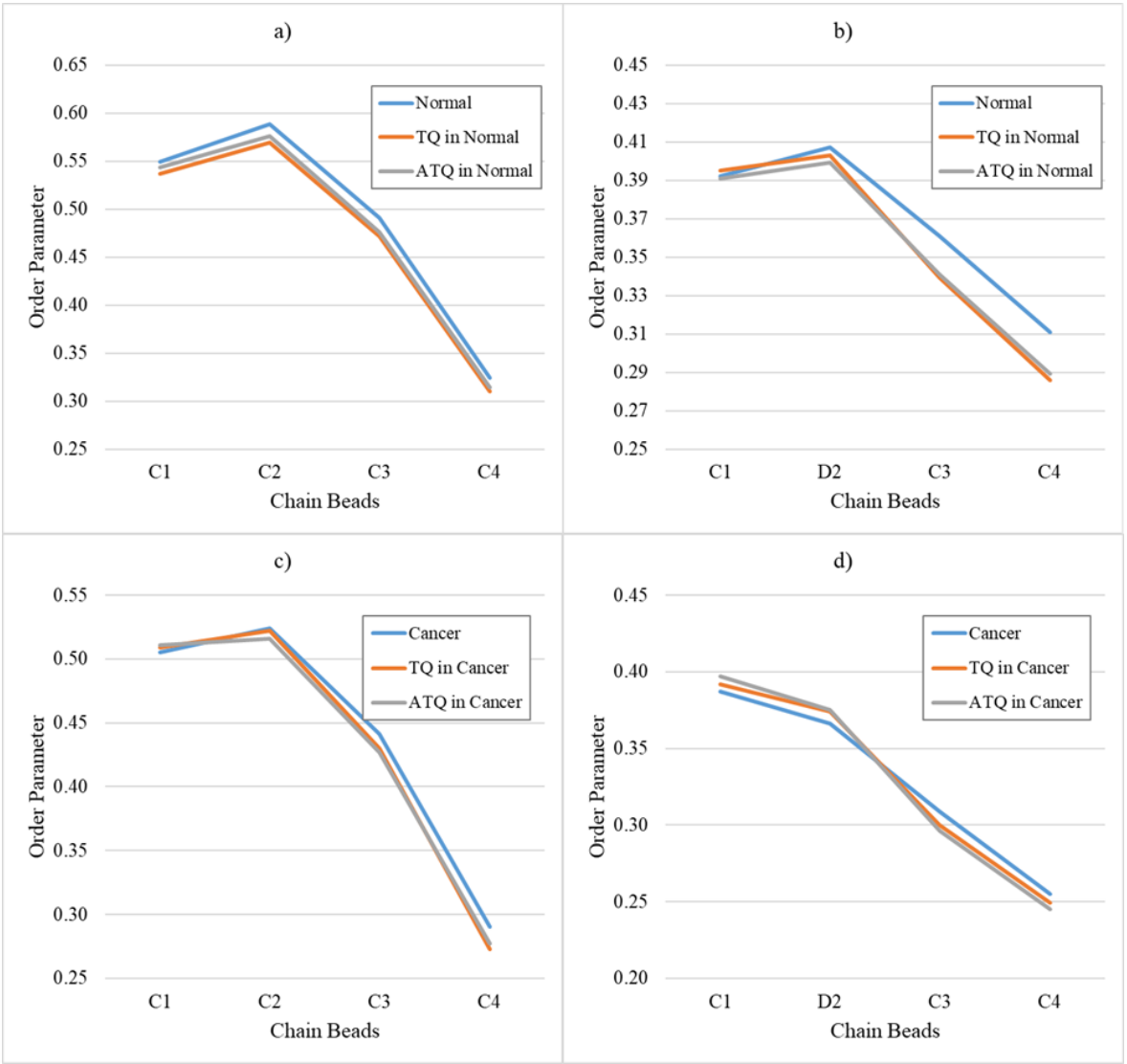

Figure 4.15. Order parameters of POPS a) sn1 and b) sn2 acyl chains in Model 1 normal cell bilayer, and c) sn1 and d) sn2 acyl chains in Model 2 cancer cell bilayer.

Thymoquinone and aminothymoquinone have similar disordering effects on the POPC lipids of normal and cancer membrane models as can be seen in Table 4.14. On the other hand, the disordering effect of thymoquinone and aminothymoquinone on POPS lipids in the normal cell membrane model is greater than in the cancer membrane model.

Table 4.16. Order parameters of acyl chains of POPC lipids in Model 2 normal and cancer cell bilayers.

		No TQ/ATQ	**100 TQ**	**100 ATQ**
Normal	**sn1 chain**	0.476	0.461	0.460
	sn2 chain	0.352	0.343	0.343
	Average	0.414	0.402	0.402
Cancer	**sn1 chain**	0.434	0.423	0.422
	sn2 chain	0.324	0.319	0.320
	Average	0.379	0.371	0.371

Table 4.17. Order parameters of acyl chains of POPS lipids in Model 2 normal and cancer cell bilayers.

		No TQ/ATQ	**100 TQ**	**100 ATQ**
Normal	**sn1 chain**	0.488	0.472	0.477
	sn2 chain	0.368	0.356	0.355
	Average	0.428	0.414	0.416
Cancer	**sn1 chain**	0.440	0.434	0.433
	sn2 chain	0.329	0.329	0.328
	Average	0.385	0.381	0.381

The percent change of the total average order parameters is calculated to compare the lipid disordering of all systems. A sample calculation of the percent difference of DOPC order parameters between Model 1 normal cell bilayer with and without thymoquinone is handled as

$$Change\% = \frac{|0.319 - 0.324|}{0.324} \times 100 = 1.62\%.$$

The changes in order parameters in presence of thymoquinone or aminothymoquinone molecules can be compared through the data given in Table 4.16. The highest disor-

dering is observed with Model 2 of normal cell membranes, and the least disordering effect is observed with Model 1 cancer cell membranes. In general, the disordering effect of the molecules have the same trend but are different in magnitude.

Table 4.18. Percent changes of order parameters between without and with thymoquinone and aminothymoquinone.

Model 1	**Normal**		**Cancer**	
	DOPC	**DOPS**	**DOPC**	**DOPS**
TQ	1.62	1.80	0.97	0.63
ATQ	0.54	0.30	0.64	0.31
Model 2	**Normal**		**Cancer**	
	POPC	**POPS**	**POPC**	**POPS**
TQ	2.90	3.27	2.11	1.04
ATQ	2.90	2.80	2.11	1.04

4.4.2. The Interaction of Thymoquinone and Aminothymoquinone with the Complex Bilayers

The angle between the thymoquinone and aminothymoquinone molecular vector and the bilayer normal was calculated to find the tilt angle of the corresponding molecules. The distribution of tilt angles demonstrates the orientation of thymoquinone and aminothymoquinone in the bilayer models. The tilt angle distributions are shown in Figure 4.16.

Both thymoquinone and aminothymoquinone have a higher probability to be between 50° and 130° in general. Thymoquinone prefers a parallel orientation in cancer membrane models while it is mostly tilted at 20°-40° in normal membrane models. Similarly, aminothymoquinone has the same trend as thymoquinone in terms of the orientations in complex bilayers, shown in Figure 4.16.

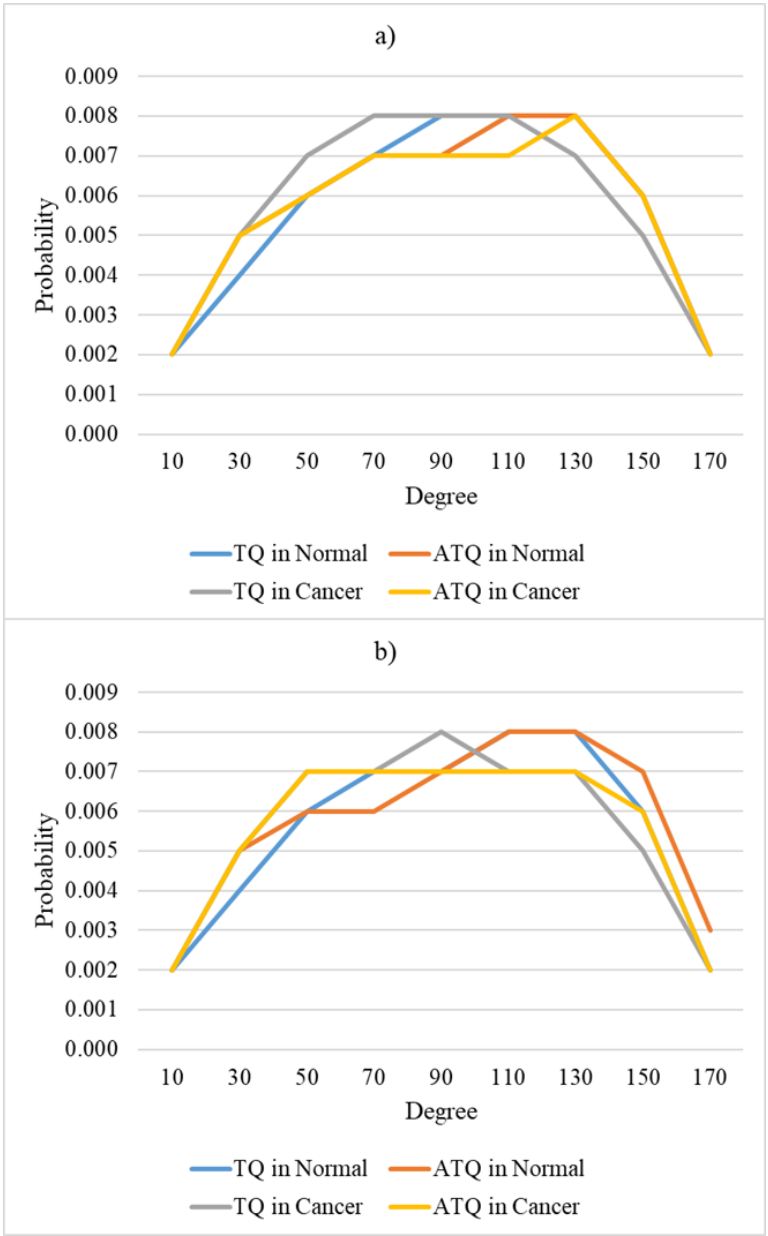

Figure 4.16. The orientation distribution of thymoquinone and aminothymoquinone in a) Model 1 and b) Model 2.

The density distribution of complex bilayers in the absence and presence of thymoquinone or aminothymoquinone are plotted with respect to the bilayer center. The graphs are given in Figures 4.17, 4.18, 4.19, and 4.20 and are zoomed in to demonstrate the distribution of thymoquinone and aminothymoquinone. The original density distributions can be found in Appendix A.5.

Thymoquinone and aminothymoquinone diffuse into the normal and cancer cell bilayer with both models. Thymoquinone is diffusing within all bilayer models, while aminothymoquinone tends to stay close to the phosphate groups. Thymoquinone is located away from the solvent due to its hydrophobicity, unlike aminothymoquinone.

In normal cell membranes of both models, thymoquinone and aminothymoquinone prefer to be more in the outer leaflet of the bilayer. The number of aminothymoquinone in the outer leaflet is higher than thymoquinone since aminothymoquinone prefers to stay near the phosphate groups. The interaction of both thymoquinone and aminothymoquinone with PC (phosphatidylcholine) lipids is higher than PS (phosphatidylserine) lipids, which is elaborated in the radial distribution function analysis.

The distribution of thymoquinone and aminothymoquinone share the same tendency in Model 1 and 2; only the peaks are sharper in Model 2 normal and cancer cell bilayers. Additionally, the ion distribution is different for normal and cancer cell bilayer models. Ions are located more in the inner leaflet of the normal bilayer, where the ratio of PC to PS lipids is 1:2 for both Model 1 and 2. The normal cell bilayer models are asymmetric and the neutralizing ions Na+ tend to stay near PS lipids. This explains the distribution of ions in the normal bilayer models. It is also important to note that the distribution of lipids, water, and ions does not change in the presence of thymoquinone and aminothymoquinone in all models.

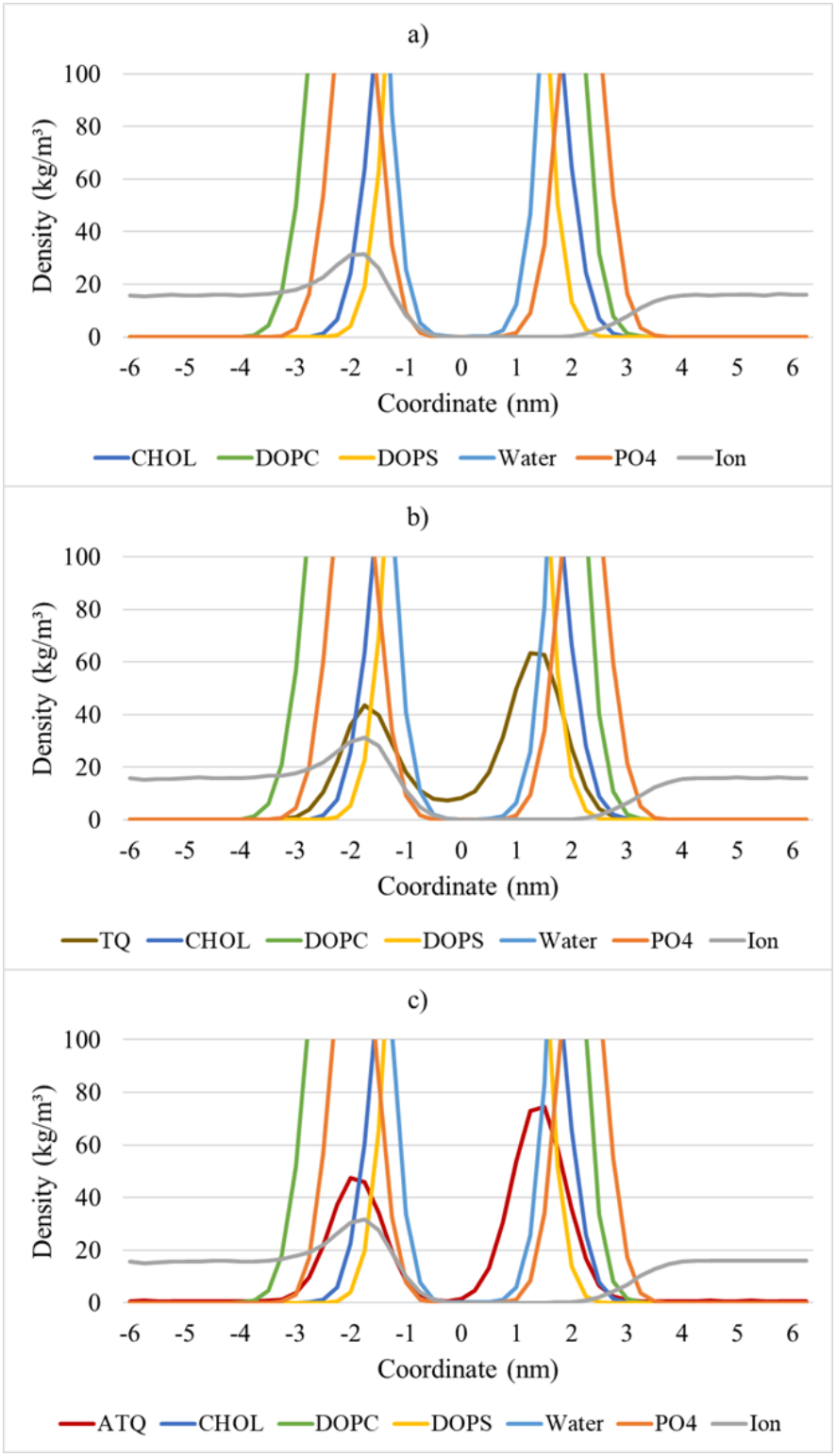

Figure 4.17. The density distribution of Model 1 normal cell bilayers a) without, and with b) thymoquinone, and c) aminothymoquinone.

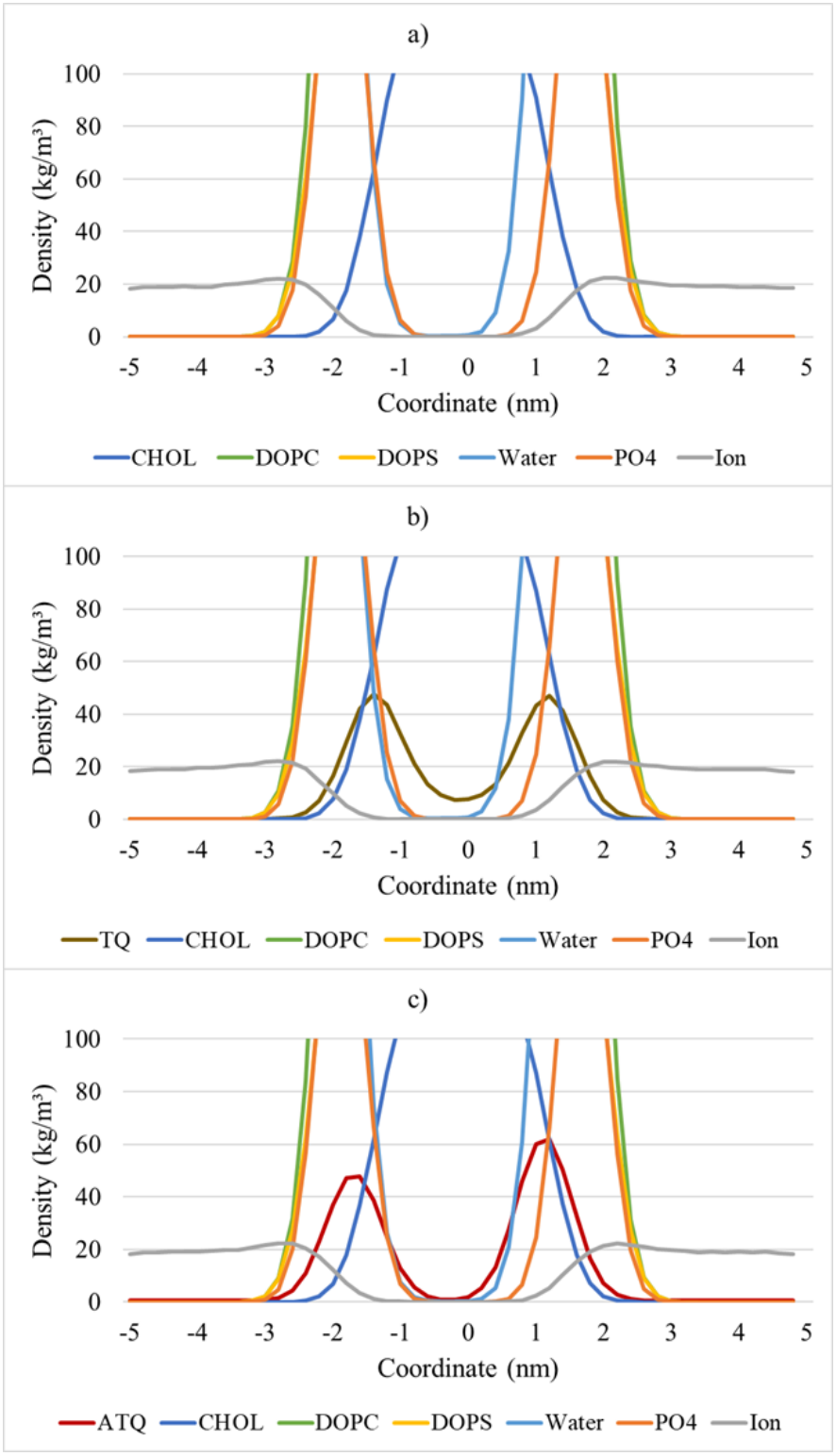

Figure 4.18. The density distribution of Model 1 cancer cell bilayers a) without, and with b) thymoquinone, and c) aminothymoquinone.

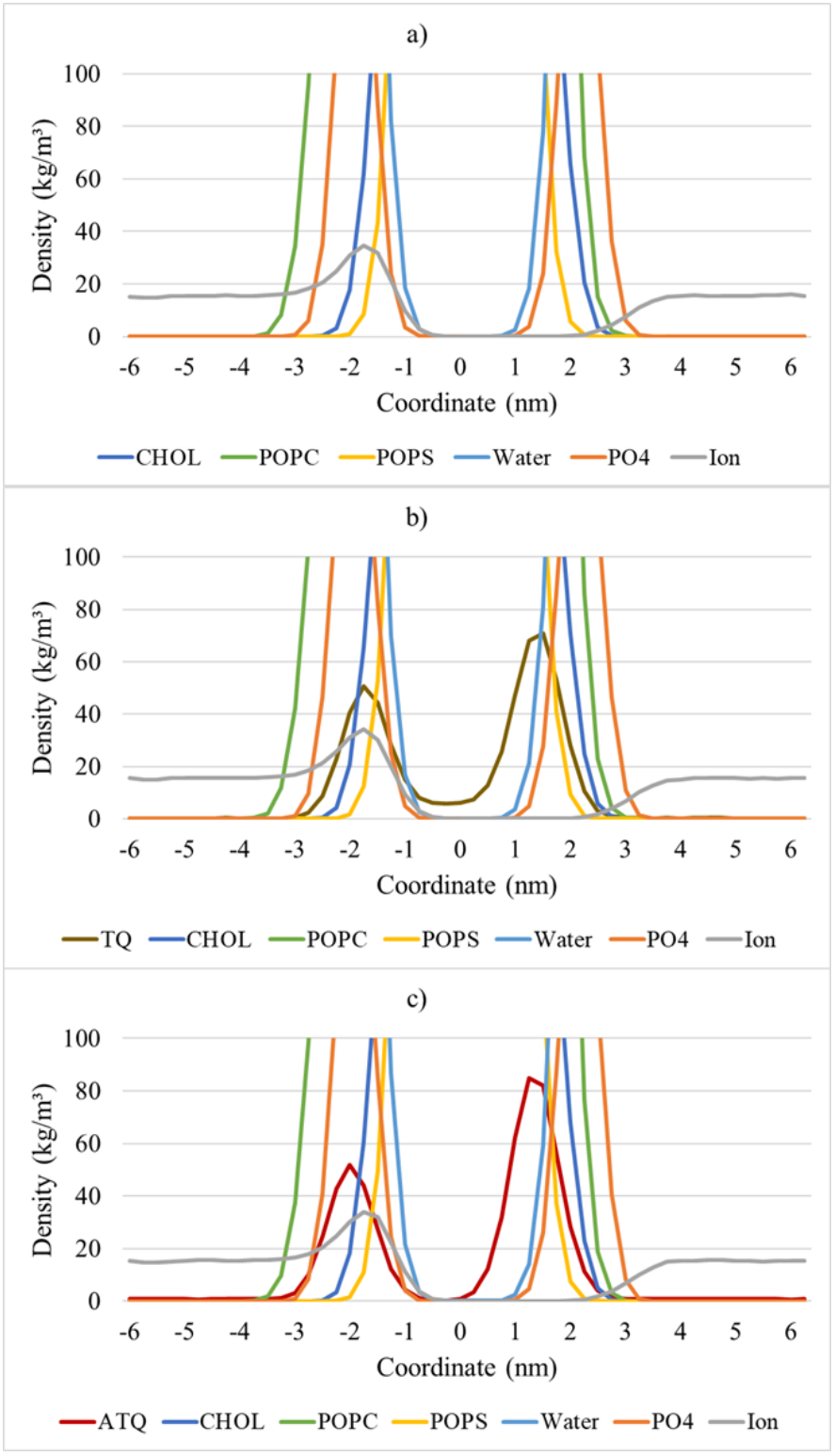

Figure 4.19. The density distribution of Model 2 normal cell bilayers a) without, and with b) thymoquinone, and c) aminothymoquinone.

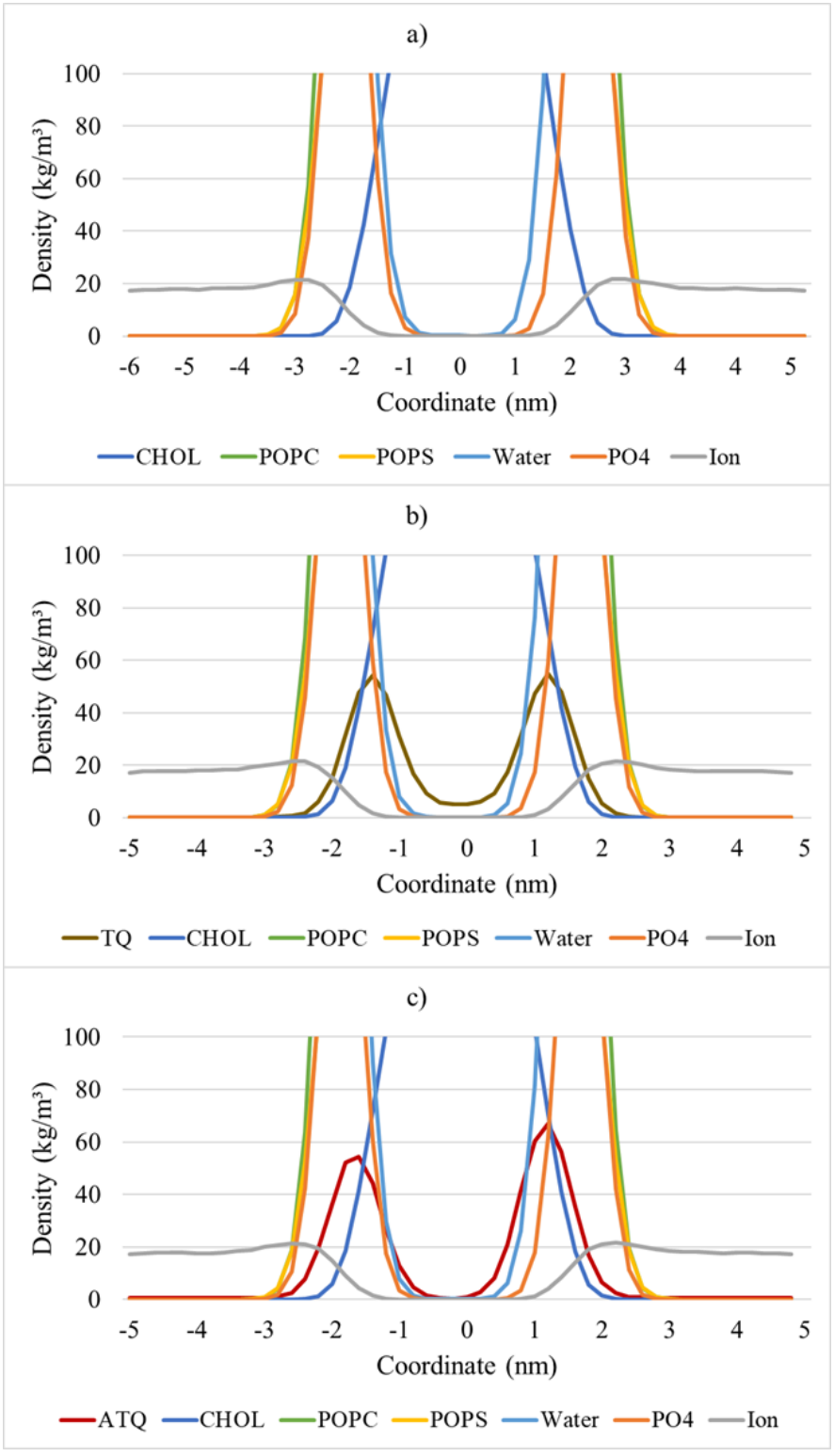

Figure 4.20. The density distribution of Model 2 cancer cell bilayers a) without, and with b) thymoquinone, and c) aminothymoquinone.

The radial distribution function of thymoquinone and aminothymoquinone with respect to cholesterol, DOPC, and DOPS molecules of Model 1, and cholesterol, POPC, and POPS molecules of Model 2 are calculated to observe their interactions with the lipids. Results are shown in Figures 4.21 and 4.22.

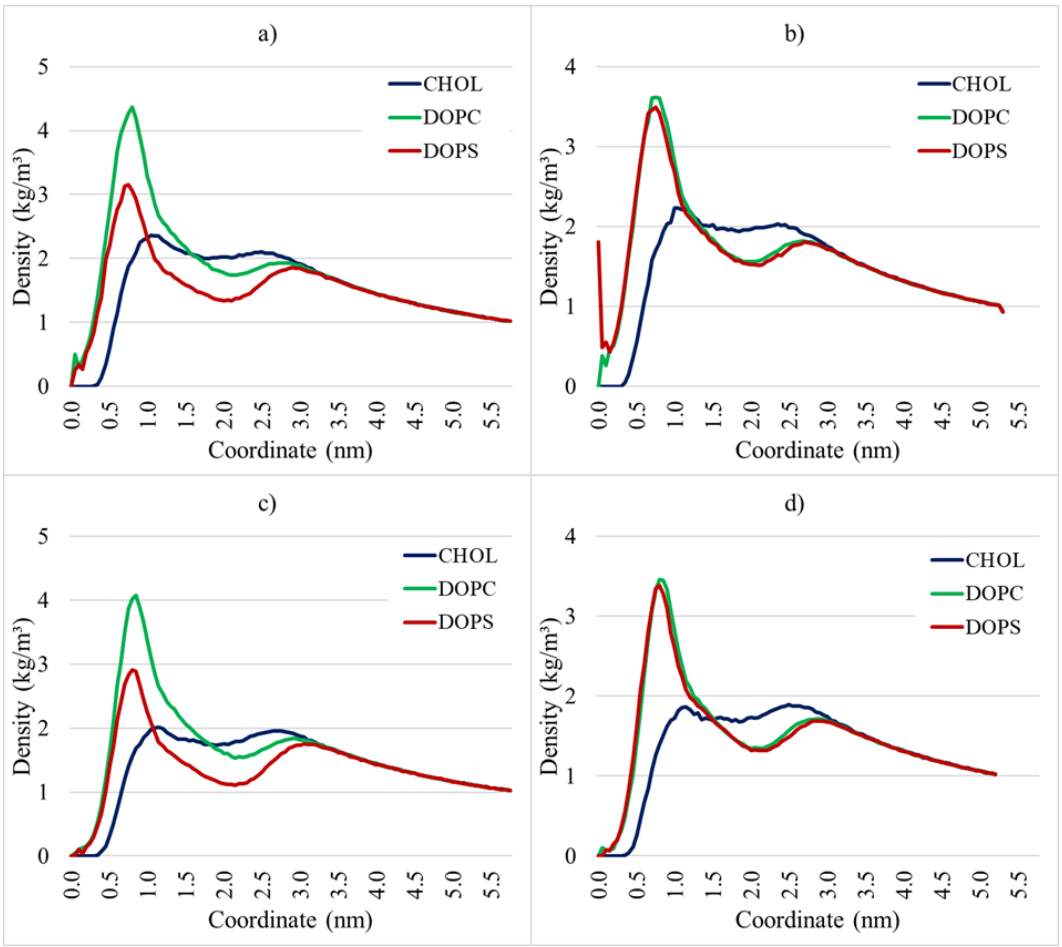

Figure 4.21. Radial distribution function of COM of thymoquinone with respect to COM of lipids of a) normal and b) cancer; and aminothymoquinone in c) normal and d) cancer bilayer Model 1.

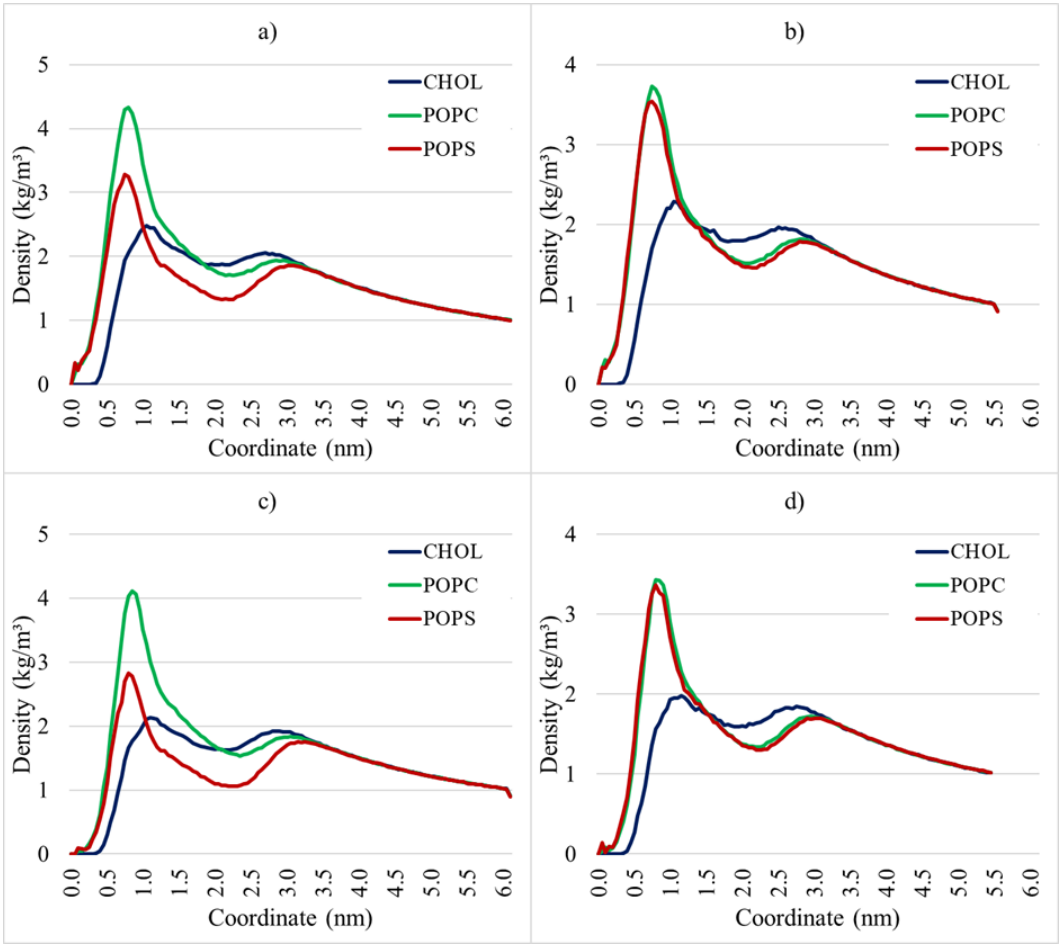

Figure 4.22. Radial distribution function of COM of thymoquinone with respect to COM of lipids of a) normal and b) cancer; and aminothymoquinone in c) normal and d) cancer bilayer Model 2.

The radial distribution of thymoquinone and aminothymoquinone show similar profiles in both normal and cancer cell membrane models. The interaction of the molecules with PS lipids is weaker in normal cell bilayers compared to cancer bilayers with both models. This finding supports the density profile of thymoquinone and aminothymoquinone molecules in normal bilayer models, showing a tendency to stay close to PC lipids, and can be seen in Figures 4.17 and 4.19. Both molecules have weaker interactions with cholesterol, where thymoquinone has slightly greater interaction than aminothymoquinone. The peaks of PC lipids are higher in normal bilayers compared to the cancer bilayer in all models, indicating that the interaction of thymoquinone and aminothymoquinone with PC lipids decreases inside the cancer bilayer

models. On the other hand, with all models the peak values for PS lipids increase in cancer cell membranes, indicating stronger interaction of the molecules with PS lipids. No significant change in the interaction of thymoquinone with cholesterol is observed in Model 1 membranes. However, the interactions slightly decrease in the cancer membrane of Model 2 in the presence of aminothymoquinone.

5. CONCLUSION

The aim of this study was to investigate the interaction between thymoquinone and its derivative aminothymoquinone with lipid bilayers using MD simulations on atomistic and coarse-grained scales. MD simulations provide the time evolution of the systems with small drug molecules that have experimental limitations. The coarse-grained models of thymoquinone and aminothymoquinone were developed to offer a practical alternative to the atomistic models and observe the behavior of these phytochemicals using a lower-cost simulation method.

The atomistic simulations were conducted to reproduce the chemical and dynamic properties of thymoquinone and aminothymoquinone using the OPLS-AA force field. Partitioning free energies in water and 1-octanol were calculated and the logP values were compared to the experimental data before the construction of the coarse-grained models. The simple bilayers, consisting of DOPC and POPC lipids, were simulated without and with one or 10 thymoquinone molecules to generate a reference for the coarse-grained bilayer simulations. The results from the analysis of bilayer-only systems were compared with the experimental findings and other computational studies.

The coarse-grained models of thymoquinone and aminothymoquinone were constructed using MARTINI 3.0.0 force field. The molecules were represented by four beads, and bonds, constraints, and improper dihedrals were defined. The logP values of thymoquinone and aminothymoquinone were calculated from the transfer free energies and compared with the ones from atomistic simulations. After obtaining a good agreement between atomistic and coarse-grained bonded and nonbonded interactions, the coarse-grained simple bilayers consisting of DOPC and POPC were run with or without thymoquinone molecules to observe the properties.

Application of coarse-grained thymoquinone and aminothymoquinone models to normal and cancer cell membrane models was performed. Two types of complex models

were used. Model 1 included cholesterol, DOPC and DOPS lipids, and Model 2 included cholesterol, POPC and POPS lipids. The properties of bilayers both in the absence and presence of thymoquinone or aminothymoquinone were analyzed to observe their properties.

The structural changes of the bilayers were measured by analyzing the area per lipid, bilayer thickness, lateral diffusion coefficient, and order parameters of lipid chains. Moreover, the interaction of thymoquinone or aminothymoquinone molecules with bilayers was demonstrated by analyzing the orientation of the molecules in the bilayers, the radial distribution functions, and the density distributions of the bilayer. From the free energy calculations of thymoquinone and aminothymoquinone, logP values were found as 2.72 and 1.82, respectively, in the atomistic simulations. These values were 2.52 and 1.65, respectively, in the coarse-grained simulations with error percentages of 7.31% and 9.34%. All logP values were in the acceptable range compared with the data from the literature.

The structural properties of DOPC/POPC-only bilayers were in the range of the reported values, with slight but acceptable deviations. The structural change in simple bilayers in the presence of thymoquinone molecules demonstrated a similar trend in DOPC and POPC bilayers by increasing the area per lipid and decreasing the bilayer thickness slightly. Introducing thymoquinone to the bilayer systems increased the lateral diffusion coefficients of the lipid phosphate groups. Thymoquinone had slight ordering and disordering effects on DOPC and POPC bilayers, respectively. The number of thymoquinone diffused into the bilayers was lower in the atomistic simulations compared to the coarse-grained ones, due to the requirement for longer simulation time. The interaction of thymoquinone with DOPC and POPC lipids was observed in an opposite trend depending on the increase of thymoquinone concentration. Thymoquinone molecules interacted with POPC lipid when its concentration increased, and the opposite effect on DOPC lipids were observed.

Both thymoquinone and aminothymoquinone had a bilayer thinning effect on the complex bilayers by increasing the area per lipid and decreasing the thickness. The diffusion coefficient of cholesterol was the greatest among the other lipids in all models, while the highest diffusion rate was obtained in Model 1 cancer membrane in the presence of aminothymoquinone. The highest disordering was observed in Model 1 cancer membranes in the presence of both thymoquinone and aminothymoquinone with the percent change in the order parameters of POPC and POPS lipids as 2.80 and 3.27, respectively. Both thymoquinone and aminothymoquinone preferred to have parallel or near parallel orientation in the membrane models. Thymoquinone diffused through the membrane models while aminothymoquinone tended to stay near the phosphate groups. Both thymoquinone and aminothymoquinone interacted the most with the PC lipids. However, the interaction of both molecules with PS lipids significantly increased in the cancer membrane models. Both molecules showed the same interaction profile in the membrane models besides demonstrating a higher interaction with PC lipids in normal membrane models.

In general, the atomistic models reproduced the properties of thymoquinone and aminothymoquinone while the coarse-grained models showed similar trends to the results from atomistic simulations. The application of thymoquinone and aminothymoquinone to the complex membrane models demonstrated that both molecules had the same trend but with different magnitude in their effects.

For further studies, a different force field can be used for the lipid-only simple bilayers, such as CHARMM, GROMOS, or AMBER force fields, to eliminate the deviations of the results in atomistic simulations from the reported experimental data. In that case, thymoquinone and aminothymoquinone parameters need to be adjusted to adapt to the corresponding forcefields. Additionally, the longer simulation time can be applied to the atomistic simulations if a study is designed to be lasted for longer time periods, in order to observe the time evolution of a system in higher resolutions. Lastly, the interaction of thymoquinone and aminothymoquinone with more complex bilayer models can be studied.

REFERENCES

1. Winston, J. C., "Pythochemicals: Guardians of Our Health", *Journal of American Dietetic Association*, Vol. 97, No. 10, pp. 199–204, 1997.

2. Dillard, C. J. and J. B. German, "Phytochemicals: Nutraceuticals and Human Health", *Journal of the Science of Food and Agriculture*, Vol. 80, No. 12, pp. 1744–1756, 2000.

3. Johnson, I. T., "Phytochemicals and Cancer", *Proceedings of the Nutrition Society*, Vol. 66, No. 2, pp. 207–215, 2007.

4. Almajali, B., H. A. N. Al-Jamal, W. R. W. Taib, I. Ismail, M. F. Johan, A. A. Doolaanea and W. N. Ibrahim, "Thymoquinone, as a Novel Therapeutic Candidate of Cancers", *Pharmaceuticals*, Vol. 14, No. 4, p. 369, 2021.

5. Darakhshan, S., A. B. Pour, A. H. Colagar and S. Sisakhtnezhad, "Thymoquinone and Its Therapeutic Potentials", *Pharmacological Research*, Vol. 95-96, pp. 138–158, 2015.

6. Schneider-Stock, R., I. H. Fakhoury, A. M. Zaki, C. O. El-Baba and H. U. Gali-Muhtasib, "Thymoquinone: Fifty Years of Success in the Battle against Cancer Models", *Drug Discovery Today*, Vol. 19, No. 1, pp. 18–30, 2014.

7. Glamoclija, U., S. Padhye, S. Spirtovic-Halilovic, A. Osmanovic, E. Veljovic, S. Roca, I. Novakovic, B. Mandic, I. Turel, J. Kljun, S. Trifunovic, E. Kahrovic, S. K. Pavelic, A. Harej, M. Klobucar and D. Završnik, "Synthesis, Biological Evaluation and Docking Studies of Benzoxazoles Derived from Thymoquinone", *Molecules*, Vol. 23, No. 12, 2018.

8. Faulkner, C., D. Santos-Carballal, D. Santos-Carballal, D. F. Plant, N. H. de Leeuw and N. H. de Leeuw, "Atomistic Molecular Dynamics Simulations

of Propofol and Fentanyl in Phosphatidylcholine Lipid Bilayers", *ACS Omega*, Vol. 5, No. 24, pp. 14340–14353, 2020.

9. Ribeiro, I. A. C., C. M. C. Faustino, R. C. Guedes, A. J. I. Alfaia, and M. H. L. Ribeiro, "Exploring Drug Diffusion through a Membrane: A Physical Chemistry Experiment for Health and Life Sciences Undergraduate Students", *Journal of Chemical Education*, Vol. 92, No. 5, pp. 924–927, 2015.

10. Dowhan, W., "Understanding Phospholipid Function: Why Are There So Many Lipids?", *Journal of Biological Chemistry*, Vol. 292, No. 26, pp. 10755–10766, 2017.

11. Miguel, V., M. E. D. Lestard, M. E. Tuttolomondo, S. B. Díaz, A. B. Altabef, M. Puiatti and A. B. Pierini, "Molecular View of the Interaction of S-methyl Methanethiosulfonate with DPPC Bilayer", *Biochimica et Biophysica Acta (BBA) - Biomembranes*, Vol. 1858, No. 1, pp. 38–46, 2016.

12. Benz, R. W., F. Castro-Román, D. J. Tobias and S. H. White, "Experimental Validation of Molecular Dynamics Simulations of Lipid Bilayers: A New Approach", *Biophysical Journal*, Vol. 88, No. 2, pp. 805–817, 2005.

13. Monticelli, L., S. K. Kandasamy, X. Periole, R. G. Larson, D. P. Tieleman and S. J. Marrink, "The MARTINI Coarse-Grained Force Field: Extension to Proteins", *Journal of Chemical Theory and Computation*, Vol. 4, No. 5, pp. 819–834, 2008.

14. Baron, R., A. H. de Vries, P. H. Hünenberger and W. F. van Gunsteren, "Comparison of Atomic-Level and Coarse-Grained Models for Liquid Hydrocarbons from Molecular Dynamics Configurational Entropy Estimates", *Journal of Physical Chemistry B*, Vol. 110, No. 16, pp. 8464–8473, 2006.

15. Kmiecik, S., D. Gront, M. Kolinski, L. Wieteska, A. E. Dawid and A. Kolinski, "Coarse-Grained Protein Models and Their Applications", *Chemical Reviews*, Vol.

116, No. 14, pp. 7898–7936, 2016.

16. Wang, J., R. M. Wolf, J. W. Caldwell, P. A. Kollman and D. A. Case, "Development and Testing of a General Amber Force Field", *Journal of Computational Chemistry*, Vol. 25, No. 9, pp. 1157–1174, 2004.

17. Brooks, B. R., C. L. B. III, A. D. M. Jr., L. Nilsson, R. J. Petrella, B. Roux, Y. Won, G. Archontis, C. Bartels, S. Boresch, A. Caflisch, L. Caves, Q. Cui, A. R. Dinner, M. Feig, S. Fischer, J. Gao, M. Hodoscek, W. Im, K. Kuczera, T. Lazaridis, J. Ma, V. Ovchinnikov, E. Paci, R. W. Pastor, C. B. Post, J. Z. Pu, M. Schaefer, B. Tidor, R. M. Venable, H. L. Woodcock, X. Wu, W. Yang, D. M. York and M. Karplus, "CHARMM: The Biomolecular Simulation Program", *Journal of Computational Chemistry*, Vol. 30, No. 10, pp. 1545–1614, 2009.

18. Christen, M., P. H. Hünenberger, D. Bakowies, R. Baron, R. Bürgi, D. P. Geerke, T. N. Heinz, M. A. Kastenholz, V. Kräutler, C. Oostenbrink, C. Peter, D. Trzesniak and W. F. van Gunsteren, "The GROMOS Software for Biomolecular Simulation: GROMOS05", *Journal of Computational Chemistry*, Vol. 26, No. 16, pp. 1719–1751, 2005.

19. Jorgensen, W. L., D. S. Maxwell, and J. Tirado-Rives, "Development and Testing of the OPLS All-Atom Force Field on Conformational Energetics and Properties of Organic Liquids", *Journal of the American Chemical Society*, Vol. 118, No. 45, pp. 11225–11236, 1996.

20. Levitt, M. and S. Lifson, "Refinement of Protein Conformations Using a Macromolecular Energy Minimization Procedure", *Journal of Molecular Biology*, Vol. 46, No. 2, pp. 269–279, 1969.

21. Marrink, S. J., H. J. Risselada, S. Yefimov, D. P. Tieleman and A. H. de Vries, "The MARTINI Force Field: Coarse Grained Model for Biomolecular Simula-

tions", *Journal of Physical Chemistry B*, Vol. 111, No. 27, pp. 7812–7824, 2007.

22. Leitzmann, C., "Characteristics and Health Benefits of Phytochemicals", *Forschende Komplementarmedizin*, Vol. 23, No. 2, pp. 69–74, 2016.

23. Liu, R. H., "Health-Promoting Components of Fruits and Vegetables in the Diet", *Advances in Nutrition*, Vol. 4, No. 3, 2013.

24. Ahmad, N., R. Ahmad, A. Al-layly, H. Al-shawi, A. Al-ali, M. Amir and A. Mostafa, "Ultra-High-Performance Liquid Chromatography-Based Identification and Quantification of Thymoquinone in Nigella Sativa Extract from Different Geographical Regions", *Pharmacognosy Magazine*, Vol. 14, No. 57, p. 471, 2018.

25. Dastjerdi, M. N., E. M. Mehdiabady, F. G. Iranpour and H. Bahramian, "Effect of Thymoquinone on P53 Gene Expression and Consequence Apoptosis in Breast Cancer Cell Line", *International Journal of Preventive Medicine*, Vol. 7, No. 1, p. 66, 2016.

26. Chen, M., N. Lee, H. Hsu, T. Ho, C. Tu, D. J. Hsieh, Y. Lin, L. Chen, W. Kuo and C. Huang, "Thymoquinone Induces Caspase-Independent, Autophagic Cell Death in CPT-11-Resistant LoVo Colon Cancer via Mitochondrial Dysfunction and Activation of JNK and P38", *Journal of Agricultural and Food Chemistry*, Vol. 63, No. 5, pp. 1540–1546, 2015.

27. Pang, J., N. Shen, F. Yan, N. Zhao, L. Dou, L. Wu, C. L. Seiler, L. Yu, K. Yang, V. Bachanova, E. Weaver, N. Y. Tretyakova and S. Liu, "Thymoquinone Exerts Potent Growth-Suppressive Activity on Leukemia through DNA Hypermethylation Reversal in Leukemia Cells", *Oncotarget*, Vol. 8, No. 21, p. 34453, 2017.

28. Yang, J., X. Kuang, P. Lv and X. Yan, "Thymoquinone Inhibits Proliferation and Invasion of Human Nonsmall-Cell Lung Cancer Cells via ERK Pathway", *Tumour Biology*, Vol. 36, No. 1, pp. 259–269, 2015.

29. Jeong, H., S. M. Yu, and S. J. Kim, "Inhibitory Effects on Melanogenesis by Thymoquinone Are Mediated through the β-Catenin Pathway in B16F10 Mouse Melanoma Cells", *International Journal of Oncology*, Vol. 56, No. 1, pp. 379–389, 2020.

30. Kou, B., W. Liu, W. Zhao, P. Duan, Y. Yang, Q. Yi, F. Guo, J. Li, J. Zhou and Q. Kou, "Thymoquinone Inhibits Epithelial-Mesenchymal Transition in Prostate Cancer Cells by Negatively Regulating the TGF-β/Smad2/3 Signaling Pathway", *Oncology Reports*, Vol. 38, No. 6, pp. 3592–3598, 2017.

31. Johnson-Ajinwo, O. R., A. Richardson and W. Li, "Synthesis and Evaluation of Thymoquinone Analogues as Anti-Ovarian Cancer Agents", *The 2nd Molecules Medicinal Chemistry Symposium (MMCS): Facing Novel Challenges in Drug Discovery*, Barcelona, Spain, 2019.

32. Bhosale, M., A. Jamadar, A. K. D. Klair and S. Padhye, "X-Ray Crystal Structure of Aminothymoquinone and Its Interaction with Human Serum Albumin at Physiological Conditions", *Biomedical Journal of Scientific & Technical Research*, Vol. 38, No. 3, 2021.

33. Salem, A. E., A. Ain, I. et Haty, I. Abdou, A. Adem and S. Attoub, "Terpene Conjugates of the Nigella Sativa Seed-Oil Constituent Thymoquinone with Enhanced Efficacy in Cancer Cells", U.S. Patent 10501428 B2, 10 December 2019, https://patents.google.com/patent/US10501428B2/en?oq=US10501428B2, accessed on July 8, 2022.

34. Gobinath, P., P. Packialakshmi, A. A. Hatamleh, M. A. Al-Dosary, Y. A. Al-Wasel, R. Balasubramani, R. Surendrakumar and A. Idhayadhulla, "Calotropis Gigantea Assisted Synthesis of Zinc Oxide Nanoparticle Catalysis: Synthesis of Novel 3-Amino Thymoquinone Connected 1,4-Dihyropyridine Derivatives and Their Cytotoxic Activity", *Journal of Nanomaterials*, Vol. 2022, No. 4, pp. 1–10, 2022.

35. Salem, M. L., "Immunomodulatory and Therapeutic Properties of the Nigella Sativa L. Seed", *International Immunopharmacology*, Vol. 5, No. 13-14, pp. 1749–1779, 2005.

36. Tekeoğlu, I., A. Dogan, L. Ediz, M. Budancamanak and A. Demirel, "Effects of Thymoquinone (Volatile Oil of Black Cumin) on Rheumatoid Arthritis in Rat Models", *Phytotheraphy Research*, Vol. 21, No. 9, pp. 895–897, 2007.

37. Mahgoub, A. A., "Thymoquinone Protects against Experimental Colitis in Rats", *Toxicology Letters*, Vol. 143, No. 2, pp. 133–143, 2003.

38. Al-Ghamdi, M. S., "The Anti-Inflammatory, Analgesic and Antipyretic Activity of Nigella Sativa", *Journal of Ethnopharmacology*, Vol. 76, No. 1, pp. 45–48, 2001.

39. Nagi, M. N. and M. A. Mansour, "Protective Effect of Thymoquinone against Doxorubicin-Induced Cardiotoxicity in Rats: A Possible Mechanism of Protection", *Pharmacological Research*, Vol. 41, No. 3, pp. 283–289, 2000.

40. Mansour, M. A., M. N. Nagi, A. S. El-Khatib and A. M. Al-Bekairi, "Effects of Thymoquinone on Antioxidant Enzyme Activities, Lipid Peroxidation and DT-Diaphorase in Different Tissues of Mice: A Possible Mechanism of Action", *Cell Biochemistry and Function*, Vol. 20, No. 2, pp. 143–151, 2002.

41. Salmani, J. M. M., S. Asghar, H. Lv and J. Zhou, "Aqueous Solubility and Degradation Kinetics of the Phytochemical Anticancer Thymoquinone; Probing the Effects of Solvents, PH and Light", *Molecules*, Vol. 19, No. 5, p. 5925, 2014.

42. Kanter, M., "Thymoquinone Attenuates Lung Injury Induced by Chronic Toluene Exposure in Rats", *Toxicology and Industrial Health*, Vol. 27, No. 5, pp. 387–395, 2010.

43. Jain, A., V. Pooladanda, U. Bulbake, S. Doppalapudi, T. A. Rafeeqi, C. Godugu and W. Khan, "Liposphere Mediated Topical Delivery of Thymoquinone in the

Treatment of Psoriasis", *Nanomedicine: Nanotechnology, Biology and Medicine*, Vol. 13, No. 7, pp. 2251–2262, 2017.

44. Woo, C., S. Loo, V. Gee, C. Yap, G. Sethi, A. P. Kumar and K. H. B. Tan, "Anticancer Activity of Thymoquinone in Breast Cancer Cells: Possible Involvement of PPAR-γ Pathway", *Biochemical Pharmacology*, Vol. 82, No. 5, pp. 464–475, 2011.

45. El-Baba, C., V. Mahadevan, F. B. Fahlbusch, S. S. Mohan, T. T. Rau, H. Gali-Muhtasib and R. Schneider-Stock, "Thymoquinone-Induced Conformational Changes of PAK1 Interrupt Prosurvival MEK-ERK Signaling in Colorectal Cancer", *Molecular Cancer*, Vol. 13, No. 1, 2014.

46. Yin, Z., Y. Song and P. H. Rehse, "Thymoquinone Blocks pSer/pThr Recognition by Plk1 Polo-Box Domain as a Phosohate Mimic", *ACS Chemical Biology*, Vol. 8, No. 2, pp. 303–308, 2013.

47. Parbin, S., a. Shilpi, S. Kar, N. Pradhan, D. Sengupta, M. Deb, S. K. Rath and S. K. Patra, "Insights into the Molecular Interactions of Thymoquinone with Histone Deacetylase: Evaluation of the Therapeutic Intervention Potential against Breast Cancer", *Molecular BioSystems*, Vol. 12, No. 1, pp. 48–58, 2016.

48. Saffari-Chaleshtori, J., E. Heidari-Sureshjani, F. Moradi and E. Heidarian, "The Effects of Thymoquinone on Viability, and Anti-Apoptotic Factors (BCL-XL, BCL-2, MCL-1) in Prostate Cancer (PC3) Cells: An In Vitro and Computer-Simulated Environment Study", *Advanced Pharmaceutical Bulletin*, Vol. 9, No. 3, p. 490–496, 2019.

49. Srivastava, N., P. Garg, P. Srivastava and P. K. Seth, "A Molecular Dynamics Simulation Study of the ACE2 Receptor with Screened Natural Inhibitors to Identify Novel Drug Candidate against COVID-19", *PeerJ*, Vol. 9, 2021.

50. Xu, H., B. Liu, Z. Xiao, M. Zhou, L. Ge, F. Jia, Y. Liu, H. Jin, X. Zhu, J. Gao, J. Akhtar, B. Xiang, K. Tan and G. Wang, "Computational and Experimental Studies Reveal That Thymoquinone Blocks the Entry of Coronaviruses Into In Vitro Cells", *Infectious Diseases and Therapy*, Vol. 10, No. 1, pp. 483–494, 2021.

51. Khan, M. T., A. Ali, X. Wei, T. Nadeem, S. Muhammad, A. G. Al-Sehemi and D. Wei, "Inhibitory Effect of Thymoquinone from Nigella Sativa against SARS-CoV-2 Main Protease. An In-Silico Study", *Brazilian Journal of Biology*, Vol. 84, 2022.

52. Alam, S., T. Mohammad, R. A. Padder, M. I. Hassan and M. Husain, "Thymoquinone and Quercetin Induce Enhanced Apoptosis in Non-Small Cell Lung Cancer in Combination through the Bax/Bcl2 Cascade", *Journal of Cellular Biochemistry*, Vol. 123, No. 2, pp. 259–274, 2022.

53. Zhou, J., S. Imani, M. D. Shasaltaneh, S. Liu, T. Lu and J. Fu, "PIK3CA Hotspot Mutations p. H1047R and p. H1047L Sensitize Breast Cancer Cells to Thymoquinone Treatment by Regulating the PI3K/Akt1 Pathway", *Molecular Biology Reports*, Vol. 49, No. 3, p. 1799–1816, 2022.

54. Taghvaei, S., F. Sabouni, and Z. Minuchehr, "Identification of Natural Products as SENP2 Inhibitors for Targeted Therapy in Heart Failure", *Frontiers in Pharmacology*, Vol. 13, 2022.

55. Yusufi, M., S. Banerjee, M. Mohammad, S. Khatal, K. V. Swamy, E. M. Khan, A. Aboukameel, F. H. Sarkar and S. Padhye, "Synthesis, Characterization and Anti-Tumor Activity of Novel Thymoquinone Analogs against Pancreatic Cancer", *Bioorganic and Medicinal Chemistry Letters*, Vol. 23, No. 10, p. 3101–3104, 2013.

56. Katiyar, R. S. and P. K. Jha, "Molecular Simulations in Drug Delivery: Opportunities and Challenges", *Wiley Interdisciplinary Reviews: Computational Molec-*

ular Science, Vol. 8, No. 4, 2018.

57. Eid, J., A. Jraij, H. Greige-Gerges and L. Monticelli, "Effect of Quercetin on Lipid Membrane Rigidity: Assessment by Atomic Force Microscopy and Molecular Dynamics Simulations", *Biochimica et Biophysica Acta (BBA) Advances*, Vol. 1, 2021.

58. Ingólfsson, H. I., P. Thakur, K. F. Herold, E. A. Hobart, N. B. Ramsey, X. Periole, D. H. de Jong, M. Zwama, D. Yilmaz, K. Hall, T. Maretzky, H. C. Hemmings, C. Blobel, S. J. Marrink, A. Kocer, J. t. Sack and O. S. Andersen, "Phytochemicals Perturb Membranes and Promiscuously Alter Protein Function", *ACS Chemical Biology*, Vol. 9, No. 8, pp. 1788–1798, 2014.

59. Saha, S., E. Panieri, S. Suzen, and L. Saso, "The Interaction of Flavonols with Membrane Components: Potential Effect on Antioxidant Activity", *Journal of Membrane Biology*, Vol. 253, No. 1, pp. 57–71, 2020.

60. Paquet, E. and H. L. Viktor, "Molecular Dynamics, Monte Carlo Simulations, and Langevin Dynamics: A Computational Review", *BioMed Research International*, Vol. 2015, pp. 1–18, 2015.

61. Gibbs, J. W., *Elementary Principles of Statistical Mechanics*, Yale University Press, New Haven, Connecticut, 1902.

62. Berendsen, H. J. C., J. P. M. Postma, W. F. van Gunsteren, A. Dinola and J. R. Haak, "Molecular Dynamics with Coupling to An External Bath", *The Journal of Chemical Physics*, Vol. 81, No. 8, pp. 3684–3690, 1984.

63. Nosé, S., "A Unified Formulation of the Constant Temperature Molecular Dynamics Methods", *The Journal of Chemical Physics*, Vol. 81, No. 1, p. 511, 1998.

64. Hoover, W. G., "Canonical Dynamics: Equilibrium Phase-Space Distributions", *Physical Review A*, Vol. 31, No. 3, p. 1695, 1985.

65. Bussi, G., D. Donadio and M. Parrinello, "Canonical Sampling through Velocity Rescaling", *The Journal of Chemical Physics*, Vol. 126, No. 1, p. 014101, 2007.

66. Parrinello, M. and A. Rahman, "Polymorphic Transitions in Single Crystals: A New Molecular Dynamics Method", *Journal of Applied Physics*, Vol. 52, No. 12, pp. 7182–7190, 1981.

67. Abraham, M. J., T. Murtola, R. Schulz, S. Páll, J. C. Smith, B. Hess and E. Lindahl, "GROMACS: High Performance Molecular Simulations through Multi-Level Parallelism from Laptops to Supercomputers", *SoftwareX*, Vol. 1-2, pp. 19–25, 2015.

68. Karplus, M. and J. A. McCammon, "Molecular Dynamics Simulations of Biomolecules", *Nature Structural Biology*, Vol. 9, No. 9, pp. 646–652, 2002.

69. Hollingsworth, S. A. and R. O. Dror, "Molecular Dynamics Simulation for All", *Neuron*, Vol. 99, No. 6, p. 1129–1143, 2018.

70. Leach, A. R., *Molecular Modelling: Principles and Applications*, Prentice Hall, 2001.

71. van Gunsteren, W. F. and H. J. C. Berendsen, "A Leap-Frog Algorithm for Stochastic Dynamics", *Molecular Simulation*, Vol. 1, No. 3, pp. 173–185, 1988.

72. Swope, W. C., H. C. Andersen, P. H. Berens and K. R. Wilson, "A Computer Simulation Method for the Calculation of Equilibrium Constants for the Formation of Physical Clusters of Molecules: Application to Small Water Clusters", *The Journal of Chemical Physics*, Vol. 76, No. 1, p. 637, 1998.

73. Hospital, A., J. R. Goñi, M. Orozco and J. L. Gelpí, "Molecular Dynamics Simulations: Advances and Applications", *Advances and Applications in Bioinformatics and Chemistry*, Vol. 8, No. 1, pp. 37–47, 2015.

74. Leckband, D. and J. Israelachvili, "Intermolecular Forces in Biology", *Quarterly Reviews of Biophysics*, Vol. 34, No. 2, pp. 105–267, 2001.

75. Chang, C. E. A., Y. M. M. Huang, L. J. Mueller and W. You, "Investigation of Structural Dynamics of Enzymes and Protonation States of Substrates Using Computational Tools", *Catalysts*, Vol. 6, No. 6, 2016.

76. May, A., R. Pool, E. van Dijk, J. Bijlard, S. Abeln, J. Heringa and K. A. Feenstra, "Coarse-Grained versus Atomistic Simulations: Realistic Interaction Free Energies for Real Proteins", *Bioinformatics*, Vol. 30, No. 3, pp. 326–334, 2013.

77. Souza, P. C. T., R. Alessandri, J. Barnoud, S. Thallmair, I. Faustino, F. Grünewald, I. Patmanidis, H. Abdizadeh, B. M. H. Bruininks, T. A. Wassenaar, P. C. Kroon, J. Melcr, V. Nieto, V. Corradi, H. M. khan, J. Domański, M. Javanainen, H. Martinez-Seara, N. Reuter, R. B. Best, I. Vattulainen, L. Monticelli, X. Periole, D. P. Tieleman, A. H. de Vries and S. J. Marrink, "Martini 3: A General Purpose Force Field for Coarse-Grained Molecular Dynamics", *Nature Methods*, Vol. 18, No. 4, pp. 382–388, 2021.

78. Marrink, S. J. and D. P. Tieleman, "Perspective on the Martini Model", *Chemical Society Reviews*, Vol. 42, No. 16, pp. 6801–6822, 2013.

79. Dodda, L. S., I. C. de Vaca, J. Tirado-Rives and W. L. Jorgensen, "LigParGen Web Server: An Automatic OPLS-AA Parameter Generator for Organic Ligands", *Nucleic Acids Research*, Vol. 45, No. W1, pp. W331–W336, 2017.

80. Humphrey, W., A. Dalke and K. Schulten, "VMD: Visual Molecular Dynamics", *Journal of Molecular Graphics*, Vol. 14, No. 1, pp. 33–38, 1996.

81. Kulig, W., M. Pasenkiewicz-Gierula and T. Róg, "Topologies, Structures and Parameter Files for Lipid Simulations in GROMACS with the OPLS-AA Force Field: DPPC, POPC, DOPC, PEPC, and Cholesterol", *Data in Brief*, Vol. 5,

pp. 333–336, 2015.

82. Shirts, M. R., J. W. Pitera, W. C. Swope and V. S. Pande, "Extremely Precise Free Energy Calculations of Amino Acid Side Chain Analogs: Comparison of Common Molecular Mechanics Force Fields for Proteins", *The Journal of Chemical Physics*, Vol. 119, No. 11, pp. 5740–5761, 2003.

83. Darden, T., D. York and L. Pedersen, "Particle Mesh Ewald: An N.log(N) Method for Ewald Sums in Large Systems", *Journal of Chemical Physics*, Vol. 98, No. 12, pp. 10089–10092, 1993.

84. Essmann, U., L. Perera, M. L. Berkowitz, T. Darden, H. Lee and L. G. Pedersen, "A Smooth Particle Mesh Ewald Method", *The Journal of Chemical Physics*, Vol. 103, No. 19, pp. 8577–8593, 1995.

85. Hess, B., H. Bekker, H. J. C. Berendsen and J. G. E. M. Fraaije, "LINCS: A Linear Constraint Solver for Molecular Simulations", *Journal of Computational Chemistry*, Vol. 18, pp. 18–1463, 1997.

86. Hess, B., "P-LINCS: A Parallel Linear Constraint Solver for Molecular Simulation", *Journal of Chemical Theory and Computation*, Vol. 4, No. 1, pp. 116–122, 2008.

87. Alessandri, R., J. Barnoud, A. S. Gertsen, I. Patmanidis, A. H. de Vries, P. C. T. Souza and S. J. Marrink, "Martini 3 Coarse Grained Force Field: Small Molecules", *Advanced Theory and Simulations*, Vol. 5, No. 1, 2022.

88. Jo, S., T. Kim, V. G. Iyer and W. Im, "CHARMM-GUI: A Web-Based Graphical User Interface for CHARMM", *Journal of Computational Chemistry*, Vol. 29, No. 11, pp. 1859–1865, 2008.

89. Radhakrishnan, N., S. C. Kaul, R. Wadhwa and D. Sundar, "Phosphatidylserine Exposed Lipid Bilayer Models for Understanding Cancer Cell Selectivity of Natu-

ral Compounds: A Molecular Dynamics Simulation Study", *Membranes (Basel)*, Vol. 12, No. 1, 2022.

90. Shahane, G., W. Ding, M. Palaiokostas and M. Orsi, "Physical Properties of Model Biological Lipid Bilayers: Insights from All-Atom Molecular Dynamics Simulations", *Journal of Molecular Modeling*, Vol. 25, No. 3, 2019.

91. Tironi, I. G., R. Sperb, P. E. Smith and W. F. van Gunsteren, "A Generalized Reaction Field Method for Molecular Dynamics Simulations", *The Journal of Chemical Physics*, Vol. 102, No. 13, p. 5451, 1998.

92. Pohorille, A., C. Jarzynski and C. Chipot, "Good Practices in Free-Energy Calculations", *Journal of Physical Chemistry B*, Vol. 114, No. 32, pp. 10235–10253, 2010.

93. Villa, A. and A. E. Mark, "Calculation of the Free Energy of Solvation for Neutral Analogs of Amino Acid Side Chains", *Journal of Computational Chemistry*, Vol. 23, No. 5, pp. 548–553, 2002.

94. Ercan, N. I., P. Stroeve, J. W. Tringe and R. Faller, "Molecular Dynamics Modeling of Methylene Blue-DOPC Lipid Bilayer Interactions", *Langmuir*, Vol. 34, No. 14, pp. 4314–4323, 2018.

95. Bennett, C. H., "Efficient Estimation of Free Energy Differences from Monte Carlo Data", *Journal of Computational Physics*, Vol. 22, No. 2, pp. 245–268, 1976.

96. Qian, H., M. P. Sheetz and E. L. Elson, "Single Particle Tracking Analysis of Diffusion and Flow in Two-Dimensional Systems", *Biophysical Journal*, Vol. 60, No. 4, pp. 910–921, 1991.

97. Yeh, I. C. and G. Hummer, "System-Size Dependence of Diffusion Coefficients and Viscosities from Molecular Dynamics Simulations with Periodic Boundary Conditions", *Journal of Physical Chemistry B*, Vol. 108, No. 40, p. 15873–15879,

2004.

98. Piggot, T. J., J. R. Allison, R. B. Sessions and J. W. Essex, "On the Calculation of Acyl Chain Order Parameters from Lipid Simulations", *Journal of Chemical Theory and Computation*, Vol. 13, No. 11, pp. 5683–5696, 2017.

99. Murtola, T., T. A. Vuorela, M. T. Hyvönen, S. J. Marrink, M. Karttunen and I. Vattulainen, "Low Density Lipoprotein: Structure, Dynamics, and Interactions of ApoB-100 with Lipids", *Soft Matter*, Vol. 7, No. 18, pp. 8135–8141, 2011.

100. Gong, H., M. Liao, X. Hu, K. Fa, S. Phanphak, D. Ciumac, P. Hollowell, K. Shen, L. A. Clifton, M. Campana, J. R. P. Webster, G. Fragneto, T. A. Waigh, A. J. McBain and J. R. Lu, "Aggregated Amphiphilic Antimicrobial Peptides Embedded in Bacterial Membranes", *ACS Applied Materials and Interfaces*, Vol. 12, No. 40, pp. 44420–44432, 2020.

101. Zimm, B. H., "The Scattering of Light and the Radial Distribution Function of High Polymer Solutions", *The Journal of Chemical Physics*, Vol. 16, No. 12, p. 1093, 2004.

102. Rennie, R., *A Dictionary of Chemistry*, Oxford University Press, 2016.

103. Johnson-Ajinwo, O. R., I. Ullah, H. Mbye, A. Richardson, P. Horrocks and W. W. Li, "The Synthesis and Evaluation of Thymoquinone Analogues as Anti-Ovarian Cancer and Antimalarial Agents", *Bioorganic and Medicinal Chemistry Letters*, Vol. 28, No. 7, pp. 1219–1222, 2018.

104. Anilkumar, K., K. Sakthivel and S. Venkatachalam, "Lipid-Based Nanocarrier Drug Delivery System for Brain Targeting Through Nasal Route: A Review", *International Journal of Pharmaceutical Sciences and Research*, Vol. 11, No. 10, pp. 4774–4783, 2020.

105. Agung, I. I. W., H. Kalim, S. W. C. B and B. Rahardjo, "Computational Analy-

sis For Revealing The Role of Thymoquinone (Active Compound from Ethanolic Extract of Nigella sativa) as Inhibitor of P65 NF-kb Activation in Preclampsia Treatment", *International Journal of Pharmaceutical and Clinical Research*, Vol. 8, No. 5, pp. 297–300, 2016.

106. Haq, A. and B. Michniak-Kohn, "Effects of Solvents and Penetration Enhancers on Transdermal Delivery of Thymoquinone: Permeability and Skin Deposition Study", *Drug Delivery*, Vol. 25, No. 1, pp. 1943–1949, 2018.

107. Dwisari, F., A. Srihardyastutie and S. M. Ulfa, "Synthesis of 2-Methyl-5-Methoxy-1,4-Benzoquinone and In-Silico Activity Profiling Toward Cytochrome P450-3A4", *IOP Conference Series: Materials Science and Engineering*, Vol. 546, No. 6, p. 062005, 2019.

108. Alkharfy, K. M., A. Ahmad, R. M. A. Khan and W. M. Al-Shagha, "Pharmacokinetic Plasma Behaviors of Intravenous and Oral Bioavailability of Thymoquinone in a Rabbit Model", *European Journal of Drug Metabolism and Pharmacokinetics*, Vol. 40, No. 3, pp. 319–323, 2015.

109. Zuhroh, N. and S. M. Ulfa, "Synthesis of 5-(4-Bromobutyl)-2,3-Dimethyl-1,4-Benzoquinone and the Solubility Test in n-Octanol/Water Partition System", *IOP Conference Series: Materials Science and Engineering*, Vol. 833, No. 1, p. 012056, 2020.

110. Froimowitz, M., "HyperChem: A Software Package for Computational Chemistry and Molecular Modeling.", *Biotechniques*, Vol. 14, No. 6, pp. 1010–1013, 1993.

111. Ulfa, S. M., F. Dwisari, L. Pangesti and M. F. Rahman, "Biological Activity and Solubility of 5-Methoxy-1,4-Benzoquinone Having Bromoheptyl and Bromodecyl Substituents in the N-Octanol/Water System", *Makara Journal of Science*, Vol. 25, No. 1, pp. 13–20, 2021.

112. Tetko, I. V. and V. Y. Tanchuk, "Application of Associative Neural Networks for Prediction of Lipophilicity in ALOGPS 2.1 Program", *Journal of Chemical Information and Computer Sciences*, Vol. 42, No. 5, pp. 1136–1145, 2002.

113. Johnson-Ajinwo, O. R., *Identification, Semi-Synthesis and Evaluation of Anti-Ovarian Cancer Compounds from Plants Used in Traditional Medicines*, Ph.D. Thesis, Keele University, 2017.

114. Swain, M., "Chemicalize.org", *Journal of Chemical Information and Modeling*, Vol. 52, No. 2, pp. 613–615, 2012.

115. Tristram-Nagle, S., H. I. Petrache and J. F. Nagle, "Structure and Interactions of Fully Hydrated Dioleoylphosphatidylcholine Bilayers.", *Biophysical Journal*, Vol. 75, No. 2, p. 917, 1998.

116. Nagle, J. F. and S. Tristram-Nagle, "Structure of Lipid Bilayers", *Biochimica et Biophysica Acta*, Vol. 1469, No. 3, pp. 159–195, 2000.

117. Liu, Y. and J. F. Nagle, "Diffuse Scattering Provides Material Parameters and Electron Density Profiles of Biomembranes", *Physical Review E - Statistical Physics, Plasmas, Fluids, and Related Interdisciplinary Topics*, Vol. 69, No. 4, p. 4, 2004.

118. Kucerka, N., S. Tristram-Nagle and J. F. Nagle, "Structure of Fully Hydrated Fluid Phase Lipid Bilayers with Monounsaturated Chains", *The Journal of Membrane Biology*, Vol. 208, No. 3, pp. 193–202, 2005.

119. Pan, J., S. Tristram-Nagle, N. Kučerka and J. F. Nagle, "Temperature Dependence of Structure, Bending Rigidity, and Bilayer Interactions of Dioleoylphosphatidylcholine Bilayers", *Biophysical Journal*, Vol. 94, No. 1, pp. 117–124, 2008.

120. Kucerka, N., J. F. Nagle, J. N. Sachs, S. E. Feller, J. Pencer, A. Jackson and J. Katsaras, "Lipid Bilayer Structure Determined by the Simultaneous Analysis

of Neutron and X-Ray Scattering Data", *Biophysical Journal*, Vol. 95, No. 5, pp. 2356–2367, 2008.

121. Kucerka, N., M. P. Nieh and J. Katsaras, "Fluid Phase Lipid Areas and Bilayer Thicknesses of Commonly Used Phosphatidylcholines as a Function of Temperature", *Biochimica et Biophysica Acta (BBA) - Biomembranes*, Vol. 1808, No. 11, pp. 2761–2771, 2011.

122. Leftin, A., T. R. Molugu, C. Job, K. Beyer and M. F. Brown, "Area per Lipid and Cholesterol Interactions in Membranes from Separated Local-Field 13C NMR Spectroscopy", *Biophysical Journal*, Vol. 107, No. 10, pp. 2274–2286, 2014.

123. Attwood, S. J., Y. Choi and Z. Leonenko, "Preparation of DOPC and DPPC Supported Planar Lipid Bilayers for Atomic Force Microscopy and Atomic Force Spectroscopy", *International Journal of Molecular Sciences*, Vol. 14, No. 2, pp. 3514–3539, 2013.

124. Kulig, W., A. Olżyńska, P. Jurkiewicz, A. M. Kantola, S. Komulainen, M. Manna, M. Pourmousa, M. Vazdar, L. Cwiklik, T. Rog, G. Khelashvili, D. Harries, V. Telkki, M. Hof, I. Vattulainen and P. Jungwirth, "Cholesterol Under Oxidative Stress — How Lipid Membranes Sense Oxidation as Cholesterol Is Being Replaced by Oxysterols", *Free Radical Biology and Medicine*, Vol. 84, pp. 30–41, 2015.

125. Erimban, S. and S. Daschakraborty, "Translocation of a Hydroxyl Functionalized Carbon Dot Across A Lipid Bilayer: An All-Atom Molecular Dynamics Simulation Study", *Physical Chemistry Chemical Physics*, Vol. 22, No. 11, pp. 6335–6350, 2020.

126. Kasparyan, G., C. Poojari, T. Rog and J. S. Hub, "Cooperative Effects of an Antifungal Moiety and DMSO on Pore Formation Over Lipid Membranes Revealed by Free Energy Calculations", *Journal of Physical Chemistry B*, Vol. 124, No. 40,

pp. 8811–8821, 2020.

127. Filippov, A., G. Orädd and G. Lindblom, "Influence of Cholesterol and Water Content on Phospholipid Lateral Diffusion in Bilayers", *Langmuir*, Vol. 19, No. 16, pp. 6397–6400, 2003.

128. Akhunzada, M. J., L. Sagresti, A. Catte, N. Bhattacharjee, T. D'Agostino and G. Brancato, "Temperature Dependence of the Structure and Dynamics of a Dye-Labeled Lipid in a Planar Phospholipid Bilayer: A Computational Study", *The Journal of Membrane Biology*, Vol. 252, No. 4-5, pp. 227–240, 2019.

129. Febo-Ayala, W., D. P. Holland, S. A. Bradley and D. H. Thompson, "Lateral Diffusion Coefficients of an Eicosanyl-Based Bisglycerophosphocholine Determined by PFG-NMR and FRAP", *Langmuir*, Vol. 23, No. 11, pp. 6276–6280, 2007.

130. Saito, H., T. Morishita, T. Mizukami, K. I. Nishiyama, K. Kawaguchi and H. Nagao, "Molecular Dynamics Study of Binary POPC Bilayers: Molecular Condensing Effects on Membrane Structure and Dynamics", *Journal of Physics: Conference Series*, Vol. 1136, No. 1, 2018.

131. Guo, Y., V. A. Baulin and F. Thalmann, "Peroxidised Phospholipid Bilayers: Insight from Coarse-Grained Molecular Dynamics Simulations", *Soft Matter*, Vol. 12, No. 1, pp. 263–271, 2015.

132. de Meyer, F. and B. Smit, "Effect of Cholesterol on the Structure of a Phospholipid Bilayer", *Proceedings of the National Academy of Sciences*, Vol. 106, No. 10, pp. 3654–3658, 2009.

133. Koobus, B. and C. Farhat, "Second-Order Time-Accurate and Geometrically Conservative Implicit Schemes for Flow Computations on Unstructured Dynamic Meshes", *Computer Methods in Applied Mechanics and Engineering*, Vol. 170, No. 1-2, pp. 103–129, 1999.

134. Sun, D., X. Lin and N. Gu, "Cholesterol Affects C60 Translocation across Lipid Bilayers", *Soft Matter*, Vol. 10, No. 13, pp. 2160–2168, 2014.

135. Petrova, S. S. and A. D. Solov'Ev, "The Origin of the Method of Steepest Descent", *Historia Mathematica*, Vol. 24, No. 4, pp. 361–375, 1997.

APPENDIX A: RESULTS OF FREE ENERGY DIFFERENCES

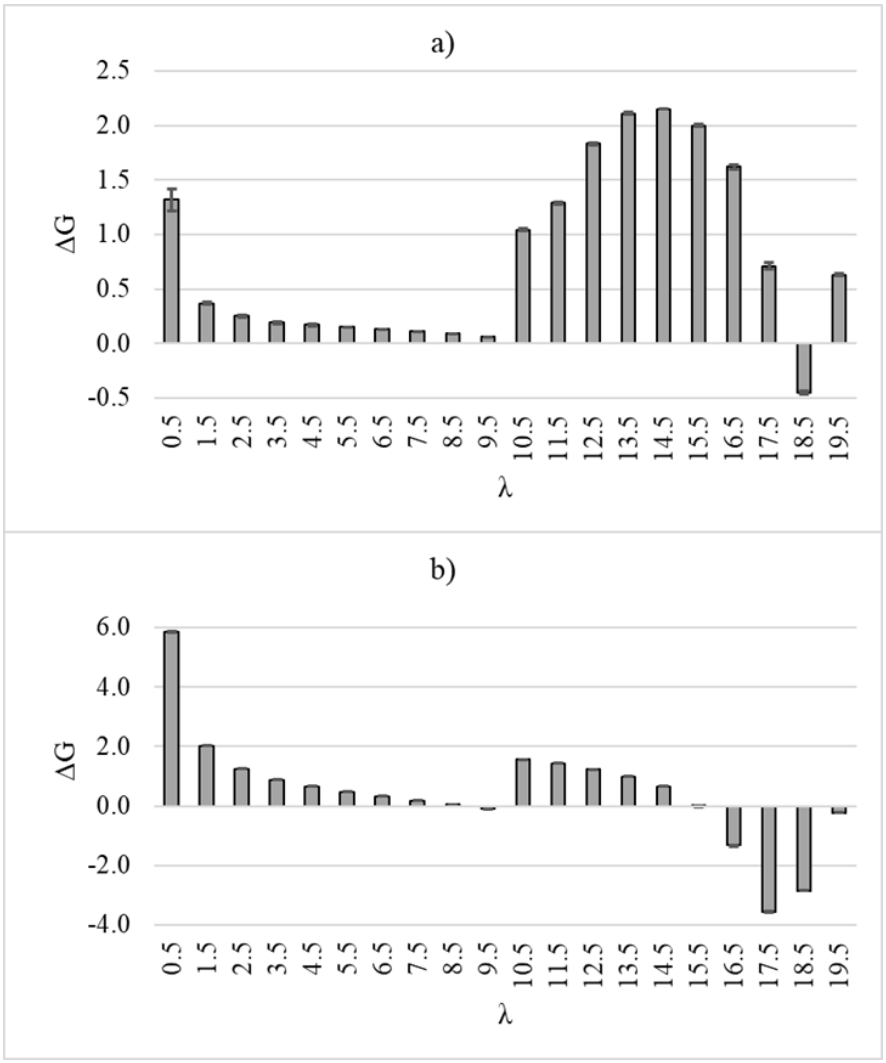

Figure A.1. Free energy differences of thymoquinone in a) 1-octanol and b) water in atomistic simulations.

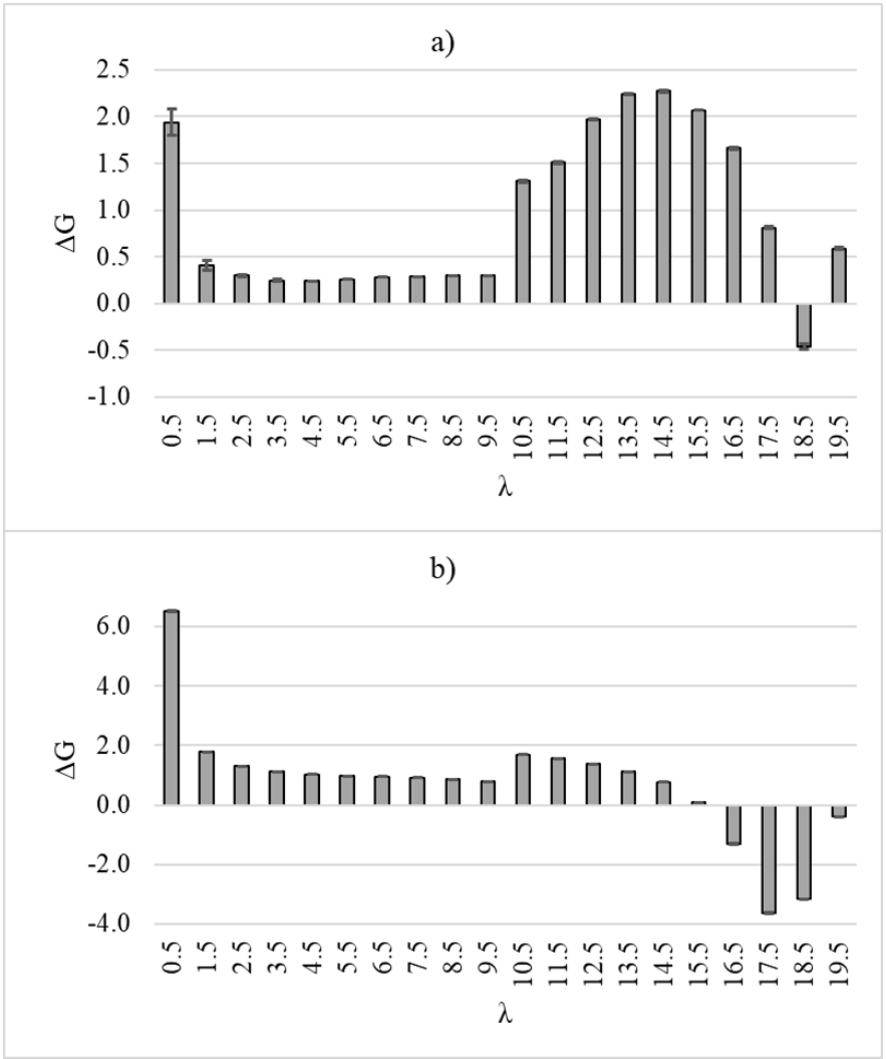

Figure A.2. Free energy differences of aminothymoquinone in a) 1-octanol and b) water in atomistic simulations.

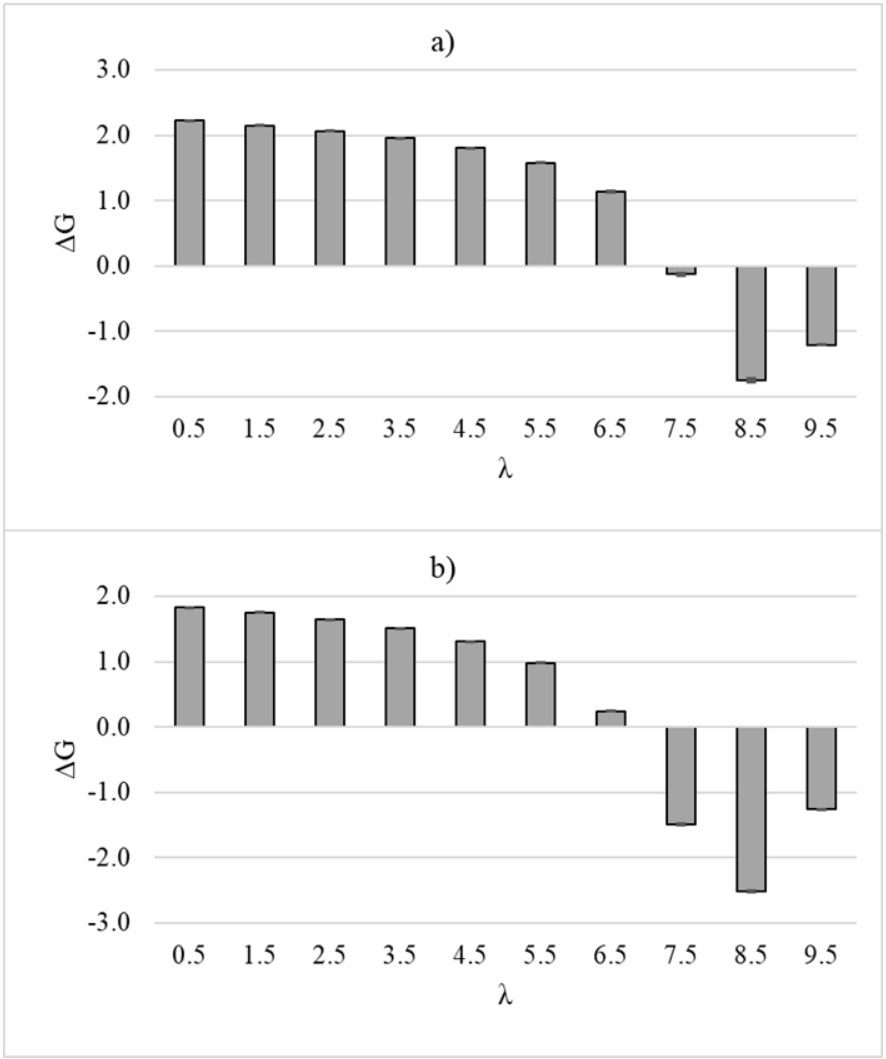

Figure A.3. Free energy differences of thymoquinone in a) 1-octanol and b) water in coarse-grained simulations.

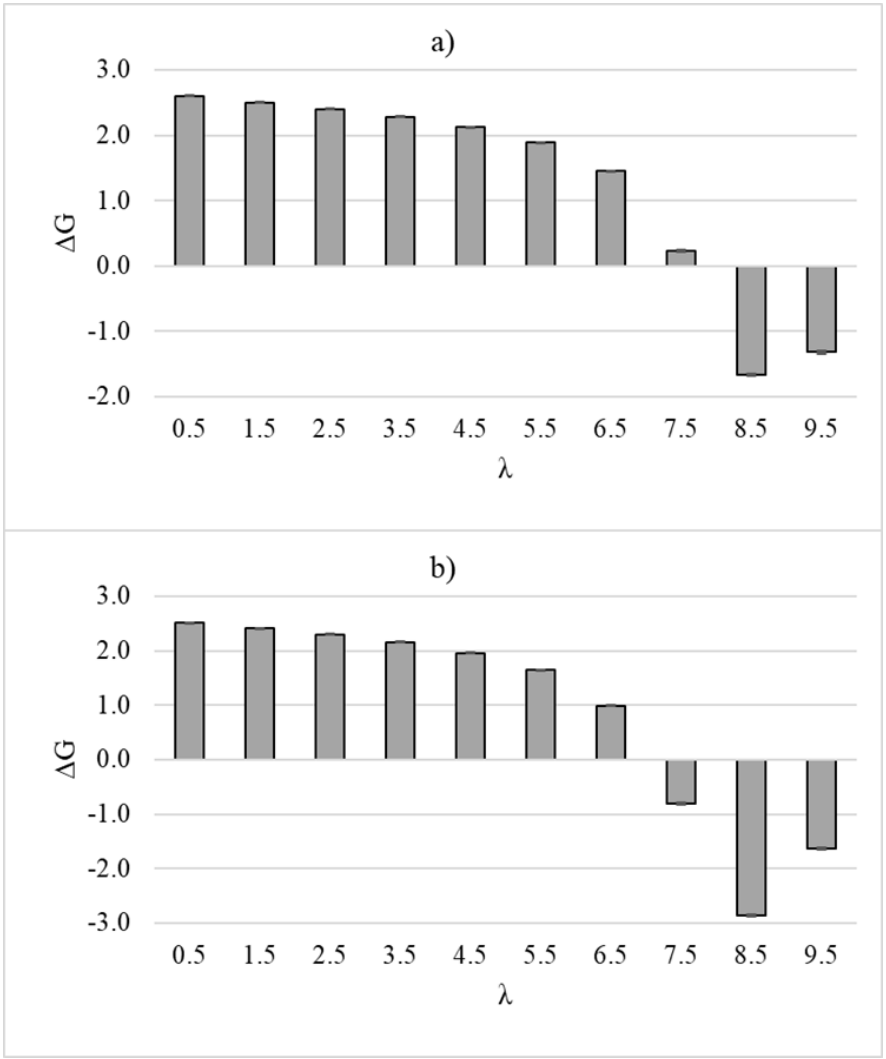

Figure A.4. Free energy differences of aminothymoquinone in a) 1-octanol and b) water in coarse-grained simulations.

APPENDIX B: ENERGY PROFILES

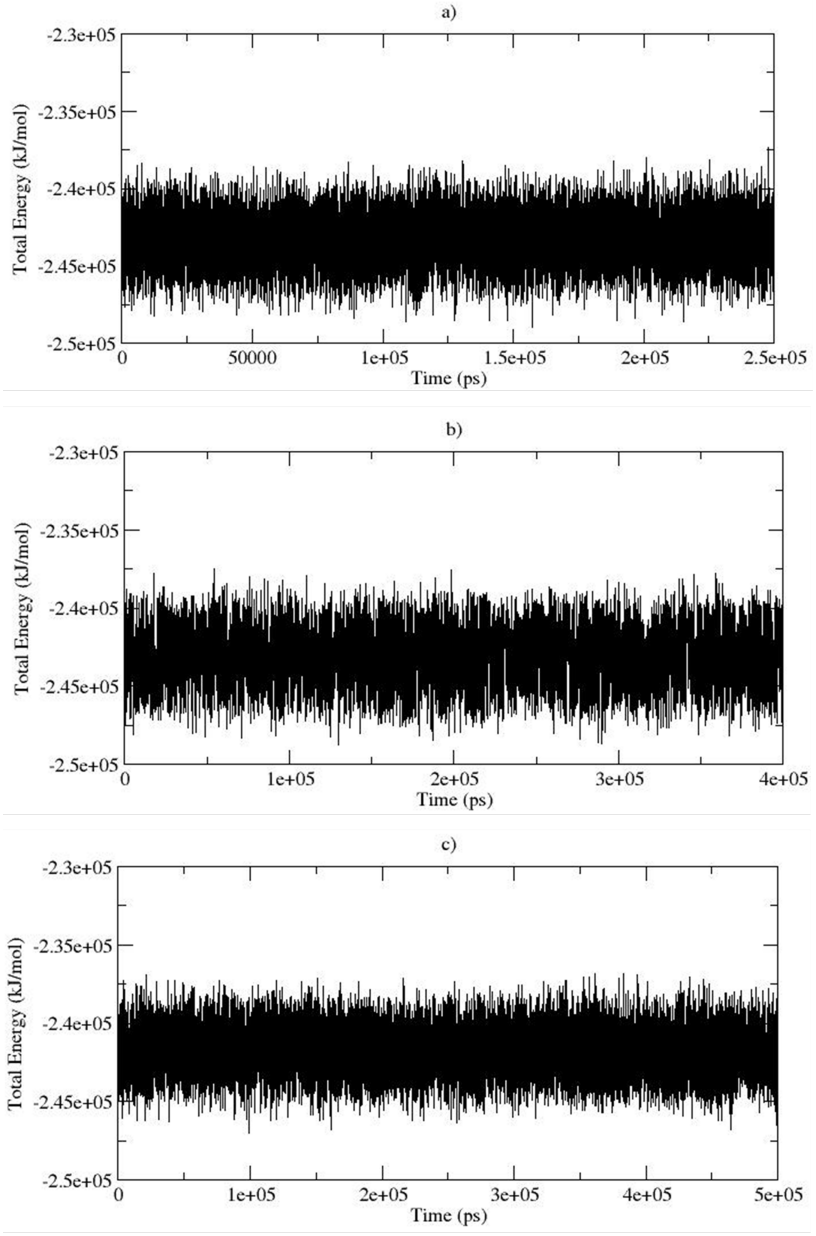

Figure B.1. Energy profiles of DOPC bilayers with a) no b) 1 and c) 10 thymoquinones in atomistic simulations.

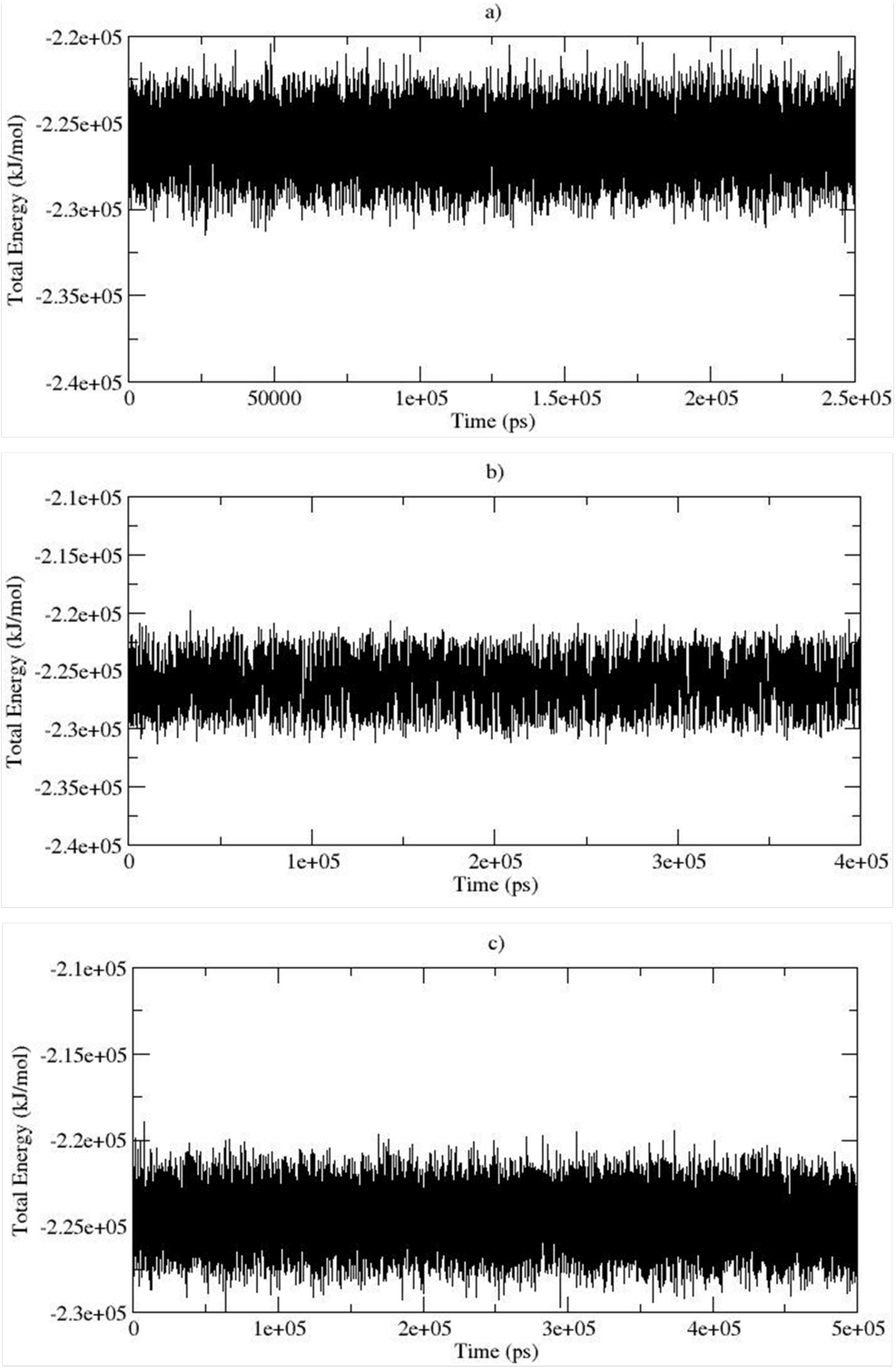

Figure B.2. Energy profiles of POPC bilayers with a) no b) 1 and c) 10 thymoquinones in atomistic simulations.

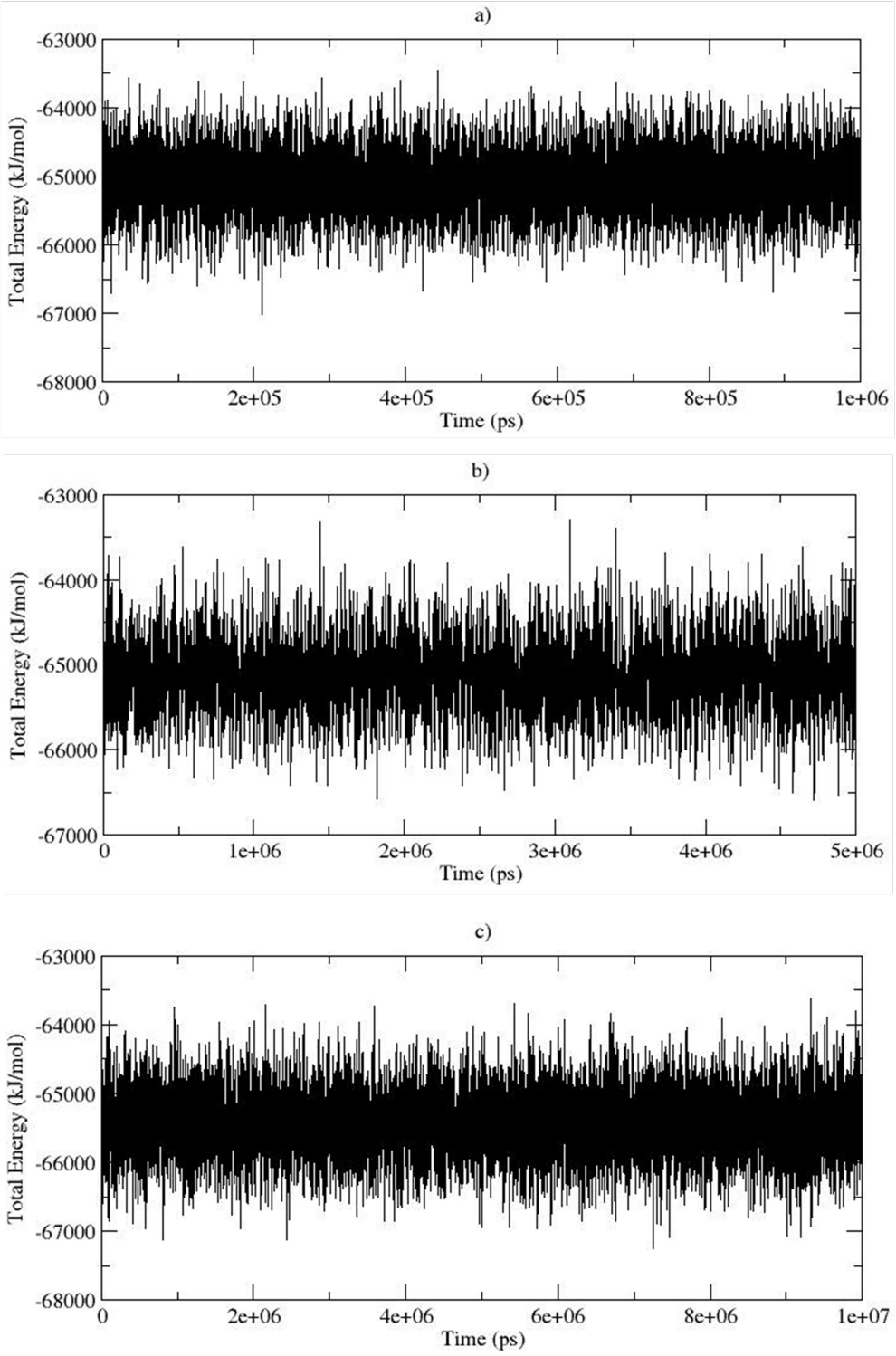

Figure B.3. Energy profiles of DOPC bilayers with a) no b) 1 and c) 10 thymoquinones in coarse-grained simulations.

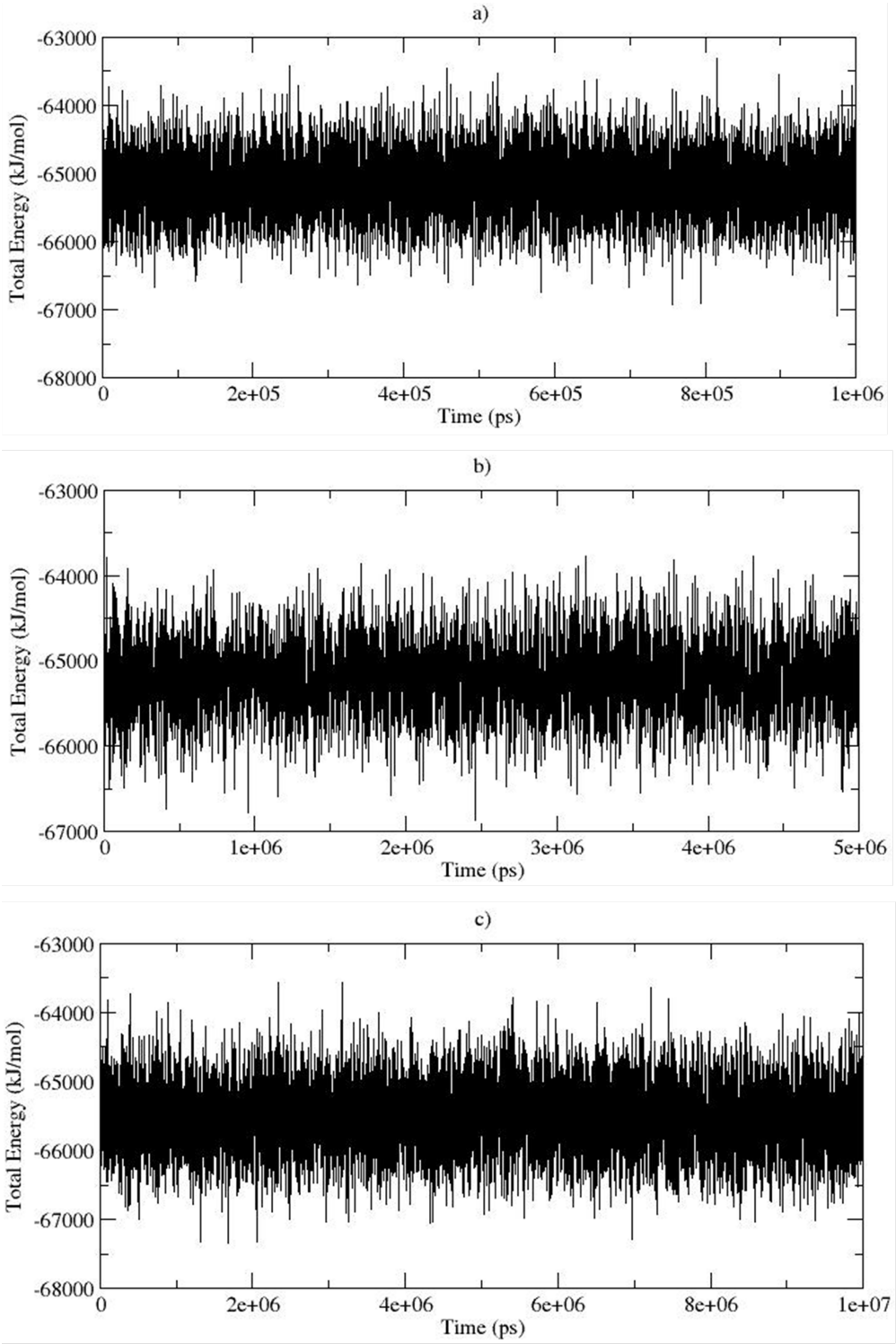

Figure B.4. Energy profiles of POPC bilayers with a) no b) 1 and c) 10 thymoquinones in coarse-grained simulations.

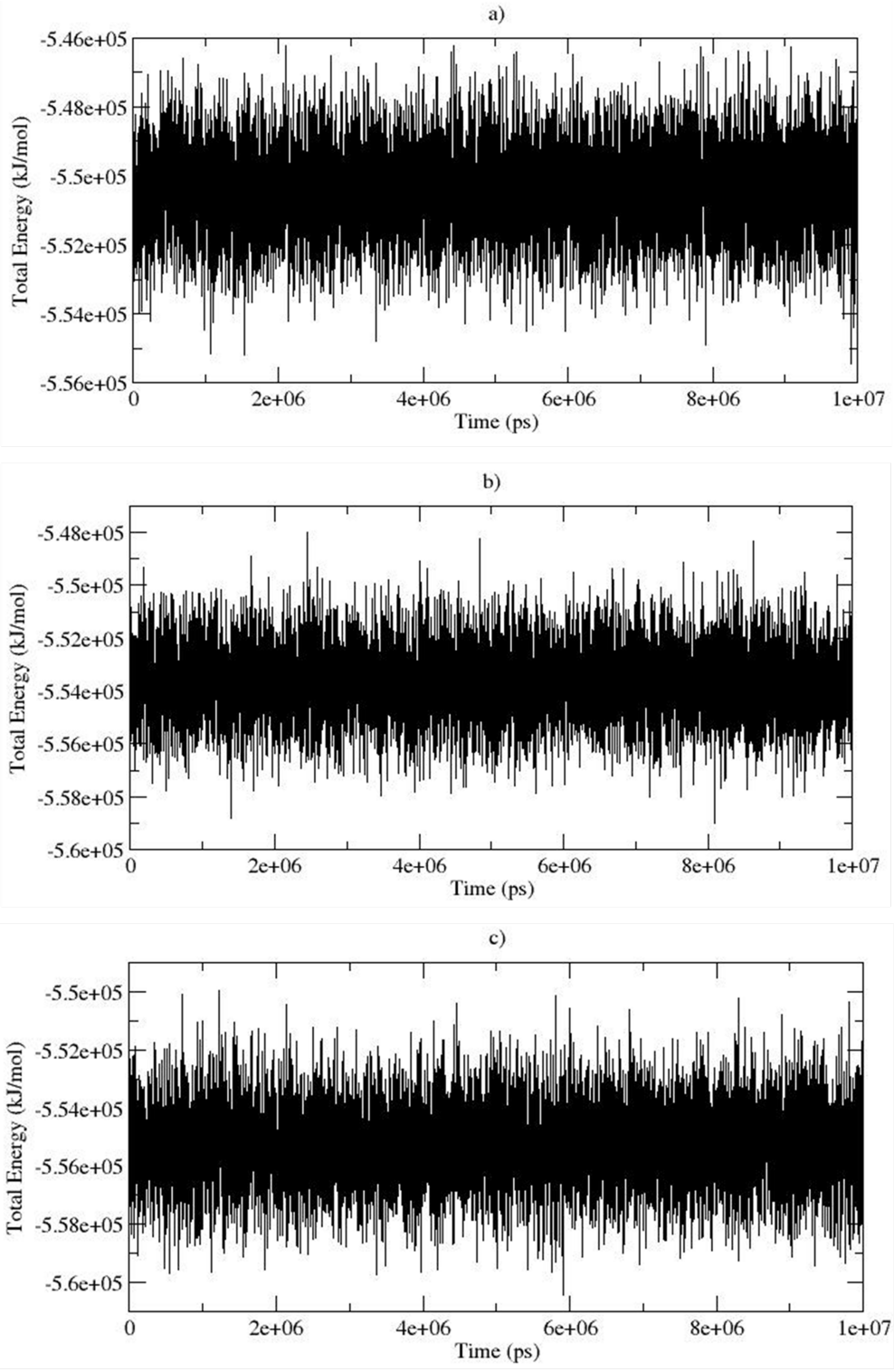

Figure B.5. Energy profiles of normal membranes of Model 1 a) without and with b) thymoquinone and c) aminothymoquinone molecules.

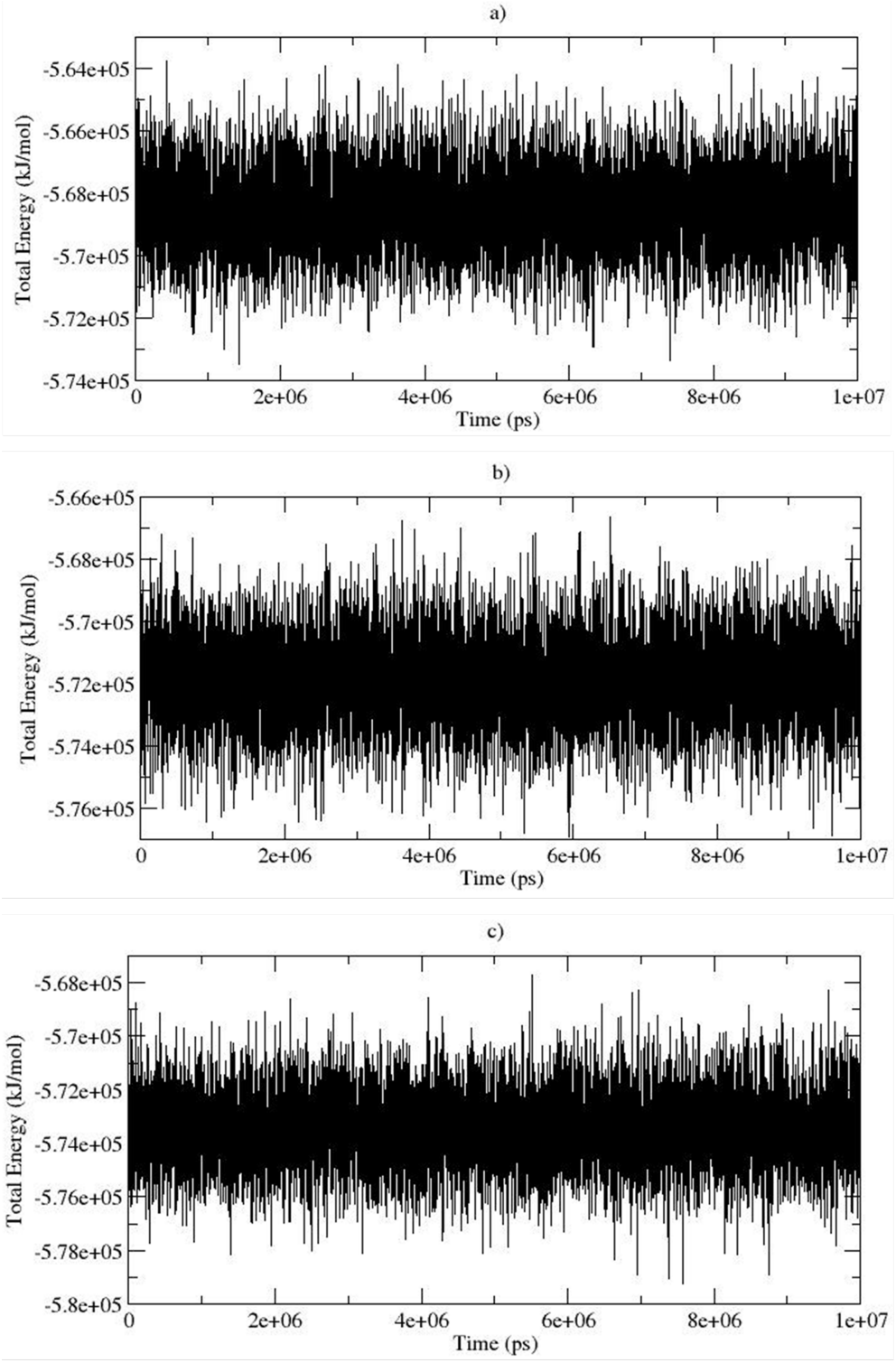

Figure B.6. Energy profiles of cancer membranes of Model 1 a) without and with b) thymoquinone and c) aminothymoquinone molecules.

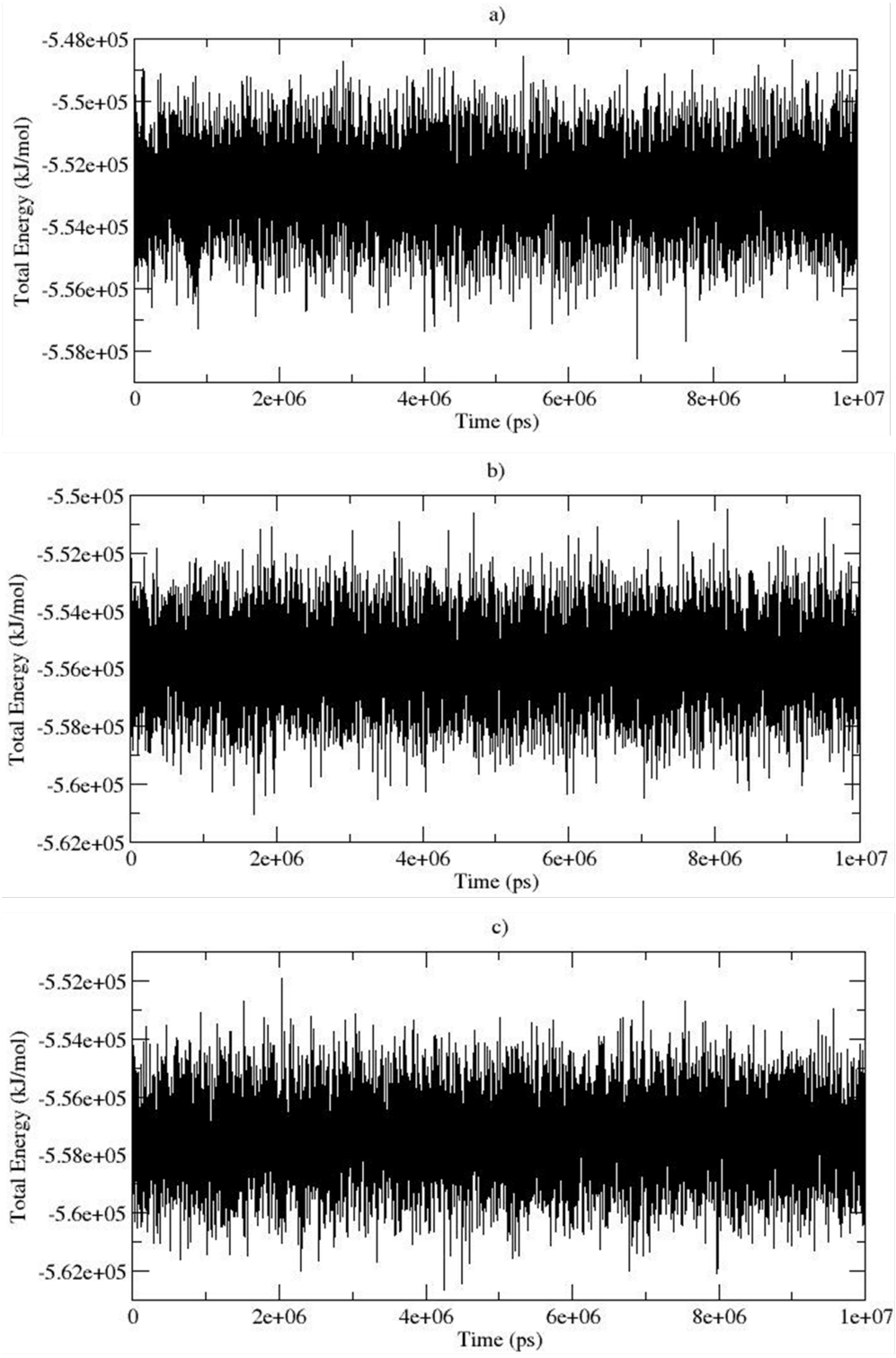

Figure B.7. Energy profiles of normal membranes of Model 2 a) without and with b) thymoquinone and c) aminothymoquinone molecules.

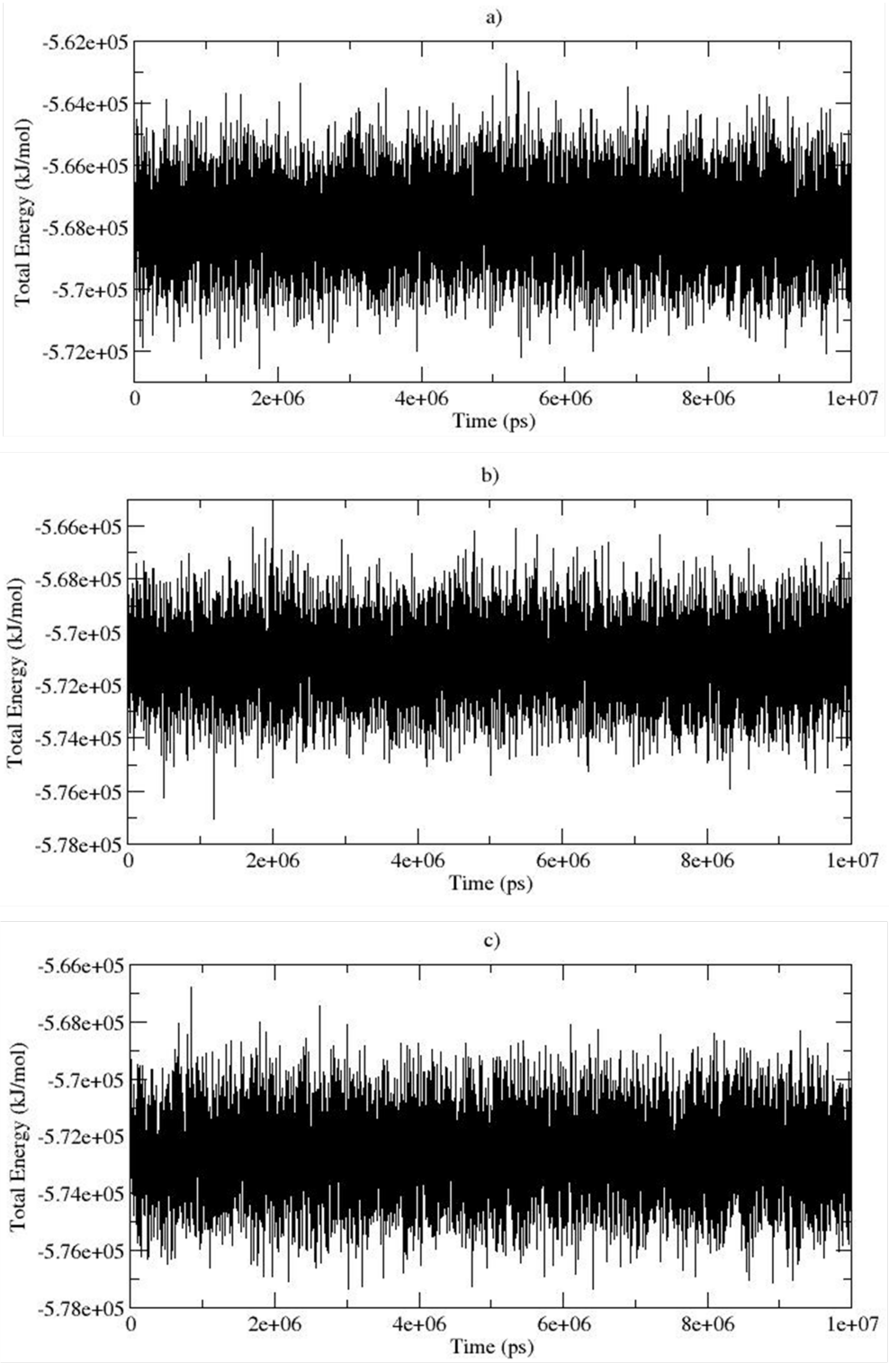

Figure B.8. Energy profiles of cancer membranes of Model 2 a) without and with b) thymoquinone and c) aminothymoquinone molecules.

APPENDIX C: GRAPHS OF AREA PER LIPID ANALYSIS

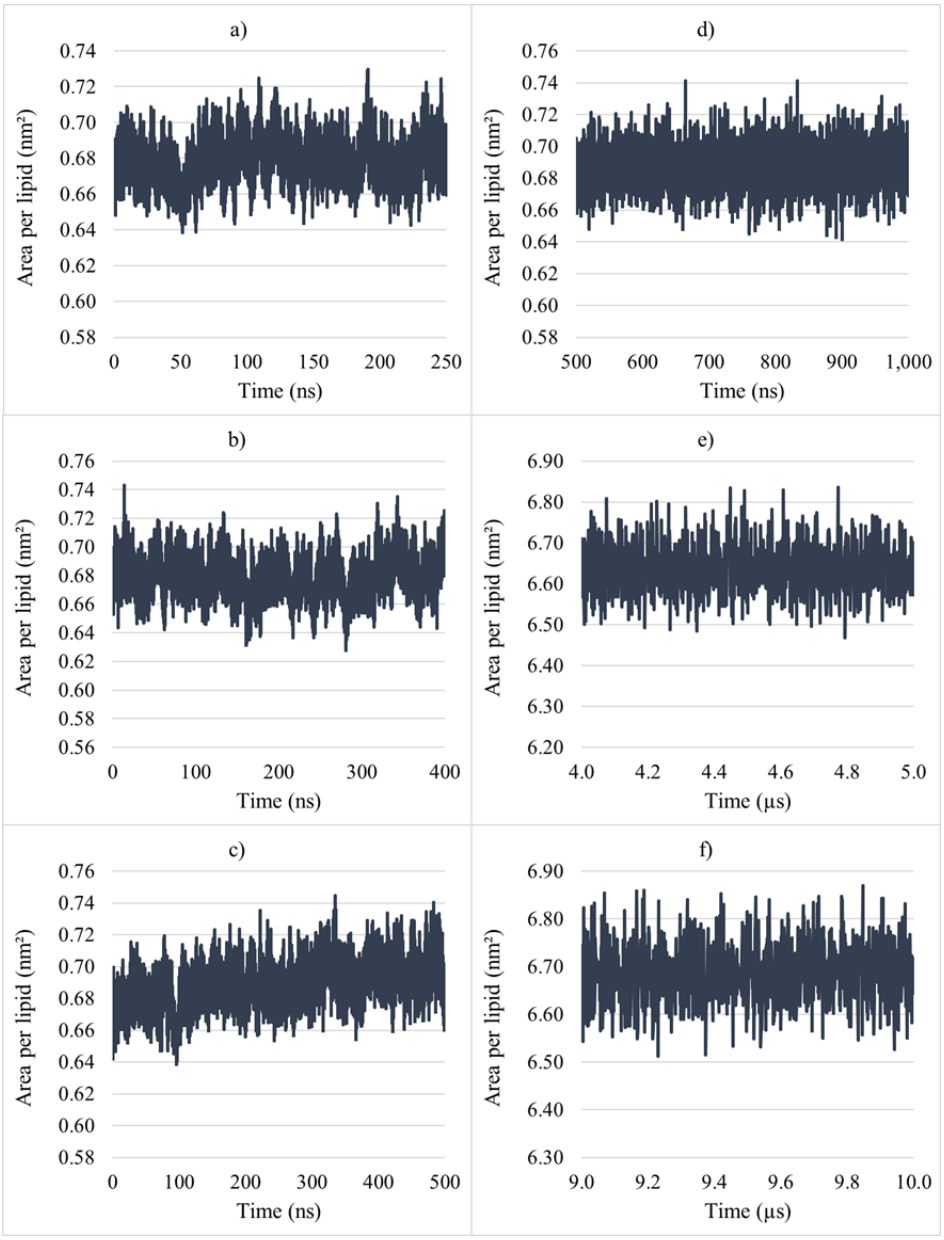

Figure C.1. Area per lipid of DOPC bilayers with a) no b) 1 and c) 10 thymoquinones in atomistic; with a) no b) 1 and c) 10 thymoquinones in coarse-grained simulations.

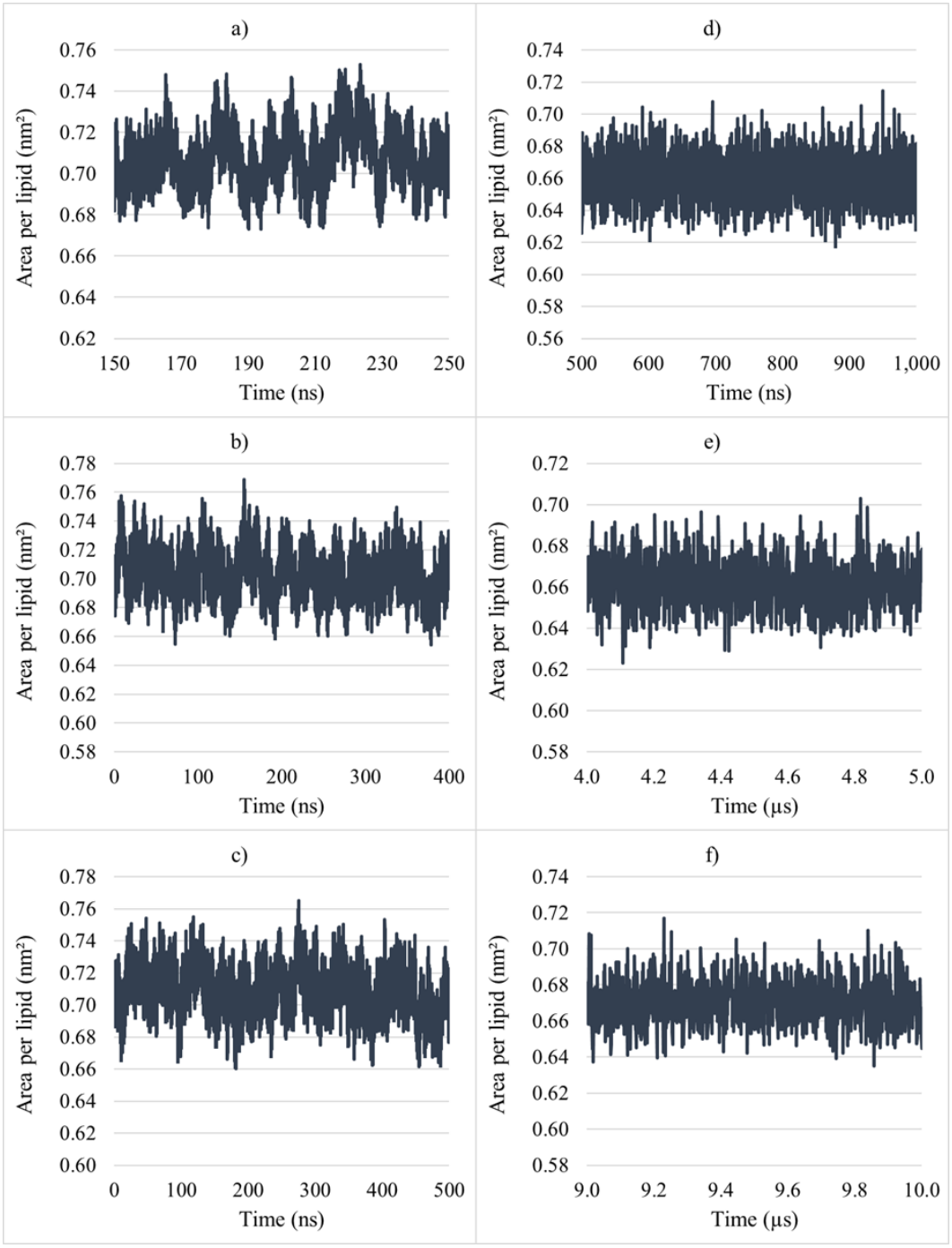

Figure C.2. Area per lipid of POPC bilayers with a) no b) 1 and c) 10 thymoquinones in atomistic; with a) no b) 1 and c) 10 thymoquinones in coarse-grained simulations.

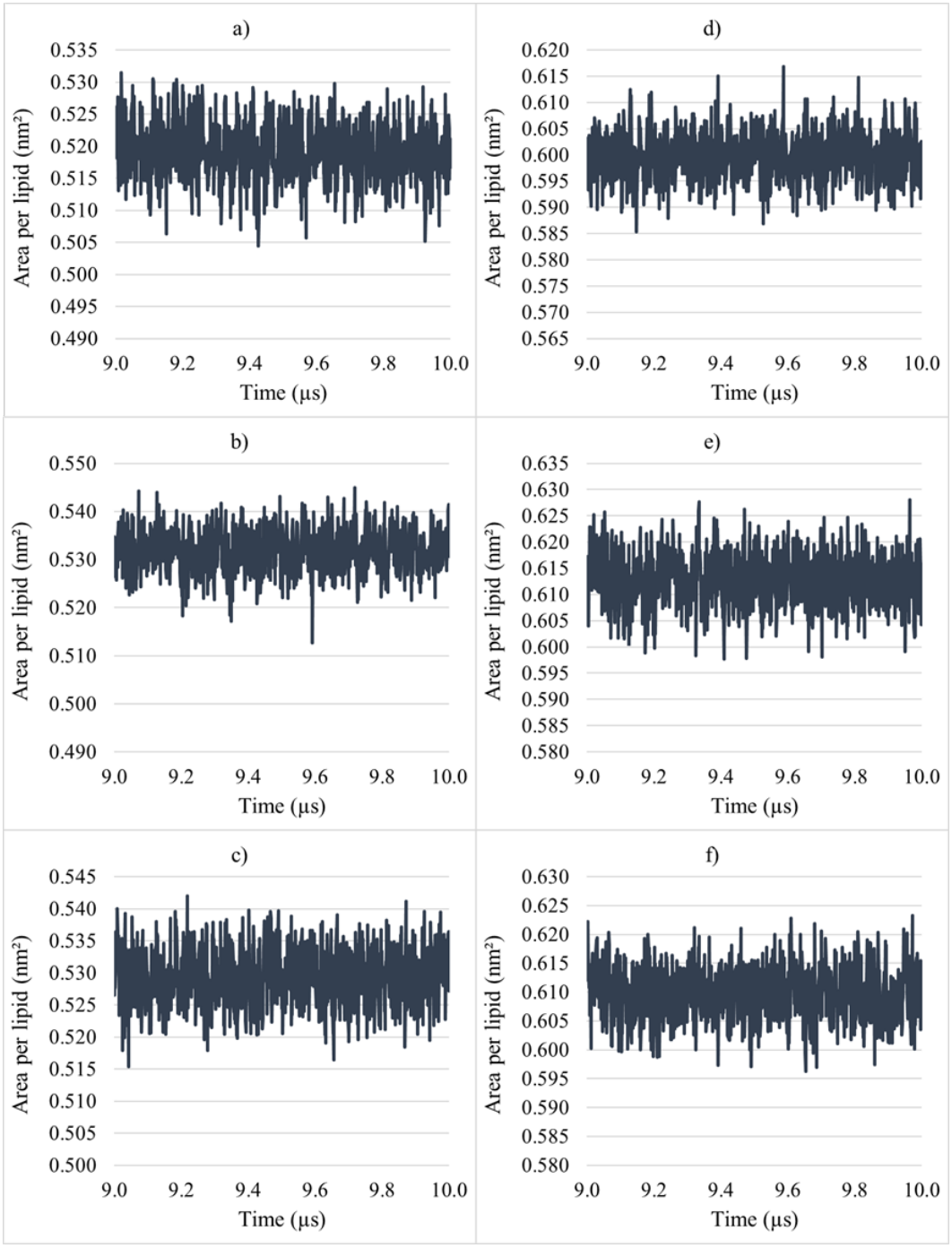

Figure C.3. Area per lipid of Model 1 membranes of normal a) without and with b) thymoquinone and c) aminothymoquinone; of cancer a) without and with b) thymoquinone and c) aminothymoquinone.

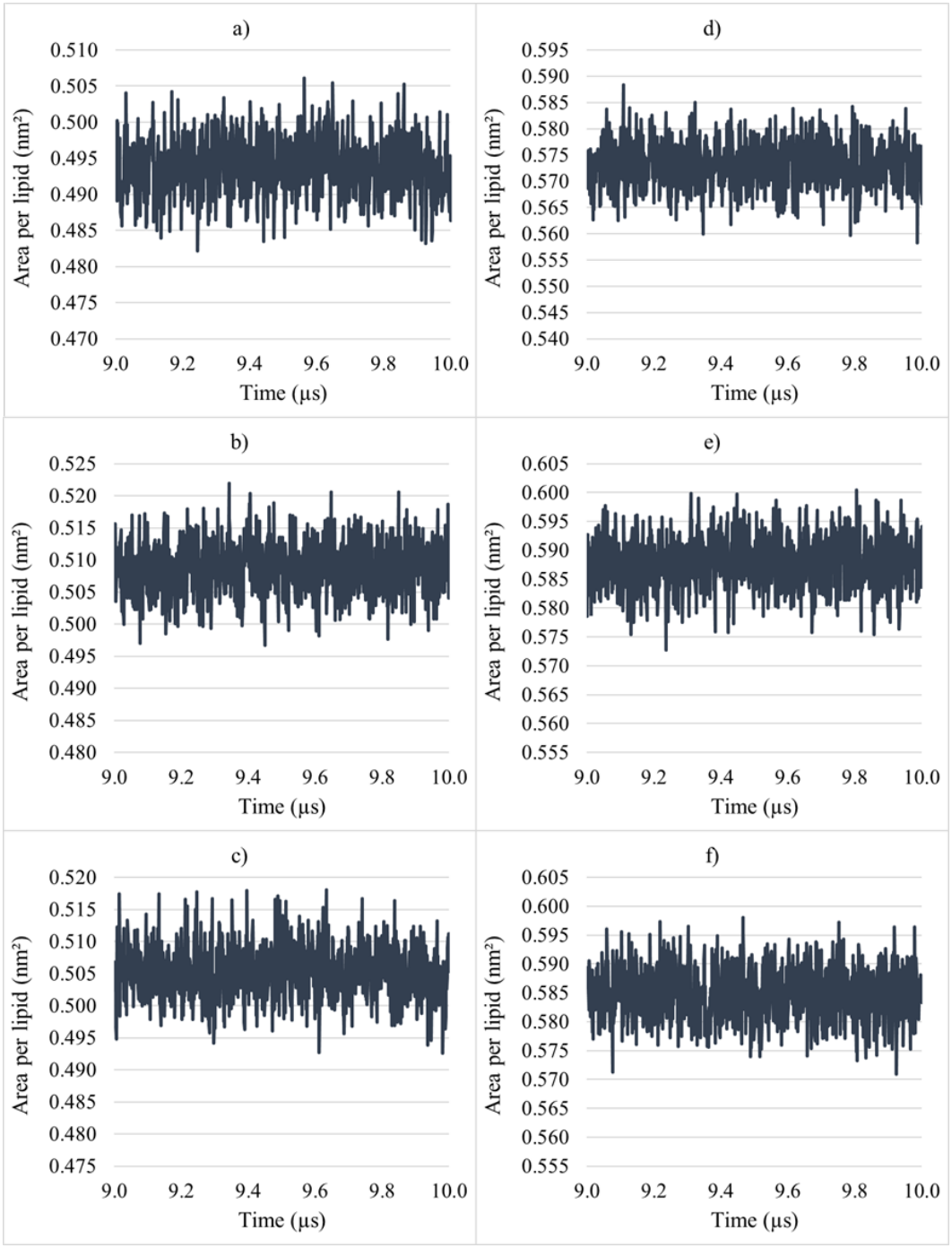

Figure C.4. Area per lipid of Model 2 membranes of normal a) without and with b) thymoquinone and c) aminothymoquinone; of cancer a) without and with b) thymoquinone and c) aminothymoquinone.

APPENDIX D: GRAPHS OF BILAYER THICKNESS ANALYSIS

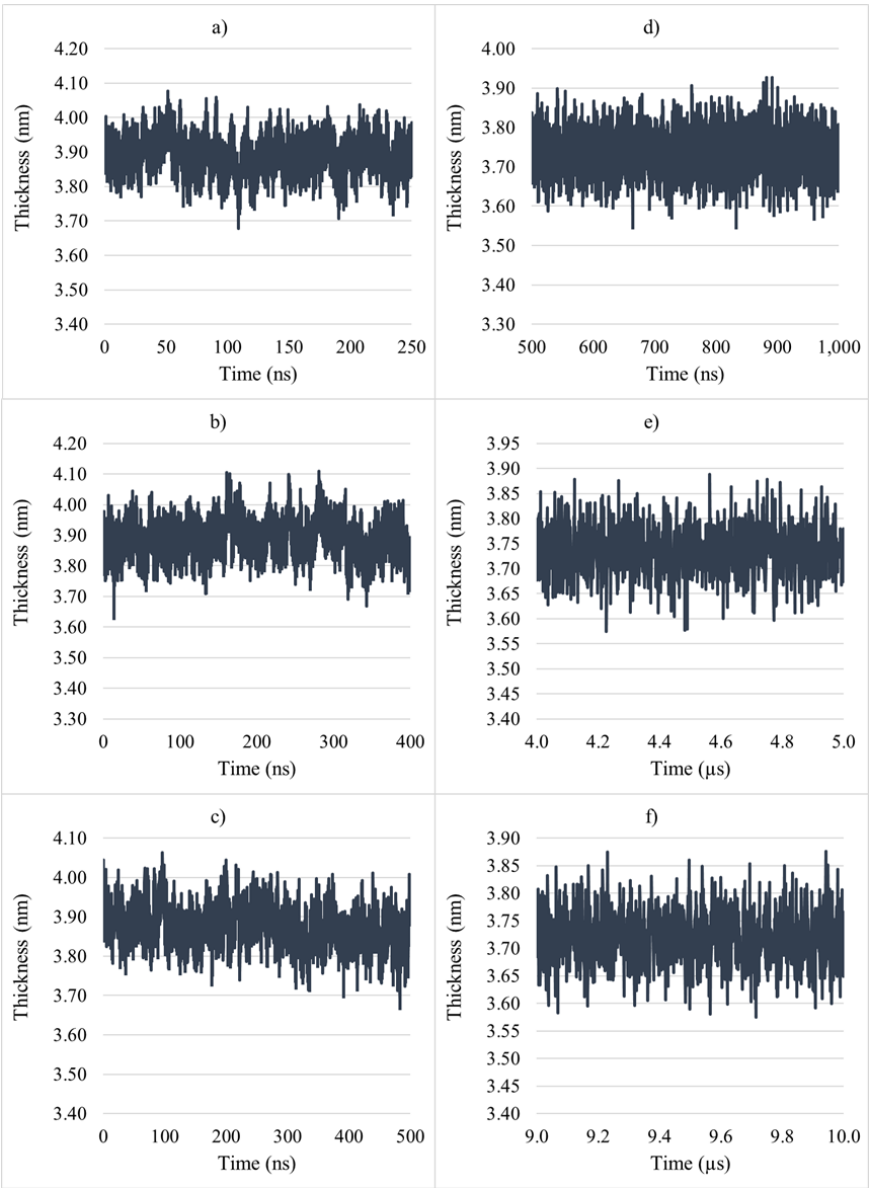

Figure D.1. Bilayer thickness of DOPC bilayers with a) no b) 1 and c) 10 thymoquinones in atomistic; with a) no b) 1 and c) 10 thymoquinones in coarse-grained simulations.

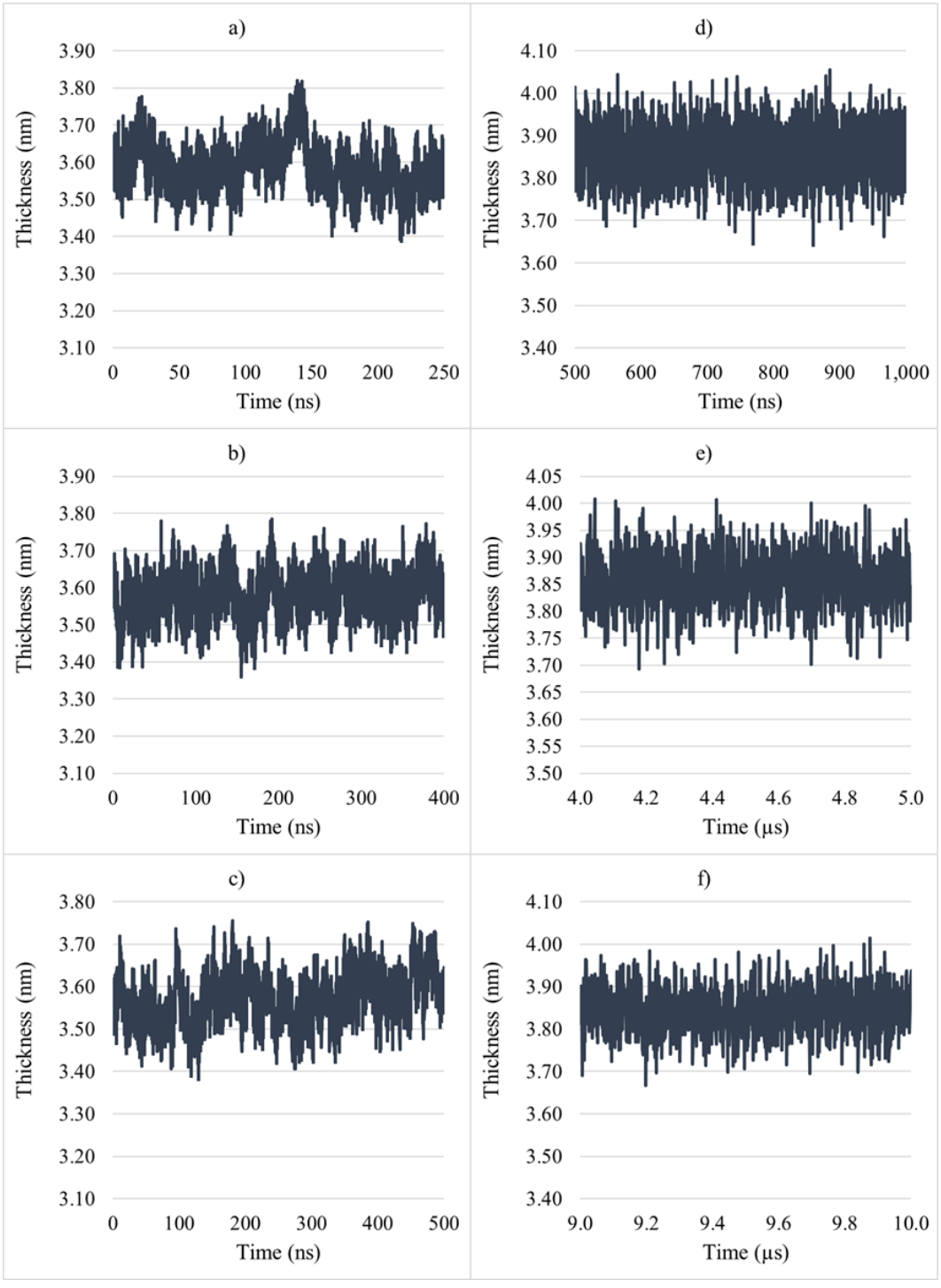

Figure D.2. Bilayer thickness of POPC bilayers with a) no b) 1 and c) 10 thymoquinones in atomistic; with a) no b) 1 and c) 10 thymoquinones in coarse-grained simulations.

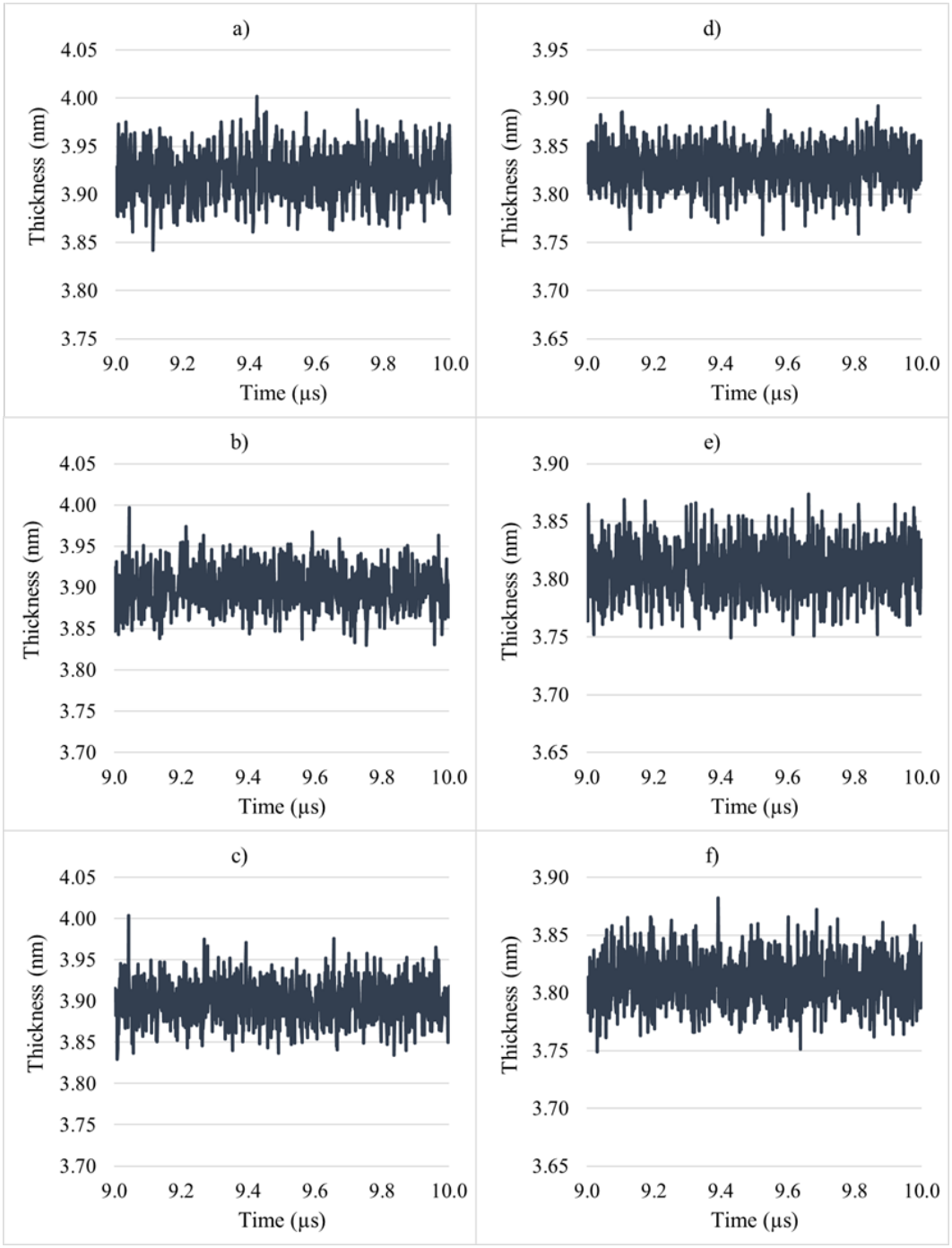

Figure D.3. Bilayer thickness of Model 1 membranes of normal a) without and with b) thymoquinone and c) aminothymoquinone; of cancer a) without and with b) thymoquinone and c) aminothymoquinone.

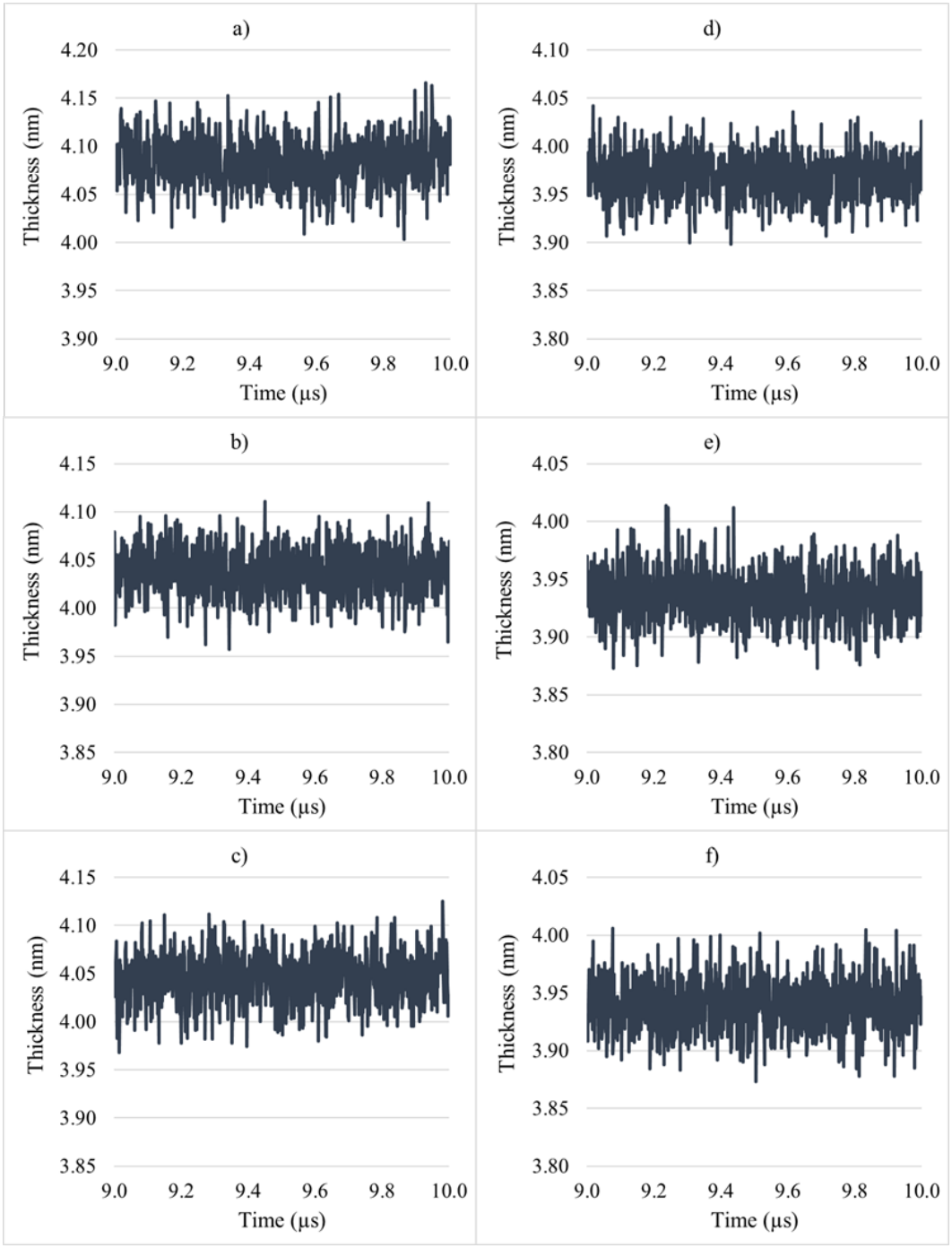

Figure D.4. Bilayer thickness of Model 2 membranes of normal a) without and with b) thymoquinone and c) aminothymoquinone; of cancer a) without and with b) thymoquinone and c) aminothymoquinone.

APPENDIX E: GRAPHS OF LATERAL DIFFUSION COEFFICIENT ANALYSIS

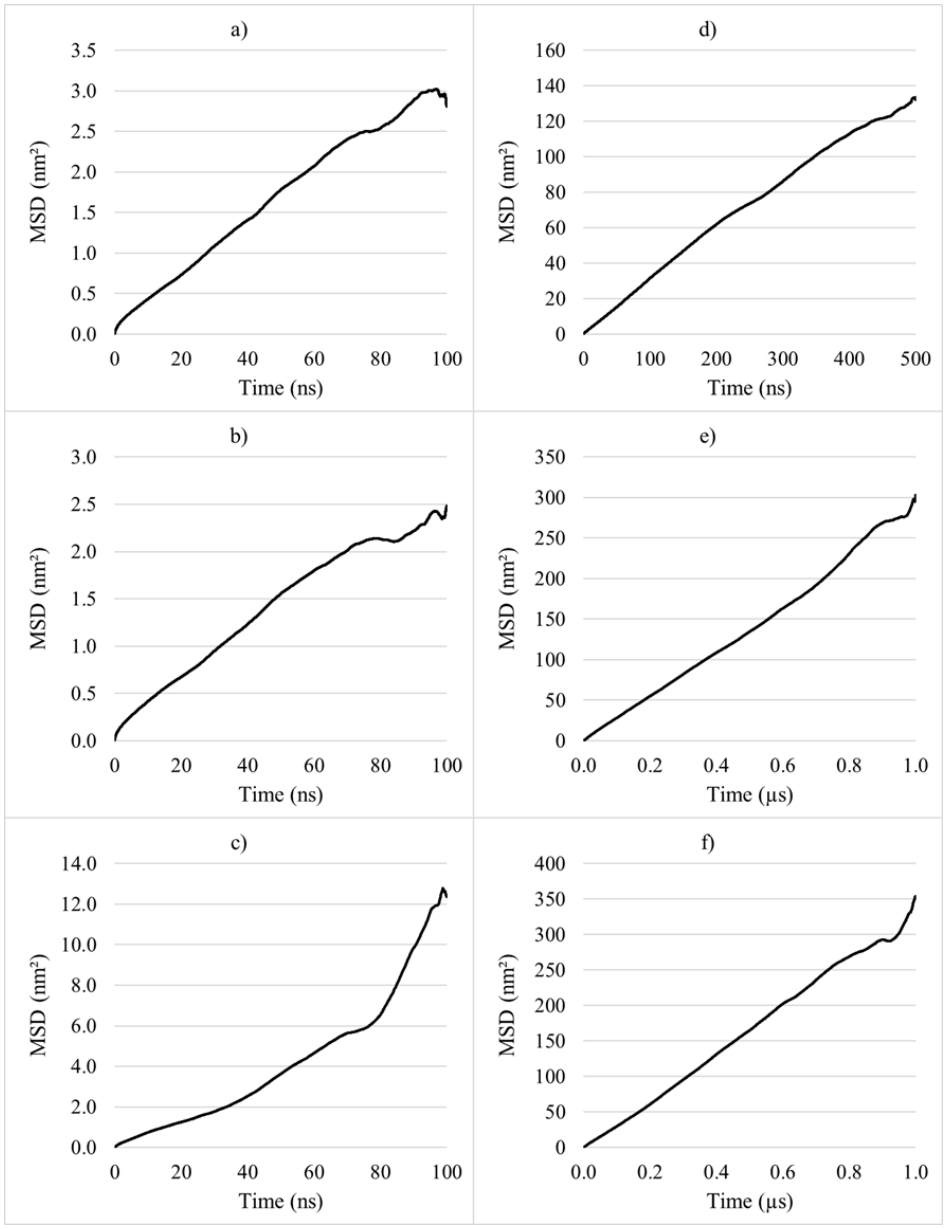

Figure E.1. MSD of DOPC lipids with a) no b) 1 and c) 10 thymoquinones in atomistic; with a) no b) 1 and c) 10 thymoquinones in coarse-grained simulations.

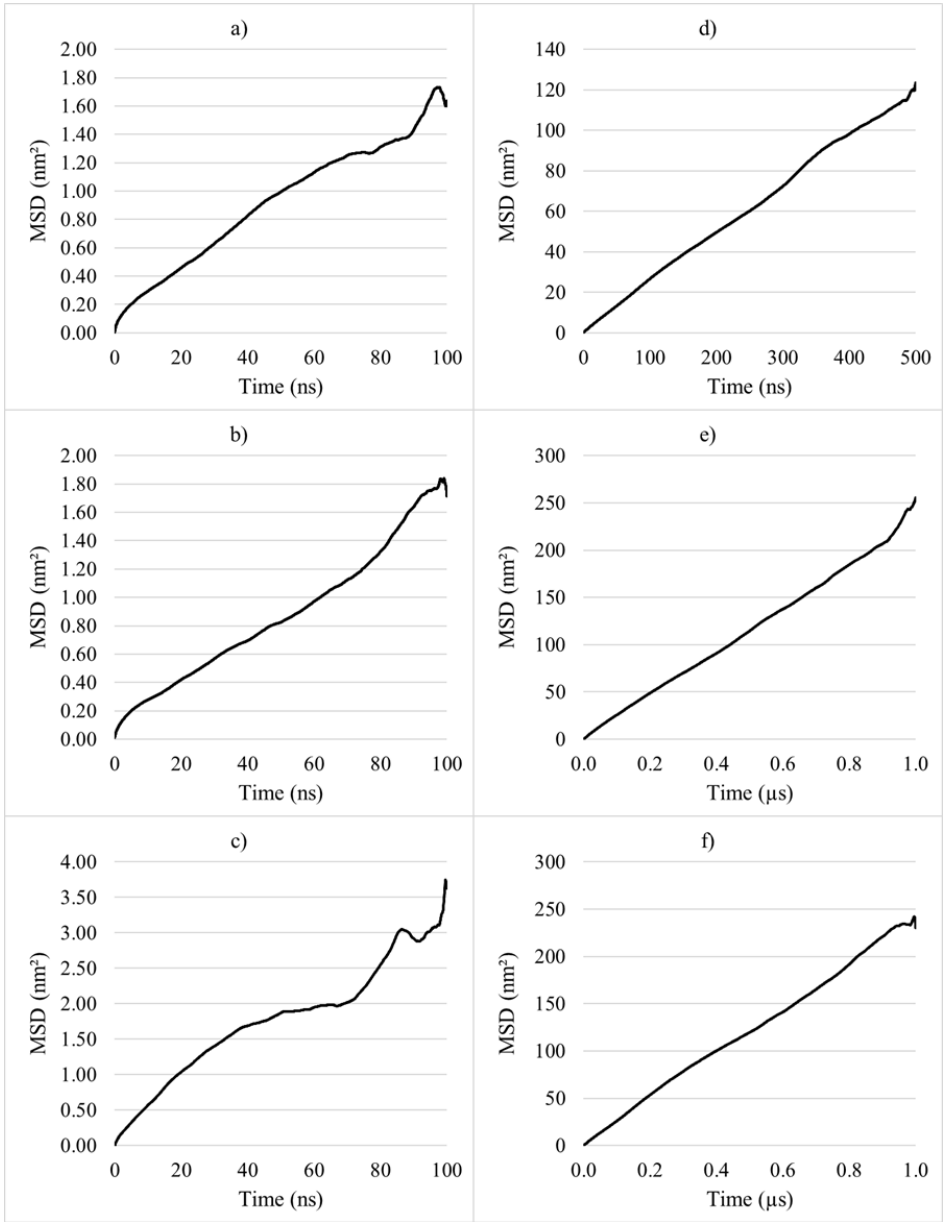

Figure E.2. MSD of POPC lipids with a) no b) 1 and c) 10 thymoquinones in atomistic; with a) no b) 1 and c) 10 thymoquinones in coarse-grained simulations.

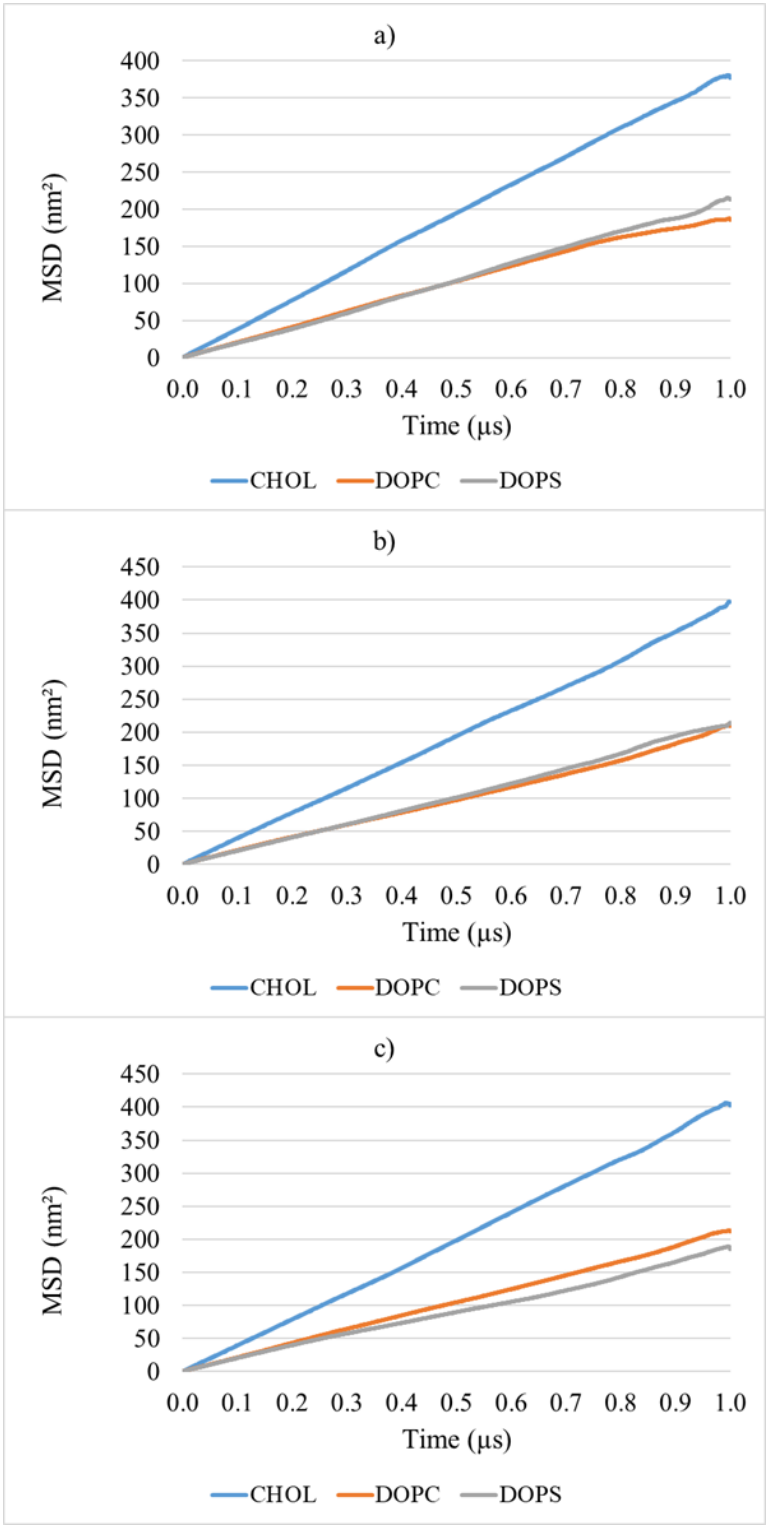

Figure E.3. MSD of Model 1 normal membrane a) without and with b) thymoquinone and c) aminothymoquinone molecules.

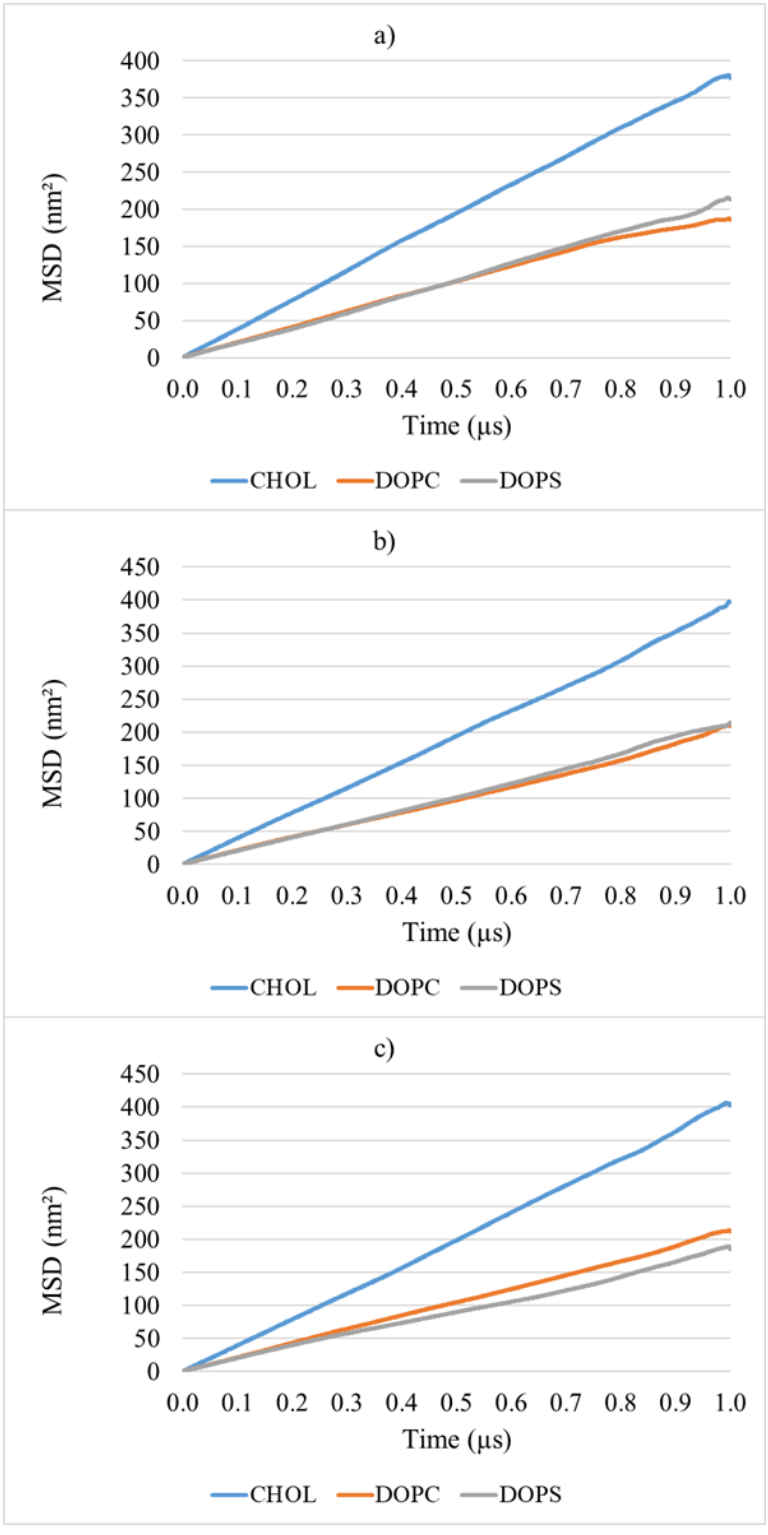

Figure E.4. MSD of Model 1 cancer membrane a) without and with b) thymoquinone and c) aminothymoquinone molecules.

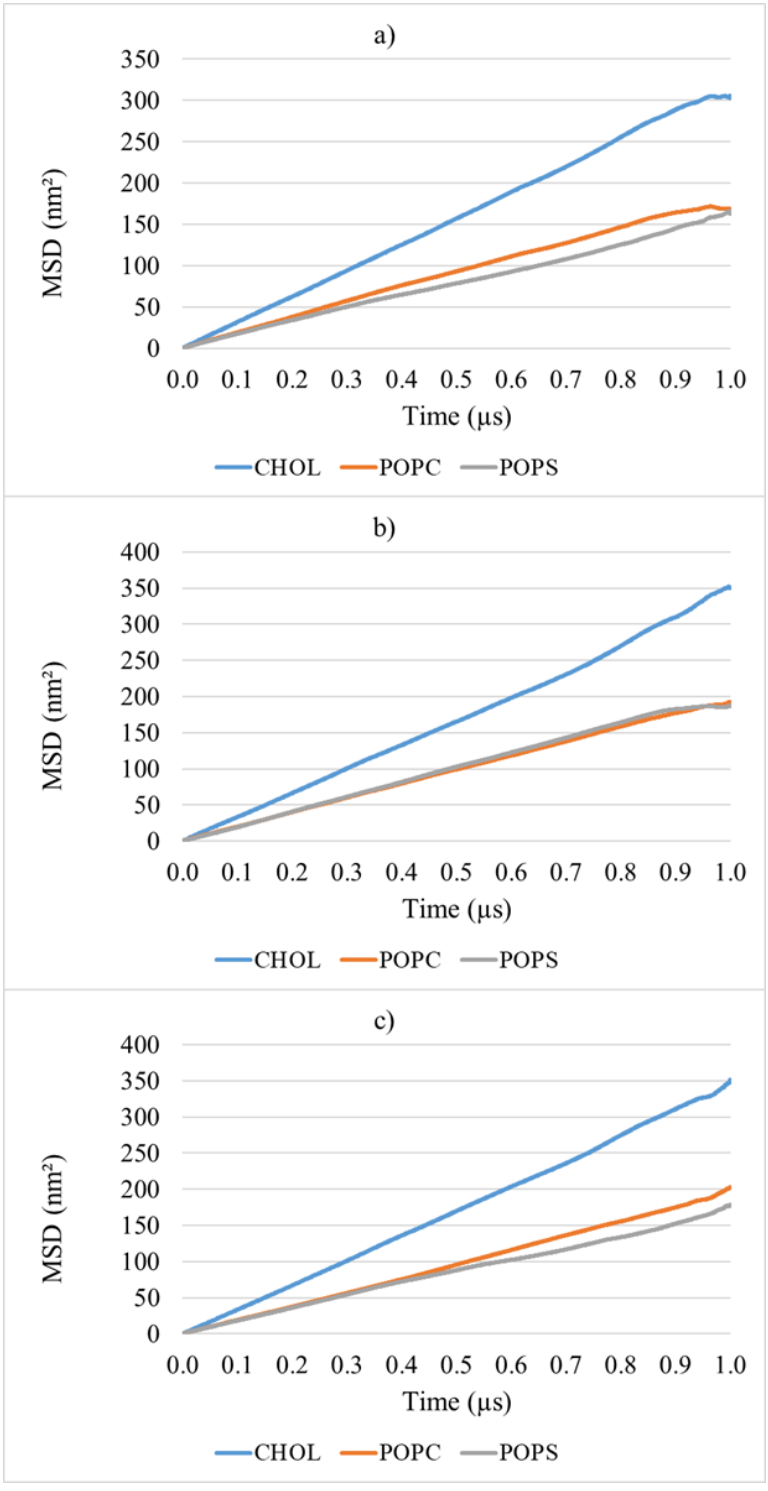

Figure E.5. MSD of Model 2 normal membrane a) without and with b) thymoquinone and c) aminothymoquinone molecules.

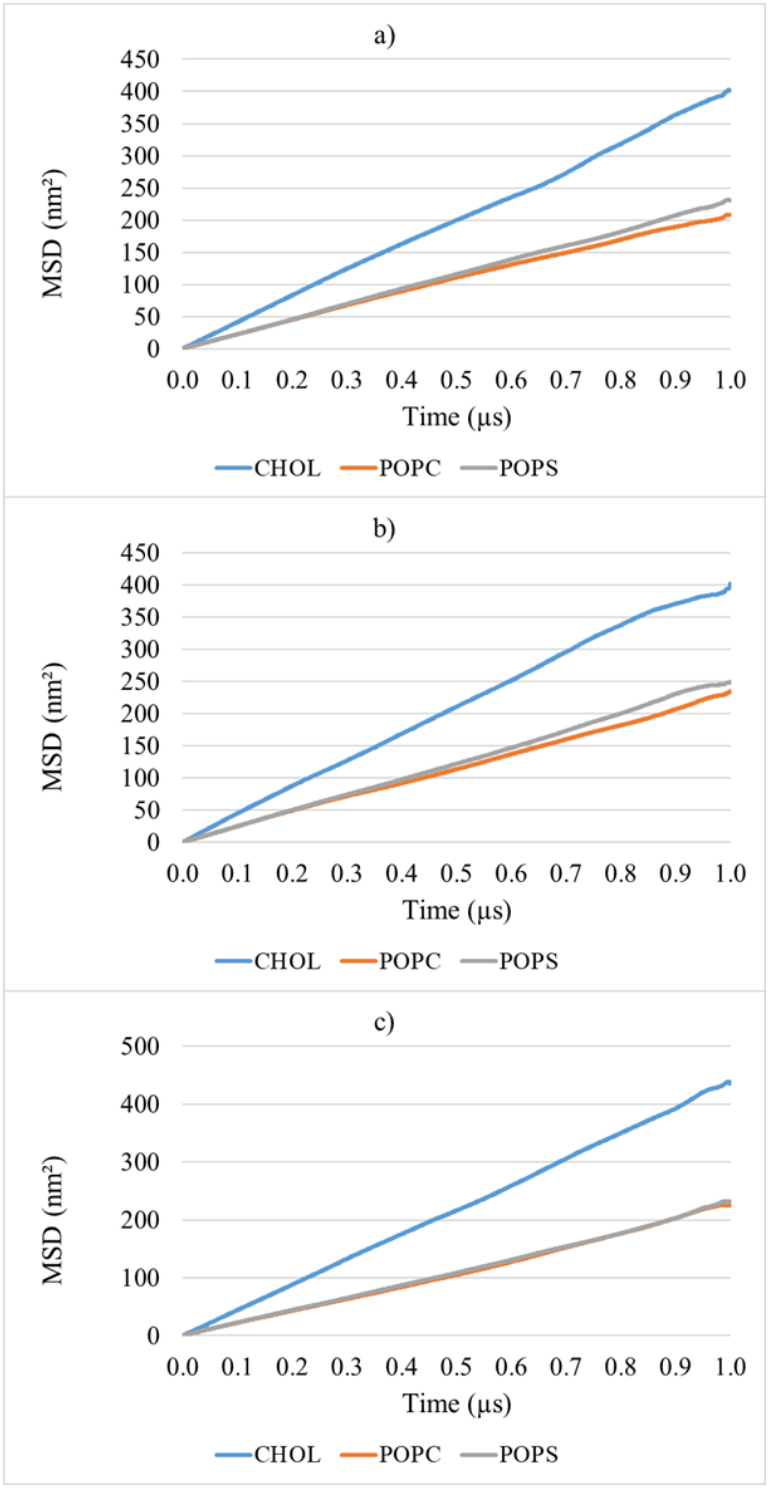

Figure E.6. MSD of Model 2 cancer membrane a) without and with b) thymoquinone and c) aminothymoquinone molecules.

APPENDIX F: GRAPHS OF DENSITY DISTRIBUTION ANALYSIS

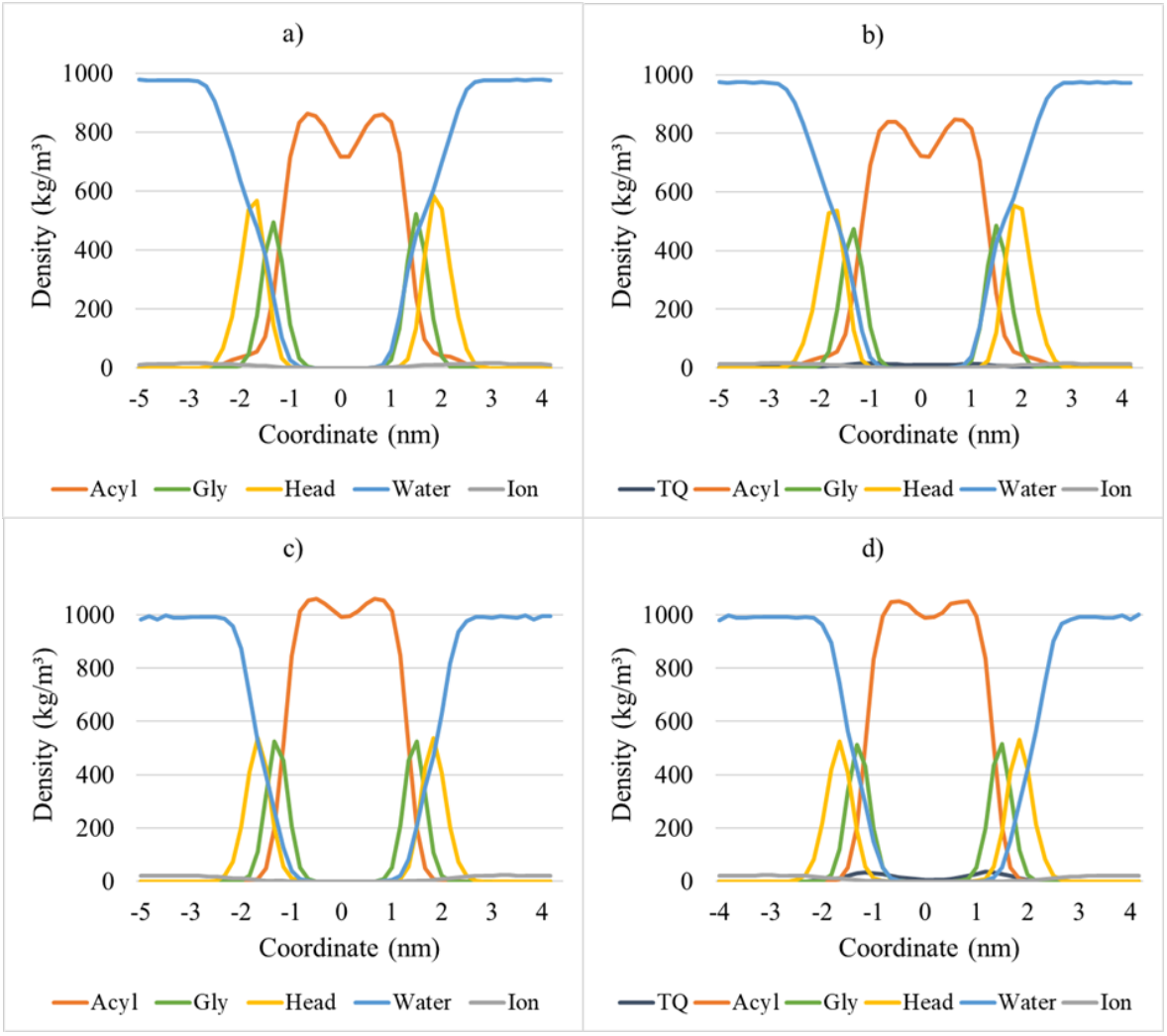

Figure F.1. Density distribution of DOPC bilayers a) without and b) with 10 thymoquinones in atomistic; c) without and d) with 10 thymoquinones in coarse-grained simulations.

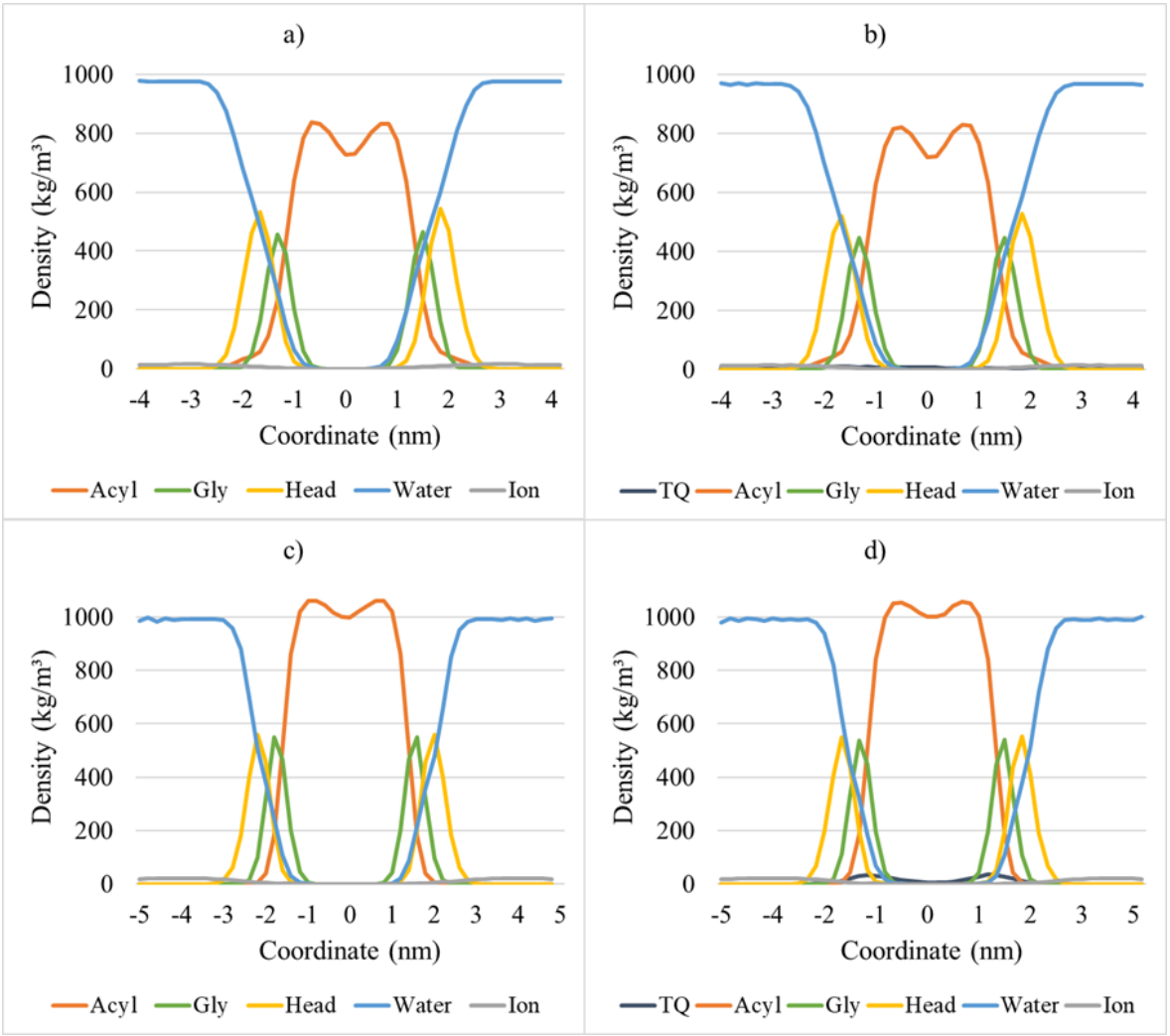

Figure F.2. Density distribution of POPC bilayers a) without and b) with 10 thymoquinones in atomistic; c) without and d) with 10 thymoquinones in coarse-grained simulations.

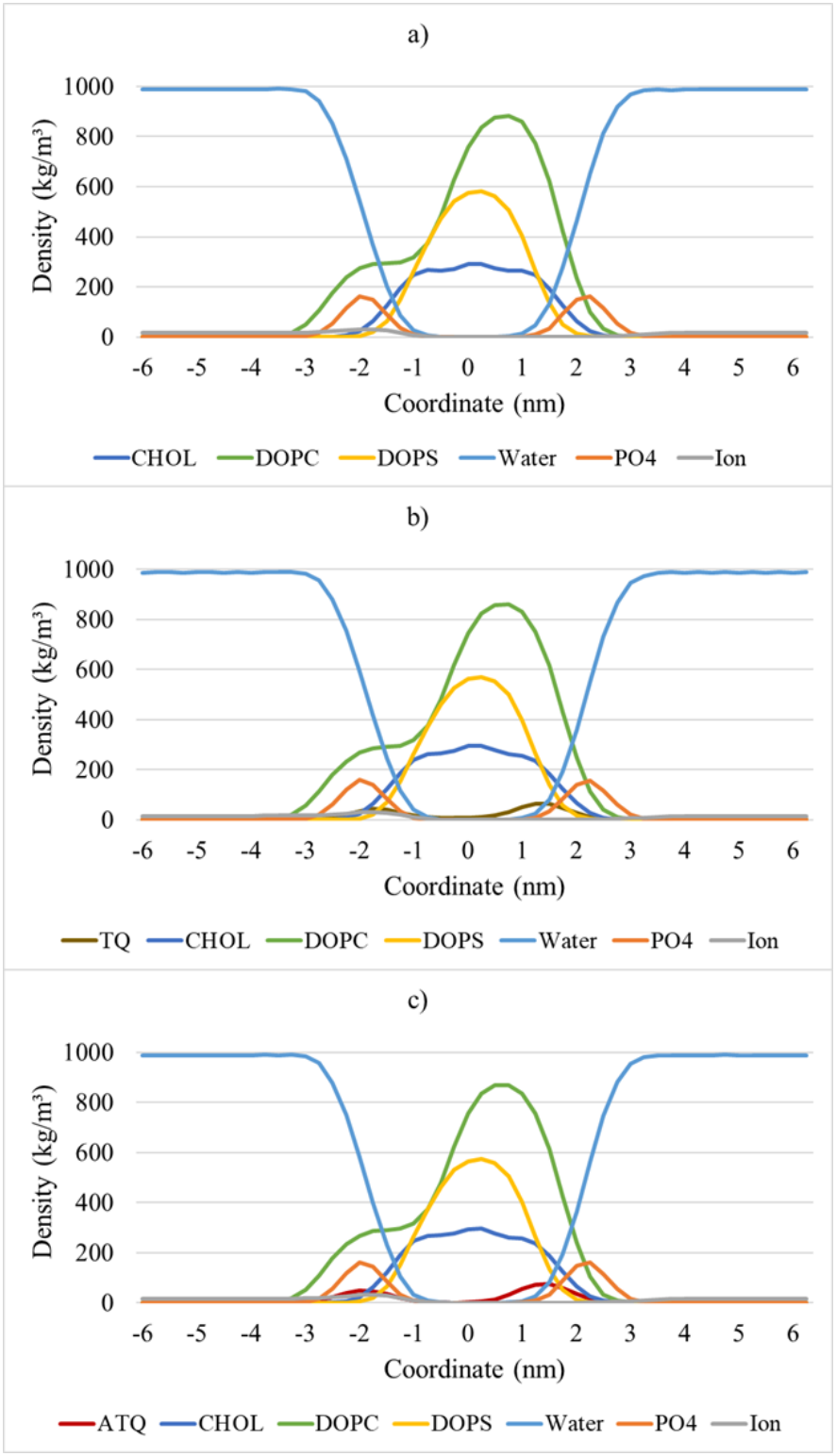

Figure F.3. The density distribution of Model 1 normal cell bilayers a) without and with b) thymoquinone and c) aminothymoquinone.

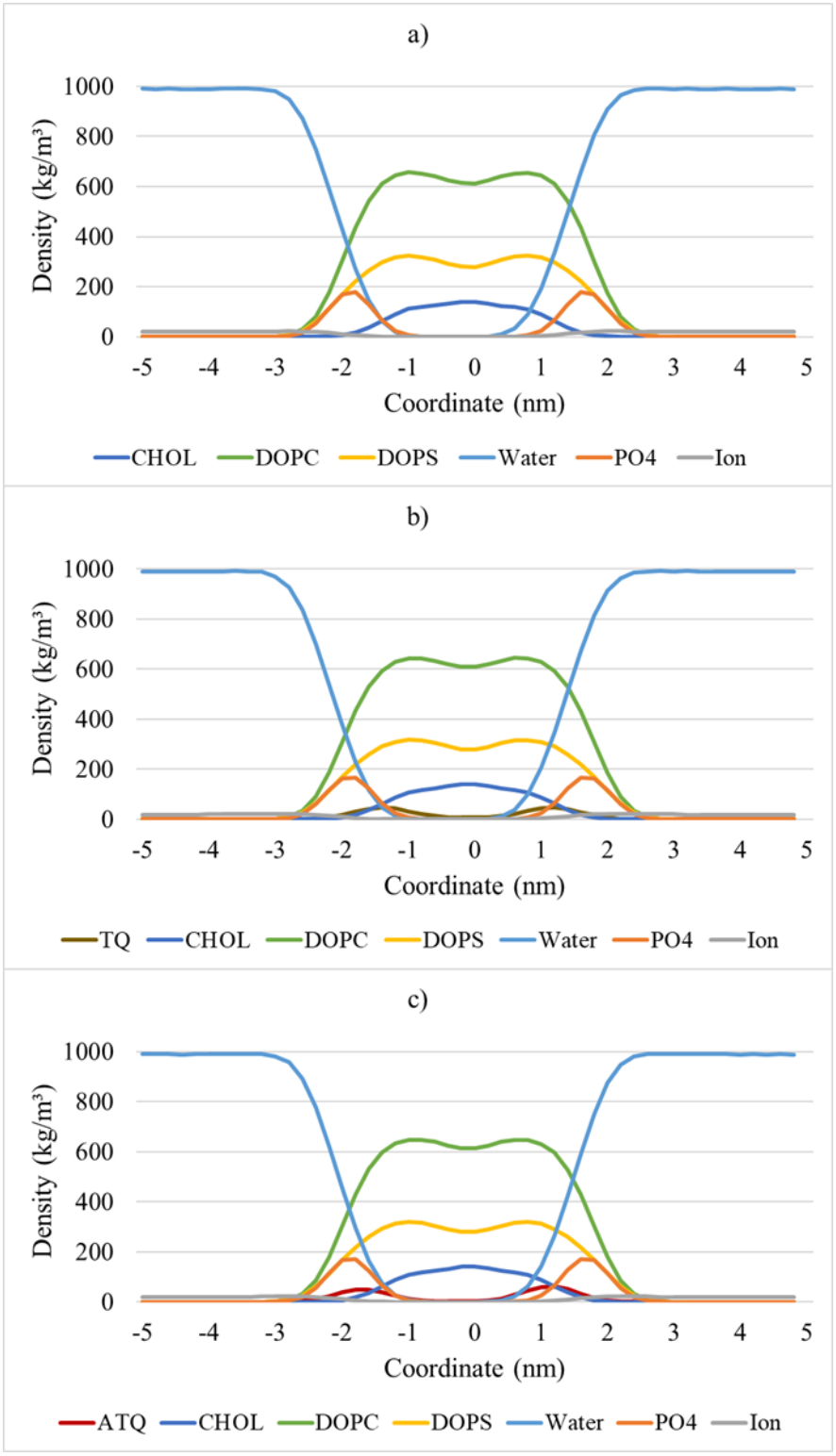

Figure F.4. The density distribution of Model 1 cancer cell bilayers a) without and with b) thymoquinone and c) aminothymoquinone.

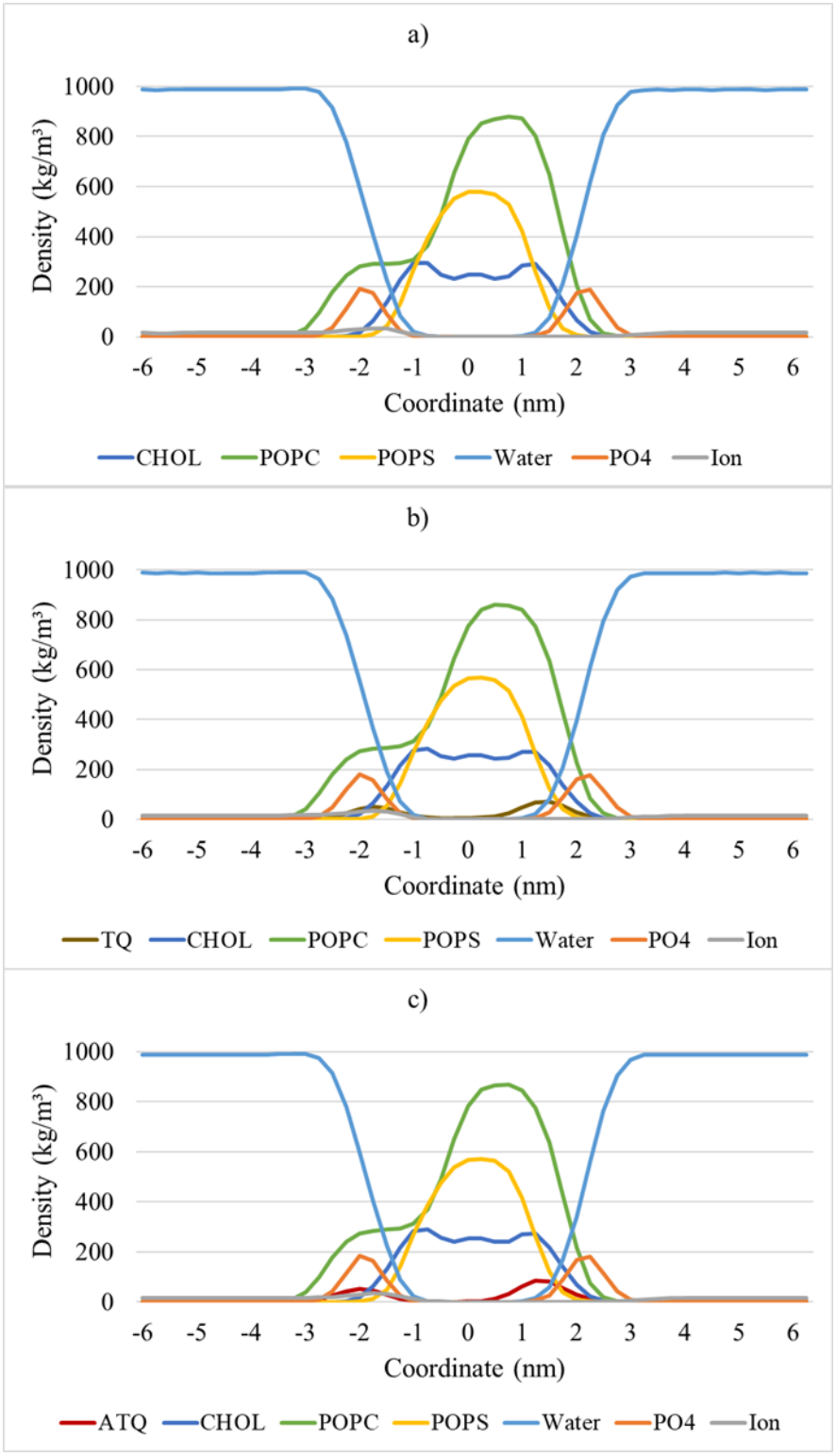

Figure F.5. The density distribution of Model 2 normal cell bilayers a) without and with b) thymoquinone and c) aminothymoquinone.

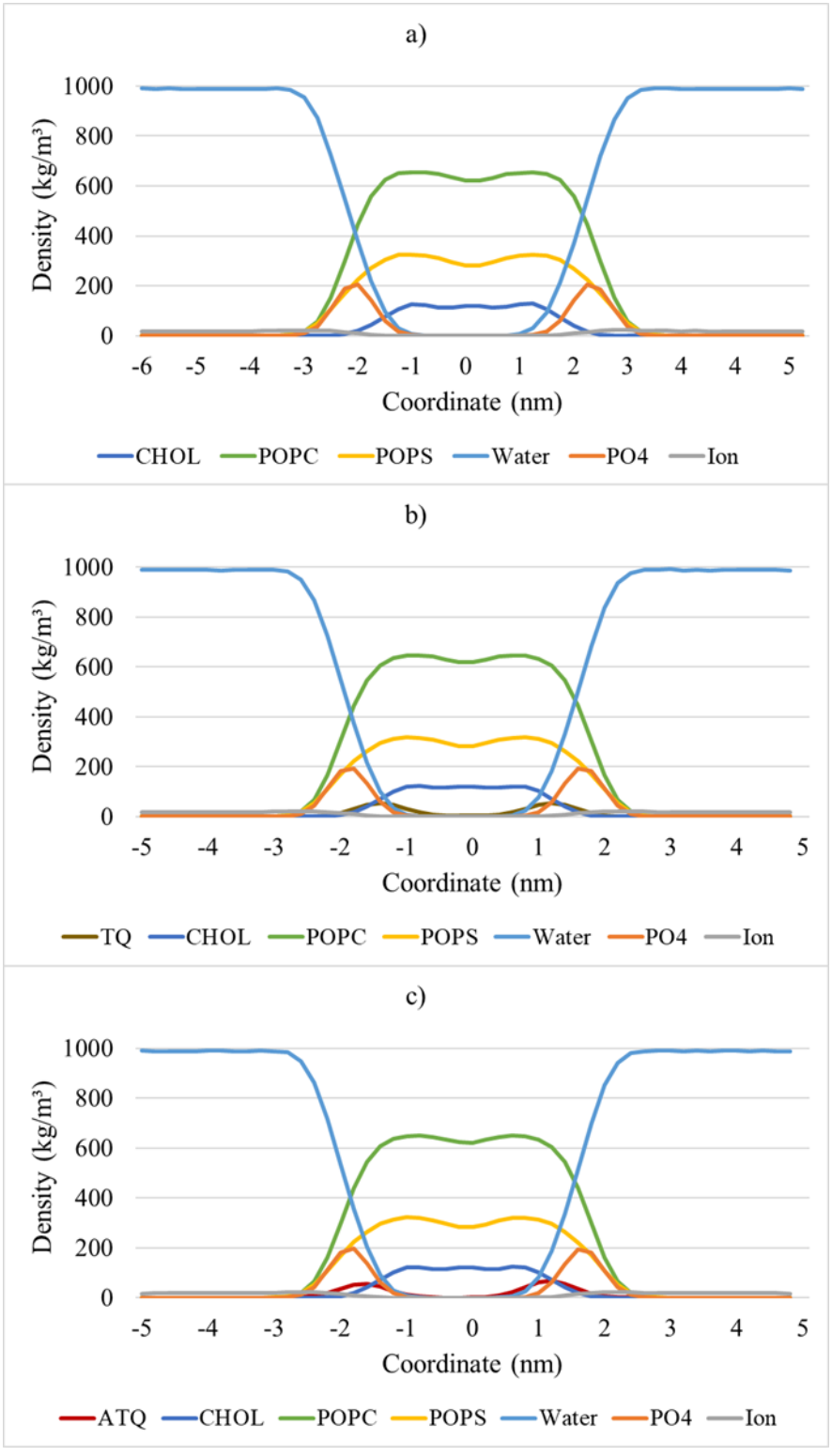

Figure F.6. The density distribution of Model 2 cancer cell bilayers a) without and with b) thymoquinone and c) aminothymoquinone.

APPENDIX G: CREDIT

Figure 3.6 is adapted with permission from Ercan, N. I., P. Stroeve, J. W. Tringe and R. Faller, "Molecular Dynamics Modeling of Methylene Blue-DOPC Lipid Bilayer Interactions", Langmuir , Vol. 34, No. 14, pp. 4314–4323, 2018. Copyright 2018, American Chemical Society.

APPENDIX H: PERMISSION FOR REUSED FIGURE 3.6

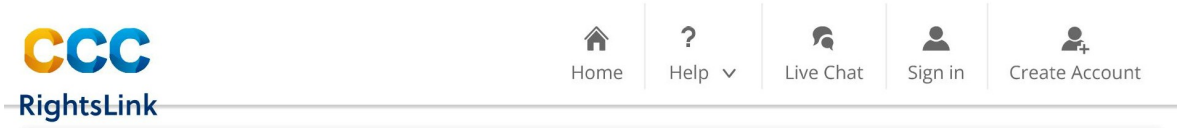

Molecular Dynamics Modeling of Methylene Blue–DOPC Lipid Bilayer Interactions

Author: Nazar Ileri Ercan, Pieter Stroeve, Joseph W. Tringe, et al

Publication: Langmuir

Publisher: American Chemical Society

Date: Apr 1, 2018

Copyright © 2018, American Chemical Society

PERMISSION/LICENSE IS GRANTED FOR YOUR ORDER AT NO CHARGE

This type of permission/license, instead of the standard Terms and Conditions, is sent to you because no fee is being charged for your order. Please note the following:

- Permission is granted for your request in both print and electronic formats, and translations.
- If figures and/or tables were requested, they may be adapted or used in part.
- Please print this page for your records and send a copy of it to your publisher/graduate school.
- Appropriate credit for the requested material should be given as follows: "Reprinted (adapted) with permission from {COMPLETE REFERENCE CITATION}. Copyright {YEAR} American Chemical Society." Insert appropriate information in place of the capitalized words.
- One-time permission is granted only for the use specified in your RightsLink request. No additional uses are granted (such as derivative works or other editions). For any uses, please submit a new request.

If credit is given to another source for the material you requested from RightsLink, permission must be obtained from that source.

BACK CLOSE WINDOW

© 2022 Copyright - All Rights Reserved | Copyright Clearance Center, Inc. | Privacy statement | Data Security and Privacy | For California Residents | Terms and ConditionsComments? We would like to hear from you. E-mail us at customercare@copyright.com